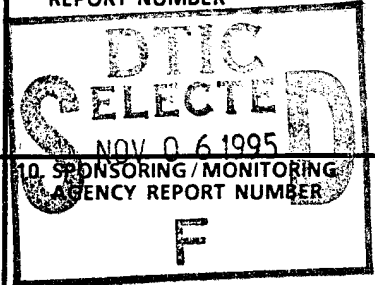


## REPORT DOCUMENTATION PAGE

Form Approved  
OMB No. 0704-0188

Public reporting burden for this collection of information is estimated to average 1 hour per response, including the time for reviewing instructions, searching existing data sources, gathering and maintaining the data needed, and completing and reviewing the collection of information. Send comments regarding this burden estimate or any other aspect of this collection of information, including suggestions for reducing this burden, to Washington Headquarters Services, Directorate for Information Operations and Reports, 1215 Jefferson Davis Highway, Suite 1204, Arlington, VA 22202-4302, and to the Office of Management and Budget, Paperwork Reduction Project (0704-0188), Washington, DC 20503.

1. AGENCY USE ONLY (Leave blank)		2. REPORT DATE 08/21/1995	3. REPORT TYPE AND DATES COVERED Final Report 11/1/89 - 05/12/95	
4. TITLE AND SUBTITLE A Continuum Model for Streamflow Synthesis			5. FUNDING NUMBERS  DAAL03-89-G-0116	
6. AUTHOR(S) Erat S. Joseph Vijay P. Singh				
7. PERFORMING ORGANIZATION NAME(S) AND ADDRESS(ES) Southern University Department of Civil Engineering Baton Rouge, LA 70813			8. PERFORMING ORGANIZATION REPORT NUMBER 	
9. SPONSORING / MONITORING AGENCY NAME(S) AND ADDRESS(ES) U.S. Army Research Office P.O. Box 12211 Research Triangle Park, NC 27709-2211			10. SPONSORING / MONITORING AGENCY REPORT NUMBER	
11. SUPPLEMENTARY NOTES The views, opinions and/or findings contained in this report are those of the author(s) and should not be construed as an official Department of the Army position, policy, or decision, unless so designated by other documentation.				
12a. DISTRIBUTION / AVAILABILITY STATEMENT  Approved for public release; distribution unlimited.			12b. DISTRIBUTION CODE  DTIC QUALITY INSPECTED 8	
13. ABSTRACT (Maximum 200 words)  In this study, three related areas were investigated with the objective of developing a continuum model for streamflow synthesis. The areas spanned surface runoff to subsurface unsaturated flow to flood-wave propagation to comparative assessment of different dynamic wave representations of the shallow water-wave theory. The surface runoff was modeled using discrete linear models for overland flow, and physically-based Muskingum methods for channel flow. Also developed was a theory of errors for a comparative evaluation of the kinematic, diffusion, and dynamic wave representations of the shallow water-wave theory. The unsaturated flow was modeled using a systems-based model for infiltration and soil moisture, and the kinematic-wave theory for movement of soil moisture. The infiltration model was a general one encompassing the popular models of Horton, Kostikov, Overton, Green and Ampt, and Philip as special cases. The models developed in the project were verified using field data. In most cases, simplified models were found to be adequate.				
14. SUBJECT TERMS Continuum model, error analysis, infiltration models, shallow water-wave theory, soil moisture movement, streamflow synthesis, subsurface unsaturated flow, systems approach, surface run			15. NUMBER OF PAGES 17	
			16. PRICE CODE	
17. SECURITY CLASSIFICATION OF REPORT UNCLASSIFIED	18. SECURITY CLASSIFICATION OF THIS PAGE UNCLASSIFIED	19. SECURITY CLASSIFICATION OF ABSTRACT UNCLASSIFIED	20. LIMITATION OF ABSTRACT UL	

19951101 103

# A CONTINUUM MODEL FOR STREAMFLOW SYNTHESIS

## COMPLETION REPORT

Accession For	
NTIS CR&I	<input checked="" type="checkbox"/>
DTIC TAB	<input type="checkbox"/>
Unannounced	<input type="checkbox"/>
Justification	
By	
Distribution/	
Availability Codes	
Dist	Avail and/or Special
A-1	

## A CONTINUUM MODEL FOR STREAMFLOW SYNTHESIS

1. INTRODUCTION
2. SURFACE RUNOFF MODELING
  - 2.1 Theory of Errors  
Physically-Based Muskingum Method
3. SUBSURFACE
  - 3.1 INFILTRATION MODELING
  - 3.2 MOVEMENT OF SOIL MOISTURE
4. LITERATURE CITED
5. PUBLICATIONS RESULTING FROM THE GRANT

## A CONTINUUM MODEL FOR STREAMFLOW SYNTHESIS

### 1. INTRODUCTION

Streamflow evolves as a continuum, and is normally comprised of three components: (1) surface runoff, (2) interflow, and (3) baseflow. These components occur concurrently, although their relative magnitudes vary with time. If we consider a sudden burst of rainfall, then surface runoff predominates during the rising part of the streamflow hydrograph, interflow predominates during the early part of its recession, and baseflow predominates during the delayed part of its recession. The mechanisms and, therefore, the governing equations, of these components are different but are influenced by dynamic interactions prevailing between them.

Although streamflow synthesis has long been a subject of scientific inquiry, treatment of streamflow as a continuum taking into account dynamic interactions amongst its components has not yet been fully developed. Most of the approaches of streamflow synthesis are based on the concepts embodied in Horton's infiltration theory of runoff (Horton, 1933). According to this theory, rainfall is absorbed for intensities not exceeding infiltration capacity, while for excess rainfall there is a constant rate of absorption as long as the infiltration capacity is unchanged. Thus, infiltration divides rainfall into two parts. One part travels over the surface giving rise to surface runoff, and the other part infiltrates into the ground resulting in replenishment of soil moisture and recharge of groundwater, and eventually in interflow and baseflow.

The three components of streamflow have been treated at various levels of mathematical sophistication but in virtual isolation with one another. Surface flow has been studied for over half a century (Woolhiser, 1982), and as a result, it is understood reasonably well (Hall, 1982). Likewise, baseflow contribution to streamflow has been studied for nearly 30 years and it too is understood reasonably well (Hall, 1982). The same, of course, cannot be said about interflow. This is not even well defined and is least understood. Also, least understood are the dynamic interactions prevailing amongst these components.

Although considerable progress has been made in mathematical and numerical treatment of the boundary value problems dealing with flows over impervious beds, the understanding of surface flows over porous beds which dynamically interact with subsurface flow is quite limited. The importance of this interaction has been pointed out in the past in the context of border irrigation (Parlange, 1973), and in the study of flood waves in ephemeral streams (Smith, 1972). These studies, however, are not based upon a coupled set of equations pertaining to surface and subsurface flow; rather the attenuation in surface flows is included by considering certain infiltration rate with time lag. The dynamic diffusion due to infiltration, therefore, remains unaccounted for.

Freeze (1972) was probably the first to develop a comprehensive quantitative treatment of hillslope hydrology considering explicit interactions between near-surface groundwater flow, surface runoff and rainfall intensity patterns. Rather limited work has since been done along the lines of Freeze. Some notable

examples are the conceptual model of Beven and Kirby (1979), the model of Hillel and Hornberger (1979), and the finite element model of Beven (1977).

The most recent work representing a major step forward in developing an analytical treatment of interdependent surface and subsurface hydrologic processes is by Smith and Hebbert (1983). In their model, the hillslope was considered to consist of two soil layers with the lower soil capable of restricting vertical flow at the interface creating a perched aquifer and subsurface stormflow. Unsaturated vertical flow was routed by a kinematic wave method and linked with an analytical infiltration model. Thus, this model attempted to integrate most of the major hydrologic response mechanisms presently identified as contributing to the hydrology of a simple hillslope. Other hillslope hydrological models (Cundy, et al., 1985; Stagnitti, et al., 1986) and surface irrigation models (Walker and Humpherys, 1983; Stagnitti, et al., 1986) and surface irrigation models (Walker and Humpherys, 1983; Ram, et al., 1983) have also been developed. However, none of these models developed a method to compute infiltration rate dynamically, although it is one of the major factors affecting runoff (or advance front) and surface water profile. Most of the models utilized empirical formulae such as Kostiaikov's or Green and Ampt's, etc. Therefore, the prevailing dynamic process between surface and subsurface flows remained unaccounted for.

Toward the goal of eventually accomplishing a continuum model for streamflow synthesis, three related areas were investigated: (1) subsurface unsaturated flow, (2) flood wave propagation, and (3) comparative assessment of

different dynamic wave representations of shallow water wave theory. In particular, we focused on (a) comparative evaluation of the kinematic-wave, diffusion-wave, and dynamic-wave representations of the shallow water wave theory ubiquitously applied to modeling surface runoff, (b) development of a systems- based model for infiltration, and (c) modeling movement of soil moisture.

## 2. SURFACE RUNOFF MODELING

The surface runoff hydrology was investigated along three lines: (a) development of a theory of errors for comparative assessment of three shallow water-wave representations: (i) kinematic-wave, (ii) diffusion-wave, and (iii) dynamic-wave; (b) development of discrete linear models for watershed runoff; and (c) physically-based Muskingum methods of channel-flow routing. A short discussion of each is in order.

### 2.1 Theory of Errors

A wide range of problems involving free-surface flows can be modeled using the shallow water-wave (SWW) theory. The SWW theory is described by the St. Venant equations or their approximations. The three most popular representations of the SWW theory are the kinematic-wave (KW), diffusion-wave (DW), and the dynamic-wave (DYW) approximations.

One of the fundamental questions to be addressed in physically-based modeling of watershed runoff is one of determining the appropriate approximation of the shallow water-wave (SWW) theory. Of the different approximations of the SWW theory, the two most popular approximations are the kinematic-wave (KW) theory and the diffusion-wave (DW) theory. How accurate are these approximations? Which approximation should be used and under what conditions? What is the spatial or temporal distribution of error of a given approximation? What is the criterion to choose between these approximations? The past studies have dealt with development of criteria for judging the adequacy of these approximations. However, these criteria are point values and do not relate to errors resulting from use of these approximations. Consequently, the error in space and/or time is not known.

The larger goal of this study was to develop a theory of errors for quantitative evaluation of the adequacy of these approximations, and, in turn, of the shallow-water-wave theory. However, because the SWW theory consists of a system of nonlinear partial differential equations of hyperbolic type, derivation of error equations is unattainable at this stage. Therefore, some realistic simplifications were made. The first was the simplification of flows being time-independent. Steady state flows are ubiquitous in nature, and much of the early hydraulics was based on this assumption.

Because spatially distributed data are seldom available, it was assumed that the full form of the SWW theory or the dynamic-wave representation was the true representation or model, and was capable of mimicking the behavior of the real

world, prototype system, and the kinematic-wave and diffusion-wave approximations were reasonable approximations, but were germane to conceptual error. The adequacy of these approximations is well documented in hydraulic literature. However, what is not known is the actual error and its distribution in time and/or space, as well as its relationship to flow characteristics, system properties and initial and boundary conditions.

The theory of errors can serve as an objective criterion for judging the adequacy of the KW and DW approximations by comparison with the DYW approximation. For time-independent flows, the theory yields error as a function of space involving infiltration, and boundary conditions. The error differential equation is ordinary in place of partial, and is more amenable to numerical solution. Even with this simplification, analytical solutions are not possible but the numerical solutions are much simpler and easy to graph.

Different criteria have been developed to evaluate the adequacy of the KW and DW theories, but no explicit relations either in time or in space between these criteria and the errors resulting from these approximations have yet been derived. Furthermore, when synthesizing streamflow, it is not clear if the kinematic-wave and the diffusion-wave approximations are valid, on one hand, for the entire hydrograph or for a portion thereof, and on the other hand, for the entire channel reach or for a portion thereof. To put differently, all of these criteria take on fixed point-values for a given rainfall-runoff event. This study, under simplified conditions, derived error equations for the kinematic-wave and diffusion-wave approximations for space-

independent as well as for time-independent flows. These equations provided a continuous description of error in the streamflow hydrograph.

With these considerations in mind, errors of kinematic-wave and diffusion wave approximations were derived for steady-state channel flows subject to finite flow at the upstream end. The diffusion-wave approximation was in excellent agreement with the dynamic wave representation for a range of the values of the Froude number and the kinematic-wave number. The kinematic-wave approximation was also in good agreement with the dynamic wave representation, but for a limited range of the values of the Froude number and the kinematic-wave number. On the other hand, the approximate diffusion-wave analogy, although leading to analytical solutions, was not accurate and should not be employed.

Under two different initial conditions and two boundary conditions, solutions of the kinematic-wave and diffusion-wave equations were derived under the simplification that the flow was temporally independent. Thereafter, error equations for the KW and DW theories were derived. It was found that the DW theory was quite accurate and for Froude number ( $F_o$ ) less than 2 and the kinematic wave number ( $K$ ) greater than 10, the DW theory would be an accurate representation of the SWW theory. Under the condition where there was no downstream control, the KW theory was an accurate representation for  $K > 30$ ,  $K F_o^2 > 5$ . The KW theory does not accommodate a downstream control and hence, as expected, did not accurately represent the SWW theory for the entire channel under any of the two boundary conditions. Details of this work are contained in Singh, Aravamuthan and Joseph (1994).

For space-independent flows, a dimensionless parameter was defined, reflecting the effect of initial depth of flow, channel-bed slope, lateral inflow, acceleration due to gravity, and channel roughness. For time-independent flows, the dimensionless parameter was the product of the kinematic-wave number and the square of the Froude number. By comparing the kinematic-wave and diffusion wave solutions with the dynamic-wave solution, error equations were derived in terms of the aforementioned dimensionless parameters. The error equations for space-independent flows turned out to have the form of the Riccati equation. The work is described in Singh, Aravamuthan and Joseph (1993).

## 2.2 Watershed Runoff

Discrete linear models were developed for estimating runoff and sediment discharge hydrographs from agricultural watersheds. A regression equation was also established relating runoff rate and sediment discharge. Tested on five small basins, the results were in good agreement with observations. For the discrete linear transfer runoff model, the values of the integral square error (ISE) were generally less than 1% for all calibration events, and around 10% with the average value of 9.36% for all verification events. For the discrete linear transfer sediment model, the calibration coefficient of determination  $R$  for all five basins was more than 97%, and the verification  $R$  was more than 91% with an average of 94.3%. Details of this work are described in Wang et al. (1991).

### 2.3. Physically - Based Muskingum Method

Flow routing in channels was investigated using the kinematic wave theory as well as the Muskingum method. For the latter method parameters were derived from the St. Venant equations. Preliminary testing showed that this method of parameter estimation made the Muskingum method more accurate than any of the conventional methods. The kinematic wave method was investigated for perennial as well as ephemeral streams. This method can be extended to include flood wave propagation due to dam rupture. This work is more fully described in Wang and Singh (1992).

## 3. SUBSURFACE FLOW

Modeling of flow of water in the unsaturated zone is far from complete, especially at the field scale. Two lines of inquiry were, therefore, launched. First, a systems approach was developed to model infiltration and soil moisture, which holds promise for unifying different infiltration models reported in the literature. This approach can also relate parameters of one infiltration to another. The second type of approach pertained to application of the kinematic wave theory. This approach has the advantage of coupling plant root extraction and evapotranspiration with soil water dynamics.

### 3.1 Infiltration Modeling

A general infiltration model was derived using systems approach. The models of Horton, Kostiaikov, Overton, Green and Ampt, and Philip are some of the

example models which are shown as special cases of the general model. An equivalence between the Green-Ampt model and the Philip two-term model was shown. The general model also provides a solution for the Holtan model expressing infiltration as a function of time. This solution of the Holtan model does not appear to have been reported in the literature. A first-order analysis was performed to quantify the uncertainty involved with the generalized model. The general infiltration model contains five parameters. Two of the parameters are physically based and can therefore be estimated from the knowledge of soil properties, antecedent soil moisture conditions, and infiltration measurements. The remaining three parameters can be determined using the least squares method. The model was verified using ten observed infiltration data sets. Agreement between observed and computed infiltration was quite good. This work is more fully described in Singh and Yu (1990).

### 3.2 Movement of Soil Moisture

The unsaturated subsurface flow serves as a link between surface runoff and groundwater runoff, and, therefore, occupies the central position in the streamflow continuum. The unsaturated flow region is the upper soil matrix which also is the principal source of interflow. For surface flow, infiltration is the major sink, and for groundwater flow, soil moisture percolation is the principal source or recharge. Much of the mathematical treatment of unsaturated flow, reported to date, is based on the Fokker-Planck equation or Richards equation. Both these equations are of the diffusion type, and do not lend themselves to analytical solutions, except for overly simplified cases.

If one ignores the effect of diffusion and models soil moisture movement using the kinematics wave theory, then, under certain simplifying but realistic conditions, it is possible to derive analytical solutions. This premise was pursued in this project. Currently available one-dimensional kinematic-wave models assume absence of sink terms. In other words, once the water gets infiltrated, it is either retained by the soil or moves downward to recharge the groundwater. This assumption is not tenable, especially in agricultural or forest watersheds. In this project, an effort was made to include a sink term in modeling of soil moisture. This sink term may represent removal of soil moisture by vegetation through the process of evapotranspiration.

Recognizing the difficulties of modeling unsaturated flow using the Richards equation, a novel approach was developed in this project. This approach was based on the kinematic wave theory in which a unique relation is hypothesized between the flux and the flow concentration or the hydraulic head.

The fundamental assumption underlying this theory is that the moisture movement is gravity-dominated and the hydraulic conductivity-soil moisture relationship is single-valued, i.e., it does not experience any hysteretic effects. Although these assumptions are not strictly valid, they do provide a reasonably accurate approximation. Another advantage of the theory is its simplicity and that it allows analytical solutions under simplified conditions. Under more complex conditions, numerical solutions are easily derived.

This unique relation, when coupled with the continuity equation expressing the conservation of mass, gives rise to a first order, nonlinear hyperbolic equation. Under simplified initial and boundary conditions, analytical solutions of this kinematic-wave equation are tractable. Following this tract, the soil moisture movement was modeled with the use of the kinematic-wave theory. However, attention is to be focused on certain aspects of the kinematic-wave modeling that are not apparent at the first glance. First, because the time history of the moisture front distinguishing between wet and dry soil is unknown, the kinematic-wave formulation of soil moisture movement results in a free-boundary problem. Second, natural watersheds have vegetation either seasonally or throughout the year. Inclusion of vegetation in modeling of soil-moisture movement gives rise to an additional free boundary, further complicating the model.

With these considerations in mind, a kinematic-wave model was developed for simulating the movement of soil moisture in unsaturated soils with plants. The model involved three free boundaries. Analytical solutions were derived when the plant-root extraction of moisture was at a constant rate, and the upstream boundary condition was time independent. If these assumptions are waived, then numerical solution is the only resort.

With the use of this theory, a comprehensive analytical treatment has been developed for soil moisture movement with plant-root extraction. The treatment involves free boundaries and to our knowledge this has not been dealt with in the literature so far. This work is described in Singh and Joseph (1994).

#### 4. LITERATURE CITED

- Beven, K.J., 1977. Experiments with a Finite Element Model of Hillslope Hydrology - The Effect of Topography. In Surface and Subsurface Hydrology, edited by H.J. Morel-Seytoux, et. al., pp. 37-51, Water Resources Publications, Fort Collins, CO.
- Beven, K. J. and Kirby, M. J., 1979. A physically-based variable contributing area model of basin hydrology. Hydro. Sci. Bull, Vol., 24, pp. 43-69.
- Cundy, T.W. and Tonto, S.W., 1985. Solution to the kinematic wave approach to overland flow routing with rainfall excess given by Philip's equation. Water Resources Research, Vol., 21, No. 8, pp. 1132-1140.
- Freeze, R.A., 1972a. Role of subsurface flow in generating surface runoff; 1. baseflow contributions to channel flow. Water Resources Research, Vol., 8, No. 3, pp. 609-623.
- Freeze, R.A., 1972b. Role of subsurface flow in generating surface runoff, 2, upstream source areas. Water Resources Research, Vol., 8, No., 5, pp. 1272-1283.
- Hall, F.R., 1982. Subsurface water contributions to streamflow. In: V.P. Singh (ed.), Rainfall-Runoff Relationship, Water Resources Publications, Littleton, CO.
- Hillel, D. and Hornberger, G.M., 1979. Physical model of the hydrology of sloping heterogeneous fields. Soil Sci. Soc. Am. J., Vol. 43, No. 3, pp. 434-439.
- Horton, R.E., 1933. The role of infiltration in the hydrologic cycle. Transactions, American Geophysical Union, Vol. 14, pp. 446-460.

- Parlange, J.Y., 1973. Note on the infiltration advance front from border irrigation. Water Resources Research, Vol. 9, No. 4, pp. 1075-1078.
- Ram, R.S., Singh, V. P. and Prasad, S. N., 1983. Mathematical modeling of surface irrigation. Technical Report WRR5, Water Resources Program, Department of Civil Engineering, Louisiana State University, Baton Rouge, LA.
- Smith, R. E., 1972. The infiltration envelop: Results from theoretical infiltrometer. Journal of Hydrology, Vol., 17, pp. 1-21.
- Smith, R.E. and Hebbert, R.H.B., 1983. Mathematical simulation of interdependent surface and subsurface hydrologic processes. Water Resources Research, Vol. 19, No. 4, pp. 987-1001.
- Stagnitti, F., Parlange, M. B., Steenhuis and Parlange, J.Y., 1986. Drainage from a uniform soil layer on a hillslope. Water Resources Research, Vol. 22, No. 5, pp. 631-634.
- Walker, W.R. and Humpherys, A.S., 1983. Kinematic-wave furrow irrigation model. Journal of Irrigation and Drainage Division, Proceedings of American Society of Civil Engineers, Vol. 109. No. 4, pp. 377-392.

# Kinematic-wave model for soil-moisture movement with plant-root extraction

V. P. Singh<sup>1</sup>, E. S. Joseph<sup>2</sup>

<sup>1</sup> Department of Civil and Environmental Engineering, Louisiana State University, Baton Rouge, LA 70803-6405, USA

<sup>2</sup> Department of Civil Engineering, Southern University, Baton Rouge, LA 70813, USA

Received: 23 September 1992

**Abstract.** A kinematic-wave model is developed for simulating the movement of soil moisture in unsaturated soils with plants. The model involves three free boundaries. Analytical solutions are derived when the plant roots are assumed to extract moisture at a constant rate and the upstream boundary condition is independent of time. Numerical solutions are the only resort when the moisture extraction and the upstream boundary condition both depend on time.

Much of the mathematical treatment of flow in unsaturated porous media has dealt with capillary-induced flow (Smith 1983). However, there exists a multitude of cases where gravity dominates vertical movement of soil moisture. Some examples include: drainage following infiltration, the water percolation deeper into the soil, the vertical movement of moisture in relatively porous soils when rainfall or surface fluxes are typically of the order of, or less than, the soil-saturated hydraulic-conductivity, to name but a few. For treatment in such cases, the kinematic-wave theory is simple yet reasonably accurate.

Although Sisson et al. (1980) applied the kinematic-wave theory to internal drainage, Smith (1983) was probably the first to apply the theory to develop a complete kinematic-wave model for soil moisture movement. Charbeneau (1984) extended Smith's work to solute transport, and Charbeneau et al. (1989) to multiple solute transport. In a series of papers, Germann and coworkers (Germann 1985; Germann and Beven 1985, 1986; German et al. 1987) extended the application of the theory to infiltration and drainage into and from soil macropores, as well as to microbial transport. Yamada and Kobayashi (1988) discussed the kinematic wave characteristics of vertical infiltration and soil moisture, with the aid of field observations on tracers. They concluded that the vertical infiltration of soil moisture had the characteristics of kinematic waves.

Correspondence to: V. P. Singh

In this study, a kinematic-wave model is formulated for soil-moisture movement with plant-root extraction. Analytical solutions are derived under the condition that the moisture extraction by plants and the surface flux are both constant in time. This condition is severe, but leads to intriguing and useful results. For more realistic conditions numerical solutions are the only resort, these together with field verification, will be reported in the near future.

## Kinematic-wave model

### Formulation

For vertical unsaturated flow with plant-root extraction and with the neglect of the flow of air, the governing equations are the law of conservation of mass and a flux law. The one-dimensional conservation of mass equation or the continuity equation can be expressed as

$$\frac{\partial \theta}{\partial t} + \frac{\partial q}{\partial z} = -e(z, \tau) \quad (1)$$

where  $\theta$  is the volumetric moisture content (dimensionless, volume of water/volume of soil),  $q$  is the vertical flux of soil moisture ( $L/T$ ),  $e(z, \tau)$  is the rate of soil moisture loss due to plant-root extraction at time  $t$  ( $1/T$ ),  $z$  is the depth ( $L$ ) measured downward from the ground surface,  $\tau$  is the time ( $T$ ) that water has stayed at location  $\tau = t - w(z)$ ,  $w(z)$  is the time history of the moisture advance front, and  $t$  is time ( $T$ ). At a fixed  $\tau$ ,  $e(\tau)$  is essentially the rate of plant-root extraction of soil moisture on a unit depth basis defined as

$$\frac{r(z, \tau)}{n} = e(z, \tau) \quad (2)$$

where  $n$  is the soil porosity, and  $r(t)$  is the soil-moisture extraction rate per unit depth at time  $t$  ( $1/T$ ). It may, however, be reasonable to assume  $e(z, \tau) = e(\tau)$ . This assumption implies spatially uniform extraction, that may be true if the plant roots are uniformly developed in the soil.

The flux law for a kinematic-wave model can be expressed as

$$q(\theta) = K(\theta) \quad (3)$$

where  $K(\theta)$  is the unsaturated hydraulic conductivity ( $L/T$ ) as a function of the soil-moisture content. A variety of expressions have been proposed for  $K(\theta)$  (Hsu and Liu 1990). Of all the expressions, the best-known perhaps is the Brooks-Corey relation (Brooks and Corey 1964) which can be written as

$$K(\theta) = K_s \left( \frac{\theta - \theta_0}{\theta_s - \theta_0} \right)^a \quad (4)$$

where  $K_s$  is the saturated hydraulic conductivity ( $L/T$ ),  $\theta_0$  is the residual value of  $\theta$  below which water cannot be extracted (or moved) by capillary forces,  $\theta_s$  is the saturated water content = porosity =  $n$ , and  $a$  is a parameter typically between 3 and 4, and is related to the pore-size distribution index.

In Eq. (1),  $\tau$  is unknown and a relation is needed whereby  $\tau$  can be determined. With such a relation, the formulation of the kinematic-wave model will be complete. To that end, when water is applied to the soil at its surface, it infiltrates into the soil and advances vertically downward, increasing the moisture content. If the soil is initially dry, the advance front, also called the shock front, will define the interface between moist and dry parts of the soil matrix. Let  $z = s(t)$  or  $t = w(z)$  be the time history of that advancing front; this time history gives the space-time coordinates of the shock front. The front is a free boundary and has to be determined along with the solution. An equation for  $z = s(t)$  or  $t = w(z)$ , therefore, has to be formulated. This can be accomplished by observing that

$$u(\theta) = u(z, t) = \frac{q(\theta)}{\theta} = \frac{K(\theta)}{\theta} \quad (5)$$

where  $u(\theta)$  is the average velocity with which  $\theta$  moves. Thus, the free-boundary equation is obtained by replacing  $z$  by  $s(t)$  or  $t$  by  $w(z)$  in  $u(z, t)$  as

$$\frac{ds(t)}{dt} = u(s(t), t) = \frac{K(\theta(s(t), t))}{\theta(s(t), t)}, \quad s(0) = 0 \quad (6)$$

or

$$\frac{dw(z)}{dz} = [u(z, w(z))]^{-1} = \frac{\theta(z, w(z))}{K(\theta(z, w(z)))}, \quad w(0) = 0. \quad (7)$$

Equation (6) is valid for  $\theta(z, t) > 0$ . Equations (6) and (7) require the advance front to move with the speed immediately behind the front.

The kinematic-wave model formulation consists of a partial differential Eq. (1), an algebraic Eq. (3), and an ordinary differential Eq. (6) or (7) with two unknowns  $\theta(z, t)$  and  $s(t)$  or  $w(t)$ . In order to derive solutions of these equations, the following can be assumed:

$$\theta(z, 0) = f(z), \quad z \geq 0, \quad (8)$$

$$\theta(0, t) = g(t), \quad 0 \leq t < T \quad (9)$$

$$= \theta_0, \quad t \geq T$$

where  $T$  is the duration for which moisture is applied at the upstream boundary. Note that  $g(0) = f(0) = \theta_0$ .

Equations (1) and (3) can be combined to produce

$$\frac{\partial \theta}{\partial t} + \frac{dK(\theta)}{d\theta} \frac{\partial \theta}{\partial z} = -e(z, \tau). \quad (10)$$

For notational simplicity, let

$$M(\theta) = \frac{dK(\theta)}{d\theta} = \frac{\partial \theta / \partial t}{\partial \theta / \partial z} = \frac{\partial z}{\partial t} \bigg|_{\theta = \text{constant}} \quad (11)$$

which is referred to as the mobility of water in soil by Irmay (1956); this is analogous to celerity, commonly used in open channel flows.

### Solution

Equation (10) is satisfied in the domain bounded by the positive  $t$  axis and the curve  $t = w(z)$  or  $z = s(t)$ . Solution of Eqs. (10) and (6) can be derived by using the method of characteristics. Accordingly, one can choose  $\sigma$  as the parameter on the  $t$ -axis and  $t$  as the parameter along the characteristics. The characteristics originate from the  $t$ -axis on the segment  $0 \leq t \leq T$ . The solution domain can be divided into two subdomains  $D_1$  and  $D_2$ , with the characteristics  $z(t, T)$  serving as the dividing line (called the bounding characteristic), as shown in Fig. 1. The characteristic curves  $z(t, \sigma)$ ,  $\theta(t, \sigma)$  passing through the points  $(0, \sigma, g(\sigma))$  in the  $(z, t, \theta)$  space, satisfy

$$\frac{d\theta(t, \sigma)}{dt} = -\sigma(\tau), \quad \theta(\sigma, \sigma) = g(\sigma), \quad (12)$$

$$\frac{dz(t, \sigma)}{dt} = M(t, \sigma), \quad z(\sigma, \sigma) = 0. \quad (13)$$

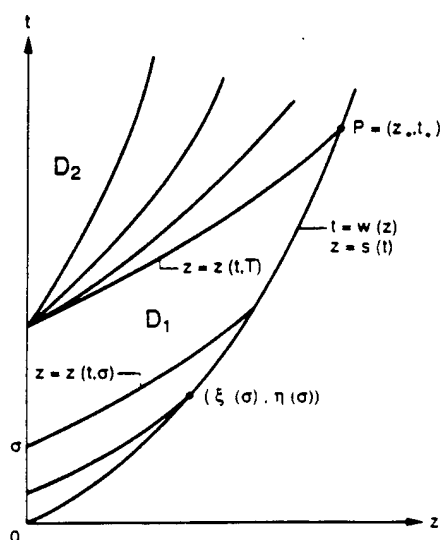


Fig. 1. Characteristic solution domain for unsaturated flow with plant-root extraction

$z(t, \sigma)$  is the position at time  $t$  of the soil-moisture content  $\theta$  which was at  $z = 0$  and at  $t = \sigma$ ;  $\theta(t, \sigma)$  is the soil-moisture content at time  $t$ . The plant-root extraction rate depends upon the nature of vegetation and availability of soil moisture. If  $e(\tau)$  is constant, which is not entirely unreasonable, especially when the soil-moisture is not limiting plant root extraction, then  $e(\tau) = e$ .

Depending upon the nature of the function  $g(t)$ , three cases can be distinguished: (1)  $g(t) = \text{constant}$ , (2)  $dg(t)/dt < 0$ , and (3)  $dg(t)/dt > 0$ . To describe the variation of soil moisture in time at a fixed  $z$  or in space at a fixed  $t$ , one may determine  $\partial\theta/\partial z$  and  $\partial\theta/\partial t$ .

#### Solution for domain $D_1$

This domain is bounded by  $0 \leq t \leq T$ ,  $z(t, T)$ , and  $z = s(t)$ . Solution of Eq. (12) is

$$\theta(t, \theta) = g(\sigma) - (t - \sigma)e. \quad (14)$$

Substitution of Eq. (14) in Eq. (13), and then integration yields

$$z(t, \sigma) = \int_0^t M(g(\sigma) - (t - \sigma)e) dt. \quad (15)$$

With the use of Eq. (4),

$$M(\theta) = \frac{K_s a}{(\theta_s - \theta_0)} \left( \frac{\theta - \theta_0}{\theta_s - \theta_0} \right)^{a-1}. \quad (16)$$

Substitution of Eq. (14) in Eq. (16) yields

$$M(\theta, \sigma) = \frac{a K_s}{(\theta_s - \theta_0)} \left[ \frac{g(\sigma) - (t - \sigma)e - \theta_0}{\theta_s - \theta_0} \right]^{a-1}. \quad (17)$$

With the use of Eq. (17), Eq. (15) leads to

$$z(t, \sigma) = \frac{K_s}{e} \left\{ \left[ \frac{g(\sigma) - \theta_0}{\theta_s - \theta_0} \right]^a - \left[ \frac{g(\sigma) - (t - \sigma)e - \theta_0}{\theta_s - \theta_0} \right]^a \right\}. \quad (18)$$

Equations (14) and (18) constitute the characteristic solution for domain  $D_1$ . By eliminating  $\sigma$  between these equations,  $\theta$  can be expressed as a function of  $z$  and  $t$ . To do that,  $z(t, \sigma)$  must be, for fixed  $t$ , either an increasing function of  $\sigma$  or a decreasing function of  $\sigma$ . Differentiating Eq. (18) with respect to  $\sigma$  yields

$$\begin{aligned} z_\sigma(t, \sigma) = \frac{\partial z(t, \sigma)}{\partial \sigma} &= \frac{a K_s}{e(\theta_s - \theta_0)} \left\{ g'(\sigma) \left[ \frac{g(\sigma) - \theta_0}{\theta_s - \theta_0} \right]^{a-1} \right. \\ &\quad \left. - \left[ \left( \frac{g(\sigma) - \theta_0}{\theta_s - \theta_0} \right)^a - \frac{ez}{K_s} \right]^{(a-1)/a} \right\} \\ &\quad - e \left[ \left( \frac{g(\sigma) - \theta_0}{\theta_s - \theta_0} \right)^a - \frac{ez}{K_s} \right]^{(a-1)/a} \end{aligned} \quad (19)$$

or

$$\begin{aligned} z_\sigma(t, \sigma) &= \frac{a K_s}{(\theta_s - \theta_0)^a} \{ g'(\sigma) [(g(\sigma) - \theta_0)^{a-1} - (\theta(t, \sigma) - \theta_0)^{a-1}] \\ &\quad - e(\theta(t, \sigma) - \theta_0)^{a-1} \}. \end{aligned} \quad (20)$$

It is seen from Eq. (20) or (19) that  $g'(\sigma) = dg/d\sigma \leq 0$  is a sufficient condition for  $z_\sigma(t, \sigma) < 0$ . The condition

$g'(\sigma) \leq 0$  includes the case of principal interest to us, namely,  $g(\sigma) = \text{constant}$ .

**Case 1.**  $g(t) = \text{constant}$ : If  $g(\sigma) = \theta_u$ , then Eq. (18) becomes

$$z(t, \sigma) = \frac{K_s}{e} \left\{ \left[ \frac{\theta_u - \theta_0}{\theta_s - \theta_0} \right]^a - \left[ \frac{\theta_u - (t - \sigma)e - \theta_0}{\theta_s - \theta_0} \right]^a \right\}. \quad (21)$$

By coupling Eqs. (41) and (21),  $\theta$  can be expressed as a function of  $z$  and  $t$  as

$$\theta(z) = \theta_0 + (\theta_s - \theta_0) \left\{ \left[ \frac{\theta_u - \theta_0}{\theta_s - \theta_0} \right]^a - \frac{ez}{K_s} \right\}^{1/a}. \quad (22a)$$

It is seen that in domain  $D_1$ ,  $\theta$  is a function of  $z$  and does not depend on  $t$ . The soil moisture profile is nonuniform but steady-state. In Eq. (22a), there are two terms within braces. The second term is due to water uptake and the first term is due to the boundary flux. If  $e = 0$ , then  $\theta(z) = \theta_u$ . The nonuniformity of soil moisture is a direct consequence of the plant-root extraction. If  $e$  were zero, then  $\theta$  would be independent of  $z$ . Thus, the alteration of the soil moisture profile is caused by plant roots. Of course, the degree of alteration depends on the value of  $e$ . On a short-time scale, the value of  $e$  is relatively small in field. Equation (22a) can be written with use of Eq. (4) as

$$\theta(z) = \theta_0 + (\theta_s - \theta_0) \left( \frac{K(\theta_u)}{K_s} \right)^{1/a} \left\{ 1 - \frac{ez}{K(\theta_u)} \right\}^{1/a}. \quad (22b)$$

In many practical cases,  $ez/K(\theta_u)$  is much less than 1, and attenuation of the  $\theta$ -profile, as a result, will be small. When Eq. (22a) is inserted into Eq. (4), the soil-moisture flux, with the aid of Eq. (3), is obtained:

$$K(\theta) = q(z) = K_s \left\{ \left[ \frac{\theta_u - \theta_0}{\theta_s - \theta_0} \right]^a - \frac{ez}{K_s} \right\}. \quad (23)$$

Similarly, the average velocity of the soil-moisture movement is obtained by substituting Eq. (22) in Eq. (5),

$$u(z) = \frac{K_s \left\{ \left[ \frac{\theta_u - \theta_0}{\theta_s - \theta_0} \right]^a - \frac{ez}{K_s} \right\}}{\theta_0 + (\theta_s - \theta_0) \left\{ \left[ \frac{\theta_u - \theta_0}{\theta_s - \theta_0} \right]^a - \frac{ez}{K_s} \right\}^{1/a}}. \quad (24)$$

Similarly, substitution of Eq. (22) in Eq. (16) yields the mobility of water:

$$M(\theta) = \frac{a K_s}{(\theta_s - \theta_0)} \left\{ \left[ \frac{\theta_u - \theta_0}{\theta_s - \theta_0} \right]^a - \frac{ez}{K_s} \right\}^{(a-1)/a}. \quad (25)$$

The behavior of the soil moisture in this case can be fully described. From Eq. (22) at a fixed  $z$ ,  $z \geq 0$ ,

$$\frac{\partial \theta}{\partial t} = 0 \quad (26)$$

and at any  $t$ ,  $0 \leq t < T$ ,

$$\frac{\partial \theta}{\partial z} = - \frac{e}{a K_s} (\theta_s - \theta_0) \left\{ \left[ \frac{\theta_u - \theta_0}{\theta_s - \theta_0} \right]^a - \frac{ez}{K_s} \right\}^{(1-a)/a}. \quad (27)$$

Equation (27) shows that at any depth within  $D_1$ ,  $\theta$  remains constant in time and at any time it decreases with increasing  $z$  from the ground surface. The gradient of  $\theta$  increases with increasing  $z$ . This corresponds to the case of a wetting event.

*Case 2.  $dg(t)/dt < 0$ :* In this case,  $\partial\theta/\partial z$  and  $\partial\theta/\partial t$  are obtained from Eqs. (14) and (18) by noting that

$$\frac{\partial\theta}{\partial z} = \frac{\partial\theta/\partial\sigma}{\partial z/\partial\sigma}, \quad \frac{\partial\theta}{\partial t} = \frac{\partial\theta/\partial\sigma}{\partial t/\partial\sigma} \quad (28)$$

To that end, with  $g' = g'(\sigma) = \partial g(\sigma)/\partial\sigma$ ,

$$\frac{\partial\theta}{\partial\sigma} = g' + e, \quad (29)$$

$$\frac{\partial z}{\partial\sigma} = \frac{K_s}{e} \frac{a}{(\theta_s - \theta_0)} \left\{ \left[ \frac{g - \theta_0}{\theta_s - \theta_0} \right]^{a-1} g' - \left[ \left( \frac{g - \theta_0}{\theta_s - \theta_0} \right)^a - \frac{ez}{K_s} \right]^{(a-1)/a} (g' + e) \right\}, \quad (30)$$

$$\frac{\partial t}{\partial\sigma} = 1 + \frac{g'}{e} \left\{ 1 - \left[ \frac{g - \theta_0}{\theta_s - \theta_0} \right]^{a-1} \left[ \left( \frac{g - \theta_0}{\theta_s - \theta_0} \right)^a - \frac{ez}{K_s} \right]^{(1-a)/a} \right\}. \quad (31)$$

Therefore, by dividing Eq. (29) by Eq. (30),

$$\frac{\partial\theta}{\partial z} = \frac{e(g' + e)(\theta_s - \theta_0)}{a K_s \left\{ \left[ \frac{g - \theta_0}{\theta_s - \theta_0} \right]^{a-1} g' - (g' + e) \left[ \left( \frac{g - \theta_0}{\theta_s - \theta_0} \right)^a - \frac{ez}{K_s} \right]^{(a-1)/a} \right\}} \quad (32)$$

It should be noted that in this characteristic method of solution,  $t$  was chosen as the parameter along characteristics. Therefore, in Eq. (18),  $z$  is the dependent variable, and  $\sigma$  is the independent variable. In order to obtain  $\partial\theta/\partial t$ , one can choose  $t$  as the dependent variable and  $z$  as the parameter along characteristics. The procedure, however, remains the same in both cases. Employment of  $t$  as the dependent variable results in

$$\frac{\partial\theta}{\partial\sigma} = g'(g - \theta_0)^{a-1} [(g - \theta_0)^a - \frac{ez}{K_s} (\theta_s - \theta_0)^a]^{(1-a)/a} \quad (32a)$$

and

$$\frac{\partial t}{\partial\sigma} = 1 - \frac{g'}{e} (g - \theta_0)^{a-1} [(g - \theta_0)^a - \frac{ez}{K_s} (\theta_s - \theta_0)^a]^{(1-a)/a}. \quad (32b)$$

By dividing Eq. (32a) by Eq. (32b),

$$\frac{\partial\theta}{\partial t} = \frac{e g' (g - \theta_0)^{a-1} [(g - \theta_0)^a - \frac{ez}{K_s} (\theta_s - \theta_0)^a]^{(1-a)/a}}{e - g' (g - \theta_0)^{a-1} [(g - \theta_0)^a - \frac{ez}{K_s} (\theta_s - \theta_0)^a]^{(1-a)/a}}. \quad (33)$$

The variation of  $\theta$  with  $z$  for a fixed  $t$  can be analyzed from Eq. (32). If  $e < g'(\sigma)$  then  $\partial\theta/\partial z > 0$ ; that means that  $\theta$  increases with increasing  $z$ . On the other hand, if  $e = g'(\sigma)$ , then  $\theta$  is independent of  $z$ . This is also the case when  $z \geq K_s/e \{ (g - \theta_0)^a - (\theta_s - \theta_0)^a \}^{1/a}$ . If  $e > g'(\sigma)$  then  $\theta$  decreases with  $z$  but can also have a complex variation. At a fixed  $z$ , the variation of  $\sigma$  can be analyzed with the aid

of Eq. (33). If  $g'(\sigma) = 0$ , then  $\theta$  is independent of  $t$ . If  $g'(\sigma) < 0$ , then  $\theta$  decreases with time. If  $e = g'(\sigma)$ , then  $\theta$  is a decreasing function. At  $z = K_s \{ (g - \theta_0)^a - (\theta_s - \theta_0)^a \}^{1/a} / e$ , then

$$\frac{\partial\theta}{\partial t} = 0 \quad \text{and} \quad (34)$$

$$\frac{\partial\theta}{\partial z} = \frac{e(g' + e)(\theta_s - \theta_0)^a}{a K_s g' (g - \theta_0)^{a-1}}. \quad (35)$$

Equation (34) shows that  $\theta$  becomes independent of  $t$  whereas Eq. (35) shows that as a function of  $z$ ,  $\theta$  decreases with  $z$ .

*Case 3.  $dg(t)/dt > 0$ :* This can be analyzed from Eqs. (32) to (35). However, Eq. (20) reveals that when  $g'(\sigma) > 0$ ,  $z_s(t, \sigma) > 0$  and this case may entail shock formation. In that case, the analytical treatment becomes unwieldy and is not discussed in this paper.

#### Determination of advance front (free boundary of domain $D_1$ )

In order to determine the shock front  $t = w(z)$ , it is convenient to express it in terms of the parameter  $\sigma$  introduced above. If one considers the characteristic curve  $z(t, \sigma)$  in the  $(z, t)$  plane, then it will intersect the free boundary at the point denoted by  $(\xi(\sigma), \eta(\sigma))$  as shown in Fig. 1. Therefore,  $z = \xi(\sigma)$ ,  $t = \eta(\sigma)$  is the parametric representation of the free boundary in terms of the parameter  $\sigma$ . For the case  $g(t) = \theta_s = \text{constant}$ , and  $e(\tau) = e = \text{constant}$ , determination of the free boundary is relatively simple. From Eq. (22), with  $t$  replaced by  $\eta(\sigma)$ ,

$$z(\eta(\sigma), \sigma) = \xi(\sigma) \quad (36)$$

$$= \frac{K_s}{e} \left[ \left( \frac{\theta_s - \theta_0}{\theta_s - \theta_0} \right)^a - \left( \frac{\theta_s - (\eta(\sigma) - \sigma)e - \theta_0}{\theta_s - \theta_0} \right)^a \right].$$

From Eqs. (6), (14) and (4), and noting that  $\theta$  does not fall below  $\theta_0$ ,

$$\frac{ds(t)}{dt} = \frac{\xi'(\sigma)}{\eta'(\sigma)} = \frac{K(\theta(\xi(\sigma), \eta(\sigma)))}{\theta(\xi(\sigma), \eta(\sigma))}$$

$$= \frac{K_s}{(\theta_s - \theta_0)} \left[ \frac{\theta_s - (\eta(\sigma) - \sigma)e - \theta_0}{\theta_s - \theta_0} \right]^{a-1}. \quad (37)$$

Equations (36) and (37) can be solved for  $\xi(\sigma)$  and  $\eta(\sigma)$ . To that end, Eq. (36) can be differentiated to yield

$$\xi'(\sigma) = \frac{a K_s}{(\theta_s - \theta_0)} \left[ \frac{\theta_s - (\eta(\sigma) - \sigma)e - \theta_0}{\theta_s - \theta_0} \right]^{a-1} (\eta'(\sigma) - 1). \quad (38)$$

On eliminating  $\xi'(\sigma)$  between Eqs. (24) and (25),

$$\eta'(\sigma) = \frac{a}{a-1}, \quad \eta(0) = 0 \quad (39)$$

which gives

$$\eta(\sigma) = \frac{a}{a-1} \sigma. \quad (40)$$

Similarly, eliminating  $\eta'(\sigma)$  between Eqs. (37) and (38) leads to

$$\xi'(\sigma) = \frac{K_s}{(\theta_s - \theta_0)} \frac{a}{(a-1)} \left[ \left( \frac{\theta_u - \theta_0}{\theta_s - \theta_0} \right)^a - \frac{\xi e}{K_s} \right]^{(a-1)/a} \quad (41)$$

which gives

$$\xi(\sigma) = \frac{K_s}{e} \left\{ \left( \frac{\theta_u - \theta_0}{\theta_s - \theta_0} \right)^a - \left[ \left( \frac{\theta_u - \theta_0}{\theta_s - \theta_0} \right) - \frac{e\sigma}{(\theta_s - \theta_0)(a-1)} \right]^a \right\}. \quad (42)$$

Equations (40) and (42) constitute the parametric representation of the free boundary. By eliminating  $\sigma$  between Eqs. (46) and (42), and noting that  $\xi$  corresponds to  $z$  and  $\eta$  to  $t$ . In terms of  $q$ ,

$$z = \frac{K_s}{e} \left\{ \left( \frac{\theta_u - \theta_0}{\theta_s - \theta_0} \right)^a - \left[ \left( \frac{\theta_u - \theta_0}{\theta_s - \theta_0} \right) - \frac{et}{a(\theta_s - \theta_0)} \right]^a \right\}, \quad (43)$$

$$z = \frac{q_0}{e} - \frac{K_s}{e} \left[ \left( \frac{q_0}{K_s} \right)^{1/a} - \frac{et}{a(\theta_s - \theta_0)} \right]^a \quad (44)$$

where  $q_0 = q(\theta_u)$ . Equation (43) or (44) expresses the advance front. It is seen from Eq. (43) that the coordinates of the point to which the free boundary can extend is given by

$$t = \frac{a}{e} (\theta_u - \theta_0), \quad z = \frac{K_s}{e} \left( \frac{\theta_u - \theta_0}{\theta_s - \theta_0} \right)^a. \quad (45)$$

To complete the solution for domain  $D_1$ , the intersection of the bounding characteristic  $z(t, T)$  and the free boundary  $z = s(t)$  is to be determined. Let that point be  $P = (z_*, t_*)$ . This point can be determined explicitly by equating Eq. (21) with  $\sigma = T$ ,  $t = t_*$  and  $z = z_*$  to Eq. (43) with  $z = z_*$  and  $t = t_*$ ; that results in

$$t_* = \frac{a}{a-1} T. \quad (46)$$

$$z_* = \frac{K_s}{e} \left\{ \left( \frac{\theta_u - \theta_0}{\theta_s - \theta_0} \right)^a - \left[ \left( \frac{\theta_u - \theta_0}{\theta_s - \theta_0} \right) - \frac{eT}{(a-1)(\theta_s - \theta_0)} \right]^a \right\}. \quad (47)$$

For the case when  $g(t)$  is not constant, we use the same parametric representation as before. Therefore, analogous to Eq. (36),

$$\xi(\sigma) = \frac{K_s}{e(\theta_s - \theta_0)^a} \{ [g(\sigma) - \theta_0]^a - [g(\sigma) - (\eta(\sigma) - \sigma)e - \theta_0]^a \} \quad (48)$$

and analogous to Eq. (37),

$$\frac{\xi'(\sigma)}{\eta'(\sigma)} = \frac{K_s}{(\theta_s - \theta_0)^a} [g(\sigma) - (\eta(\sigma) - \sigma)e - \theta_0]^{a-1}. \quad (49)$$

Differentiating Eq. (48) and then substituting the differential in Eq. (49) yield

$$\begin{aligned} \frac{d\eta}{d\sigma} + \frac{a}{e(a-1)} \frac{g'(\sigma)[g(\sigma) - \theta_0]^{a-1}}{[g(\sigma) - (\eta(\sigma) - \sigma)e - \theta_0]^{a-1}} \\ = \frac{a}{e(a-1)} (g'(\sigma) + e), \quad \eta(0) = 0. \end{aligned} \quad (50)$$

Equation (50) cannot, in general, be solved in terms of simple forms of  $g(t)$ , an analytical solution for  $\eta(\sigma)$  is tractable. With substitution of this solution in Eq. (48),  $\xi(\sigma)$  is obtained. If, however,  $g'(\sigma) = 0$ , Eq. (50) reduces to Eq. (39).

#### Another method to determine the advance front

The velocity of the front can be expressed as

$$\frac{ds(t)}{dt} = u(s(t), t) = \frac{q(\theta_2) - q(\theta_1)}{\theta_2 - \theta_1}. \quad (51)$$

Representing  $\theta_1$  by  $\theta_0$  and  $\theta_2$  by  $\theta$ , and taking advantage of Eqs. (22) and (23), Eq. (46) can be written for the case  $g(t) = \text{constant}$ , as

$$\frac{ds(t)}{dt} = \frac{K_s^{1/a}}{\theta_s - \theta_0} (q - ez)^{(a-1)/a} \quad (52)$$

which, when integrated, leads to

$$z = s(t) = \frac{q}{e} - \frac{K_s}{e} \left[ \left( \frac{q}{K_s} \right)^{1/a} - \frac{te}{a(\theta_s - \theta_0)} \right]^a \quad (53)$$

which is the same as Eq. (44).

#### Solution for domain $D_2$

Domain  $D_2$  is bounded by  $T \leq t$ ,  $z = z(t, T)$ ,  $z = s(t)$  beyond the point  $p = (z_*, t_*)$ . In this case,  $\theta(0, t) = \theta_0$  for  $t \geq T$ ;  $\theta_0 < \theta_u$ . Let  $g(t, \varepsilon)$  be a continuous function of  $t$  coinciding with  $g(t)$  on  $0 \leq t < T$ ,  $g(t, \varepsilon) = \theta_0$  on  $t \geq T + \varepsilon$ , as shown in Fig. 2. Then, it is seen from Eqs. (14) and (18) that the characteristics  $z = z(t, \sigma, \varepsilon)$ ,  $T \leq \sigma \leq T + \varepsilon$ , cover the region above  $z = z(t, T)$  completely.

$$\begin{aligned} z(t, \sigma, \varepsilon) = \frac{K_s}{e} \left\{ \left[ \frac{\theta(t, \sigma, \varepsilon) + (t - \sigma)e - \theta_0}{\theta_s - \theta_0} \right]^a - \left[ \frac{\theta(t, \sigma, \varepsilon) - \theta_0}{\theta_s - \theta_0} \right]^a \right\}. \end{aligned} \quad (54a)$$

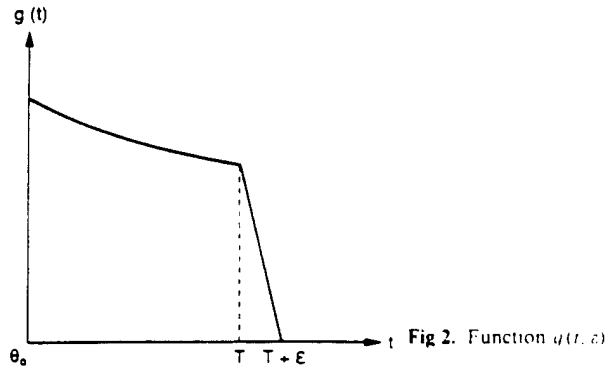


Fig. 2. Function  $g(t, \varepsilon)$

By letting  $\varepsilon \rightarrow 0$  and  $\sigma \rightarrow T$ , one obtains

$$z(\theta, t) = \frac{K_s}{e} \left[ \left( \frac{\theta + e(t - T) - \theta_0}{\theta_s - \theta_0} \right)^a - \left( \frac{\theta - \theta_0}{\theta_s - \theta_0} \right)^a \right]. \quad (54b)$$

This equation expresses the soil-moisture  $\theta$  as a function of  $z$  and  $t$  in domain  $D_2$ ;  $\theta$  varies from  $\theta_u$  to  $\theta_0$ . The reduction in  $\theta$  is caused by the plant-root extraction, and hence the water uptake is the dominant factor for variation of water content. This can be easily shown for a special case when  $a$  is an integer. To that end, Eq. (54b) can be written as

$$z(\theta, t) = \frac{K_s}{e} \left( \frac{\theta - \theta_0}{\theta_s - \theta_0} \right)^a \left\{ \left[ \frac{e(t - T)}{\theta - \theta_0} + 1 \right]^a - 1 \right\}. \quad (55a)$$

With use of the binomial theorem, this can be written as

$$z(\theta, t) = \frac{K_s}{e} \left( \frac{\theta - \theta_0}{\theta_s - \theta_0} \right)^a \left\{ \sum_{i=0}^{a-1} \binom{a}{i} \left( \frac{e(t - T)}{\theta - \theta_0} \right)^{a-i} \right\} \quad (55b)$$

$$= K_s \left( \frac{\theta - \theta_0}{\theta_s - \theta_0} \right)^a \left\{ \sum_{i=0}^{a-1} \binom{a}{i} (e)^{a-i-1} \left( \frac{t - T}{\theta - \theta_0} \right)^{a-i} \right\}.$$

It is seen that each term in the series is affected by the plant-root extraction  $e$  raised to the power  $(a-i-1)$ . Assume that only the first term of the series is most significant. Then,

$$z(\theta, t) = K_s \left( \frac{\theta - \theta_0}{\theta_s - \theta_0} \right)^a a e^{a-1} \left( \frac{t - T}{\theta - \theta_0} \right)^a. \quad (55c)$$

Thus the reduction in  $\theta$  is primarily caused by water uptake.

The characteristics in domain  $D_2$  are given by

$$z = \frac{K_s}{e} \left[ \left( \frac{\theta_i - \theta_0}{\theta_s - \theta_0} \right)^a - \left( \frac{\theta_i - e(t - T) - \theta_0}{\theta_s - \theta_0} \right)^a \right] \quad (56)$$

where  $\theta_i$  is the initial soil-moisture  $\theta_0 < \theta_i < \theta_u$ , that is carried out by the  $i$ -th characteristic.

#### Determination of free boundaries for domain $D_2$

Domain  $D_2$  has two free boundaries FB2 and FB3 as shown in Fig. 3. Along FB3 that starts at  $t = T$  and  $x = 0$ ,  $\theta(z, t) = \theta_0$ ; thus, this is the locus defined by  $\theta_0$ . This is the time history of the drying front as it advances from  $x = 0$ . From Eq. (14), we have

$$\theta_0 = g(\sigma) - (t - \sigma)e, \quad T \leq \sigma \leq T + \varepsilon. \quad (57)$$

Thus, from Eq. (18), we obtain

$$z(t, \sigma, \varepsilon) = \frac{K_s}{e} \left[ \frac{(t - \sigma)e}{\theta_s - \theta_0} \right]^a. \quad (58)$$

Letting  $\varepsilon \rightarrow 0$ ,  $\sigma \rightarrow T$ , we get the free boundary FB3

$$z(t) = \frac{K_s}{e} \left[ \frac{e(t - T)}{\theta_s - \theta_0} \right]^a. \quad (59)$$

Between  $z = 0$  and Eq. (59),  $\theta(z, t) = \theta_0$ .

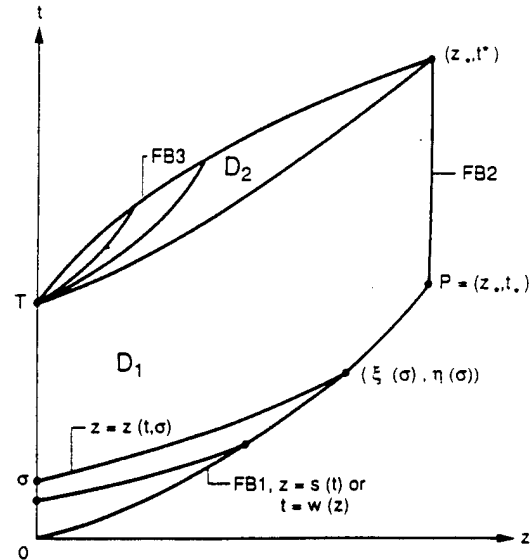


Fig. 3. Characteristic solution domain for the case  $g'(t) = 0$ ,  $0 \leq t \leq T$

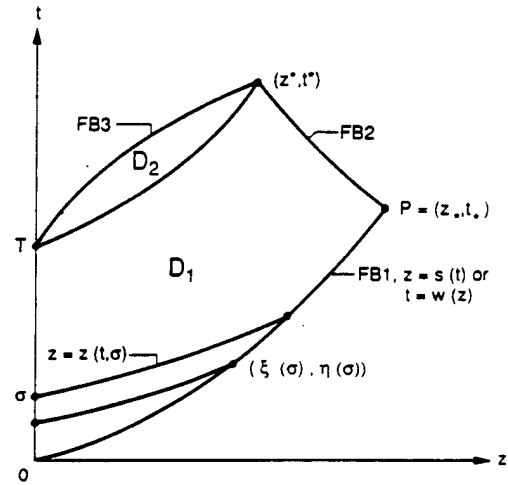


Fig. 4. Characteristic solution domain for the case when  $e = \text{constant} > 0$ ,  $-e < g'(t) < 0$ ,  $0 \leq t \leq T$

It is seen from Eq. (56) that the maximum distance that the characteristics will travel is given by

$$z^* = \frac{K_s}{e} \left( \frac{\theta_u - \theta_0}{\theta_s - \theta_0} \right)^a \quad (60)$$

which is the same as given by Eq. (45). This shows that FB2 (the locus  $\theta(z, t) = \theta_0$ ) is a vertical wall with lower end given by Eq. (45) and the upper end by Eq. (56) and

$$t^* = T + \frac{1}{e} (\theta_u - \theta_0). \quad (61)$$

In the case when  $g(t)$  is not constant, we get the parametric representation of FB2:

$$z_{\text{FB2}} = \frac{K_s}{e} \left[ \frac{g(\sigma) - \theta_0}{\theta_s - \theta_0} \right]^a. \quad (62)$$

DRAINAGE PERIOD = 6 H,  $e = 0.2/\text{DAY}$   
 BROOK AND COREY RELATION  
 FIXED DEPTH = 10, 20, 30 CM

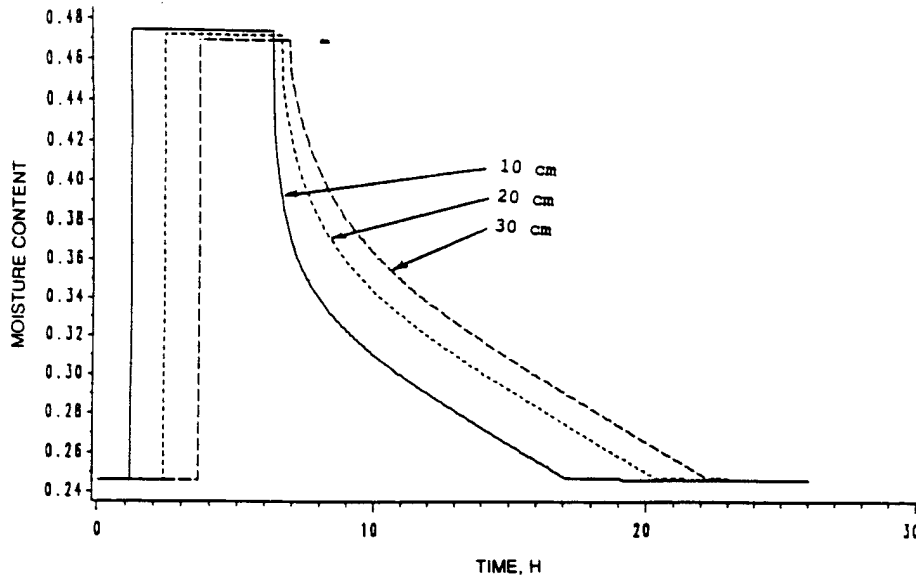


Fig. 5. Moisture content as a function of time for fixed values of depth

DRAINAGE PERIOD = 6 H,  $e = 0.2/\text{DAY}$   
 BROOK AND COREY RELATION  
 FIXED TIME = 2, 7, 10 H

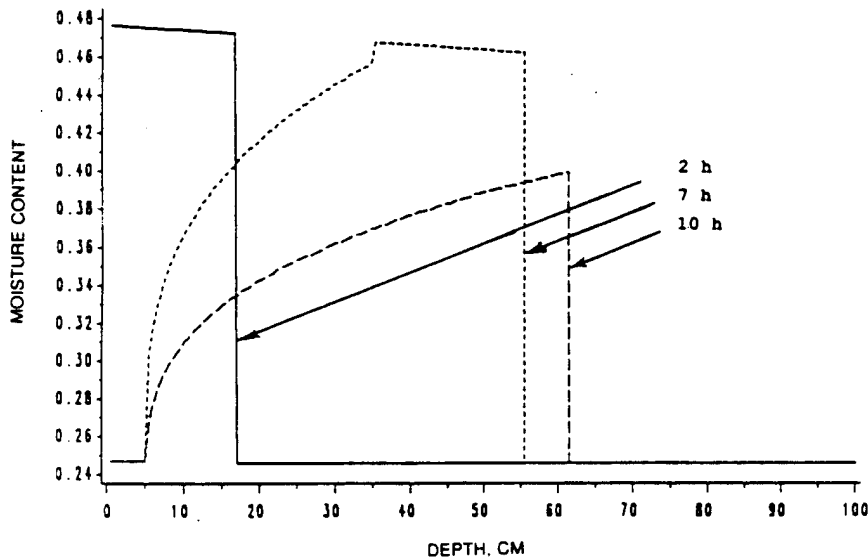


Fig. 6. Moisture content as a function of depth for fixed values of time

$$t_{FB2} = \sigma + \frac{g(\sigma) - \theta_0}{e} \quad (63)$$

Thus

$$\frac{dz}{dt} = \frac{z'(\sigma)}{t'(\sigma)} = \frac{aK_s g'(\sigma) (g(\sigma) - \theta_0)^a}{(\theta_s - \theta_0)^a (e + g'(\sigma))} \quad (64)$$

Since  $g'(\sigma) \leq 0$ , we have for FB2,  $-e \leq g'(\sigma) \leq 0 \rightarrow dz/dt \leq 0$ , and  $g'(\sigma) < -e \rightarrow dz/dt > 0$ . Under the condition  $-e < g'(\sigma) < 0$ ,  $0 < \sigma < T$ , the front wall of water recedes ( $dz/dt < 0$ ) when its moisture content is  $\theta_0$ . In this case, the appearance of FB2 is as shown in Fig. 4. If  $g'(\sigma) = 0$ ,  $0 \leq \sigma \leq T$ , the front wall of water is stationary ( $dz/dt = 0$ ), as shown in Fig. 3, when it has moisture content  $\theta_0$ .

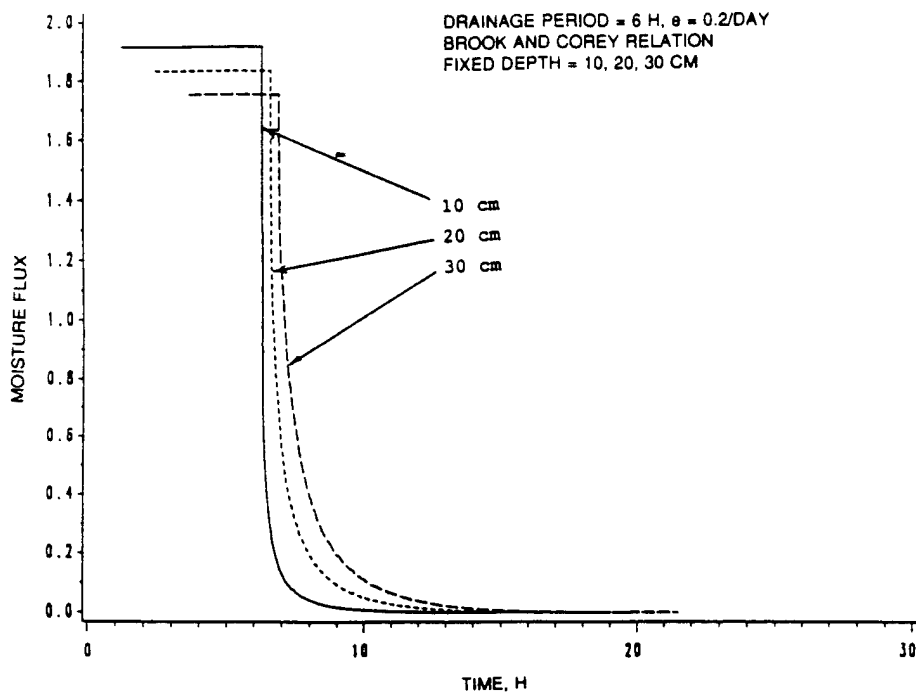


Fig. 7. Moisture flux as a function of time for fixed values of depth

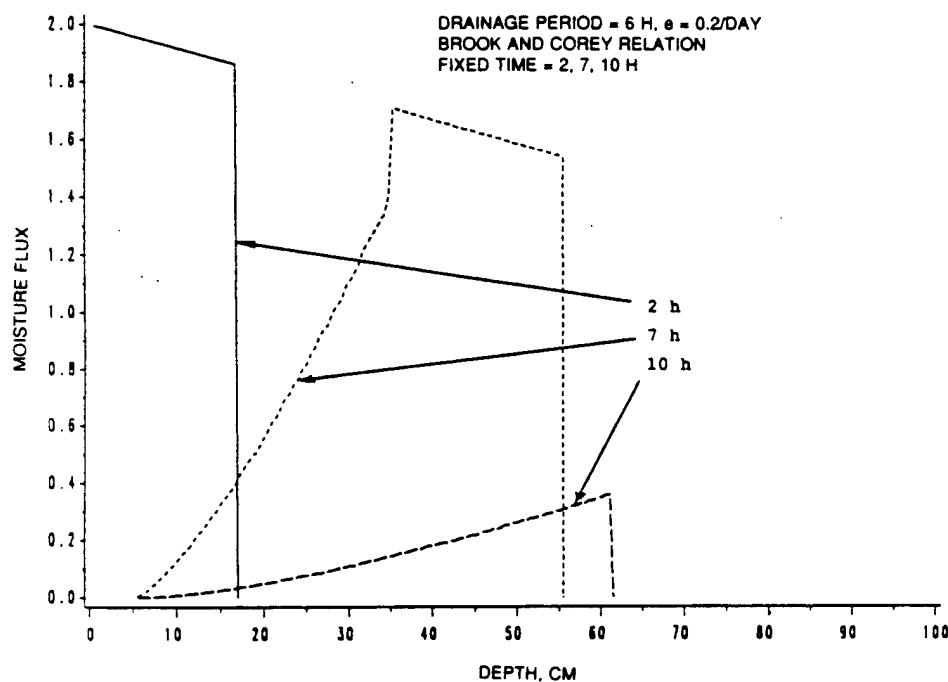


Fig. 8. Moisture flux as a function of depth for fixed values of time

#### Total moisture content

The total moisture content  $W$  varies within the region, and can be determined by integrating the moisture profile from  $z = 0$  to a particular depth  $z = L$ . Let  $L < z^*$ . Referring to Fig. 1, at  $t = 0$ , the initial total moisture content  $W_i = \theta_0 L$ . For  $0 < t < T$ , say,  $t = t_1$ , when  $g(t) = \text{constant}$ ,

$$W = \theta_1 z_1 + \theta_0 (L - z_1) \quad (65)$$

where  $z_1$  is the point of intersection of  $t = t_1$  and  $z = s(t)$ . For  $t > t^*$ ,

$$W(t, L) = \int_0^L \theta(z, t) dz \quad (66)$$

where  $\theta(z, t)$  is prescribed by Eq. (55). An explicit solution of this integral is, however, not tractable.

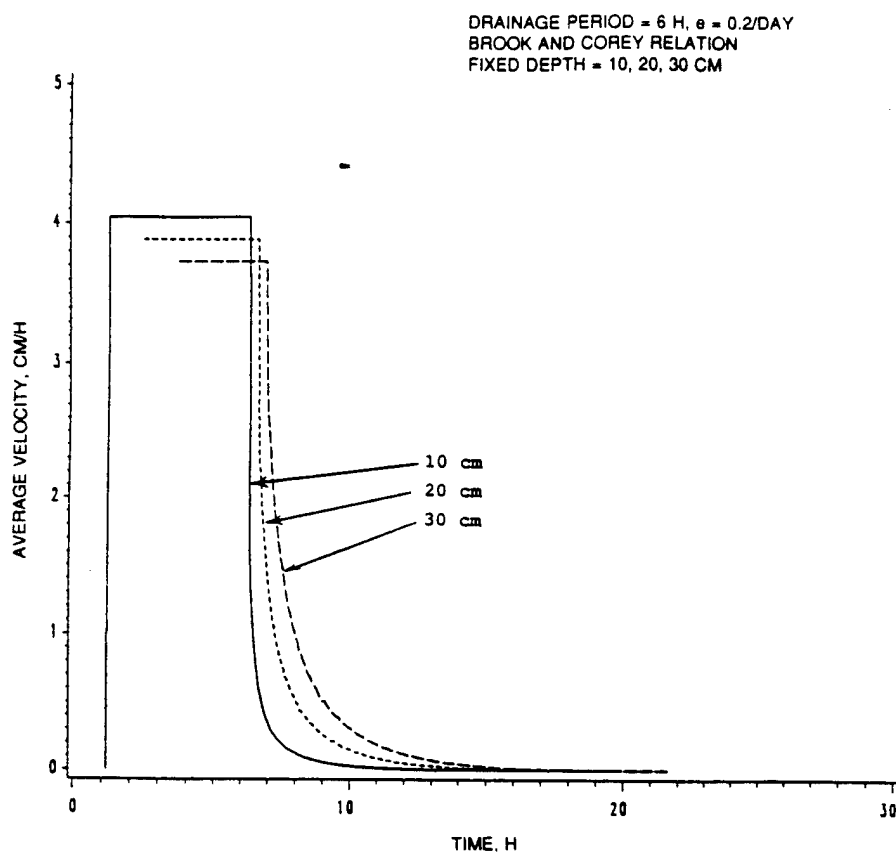


Fig. 9. Average velocity as a function of time for fixed values of depth

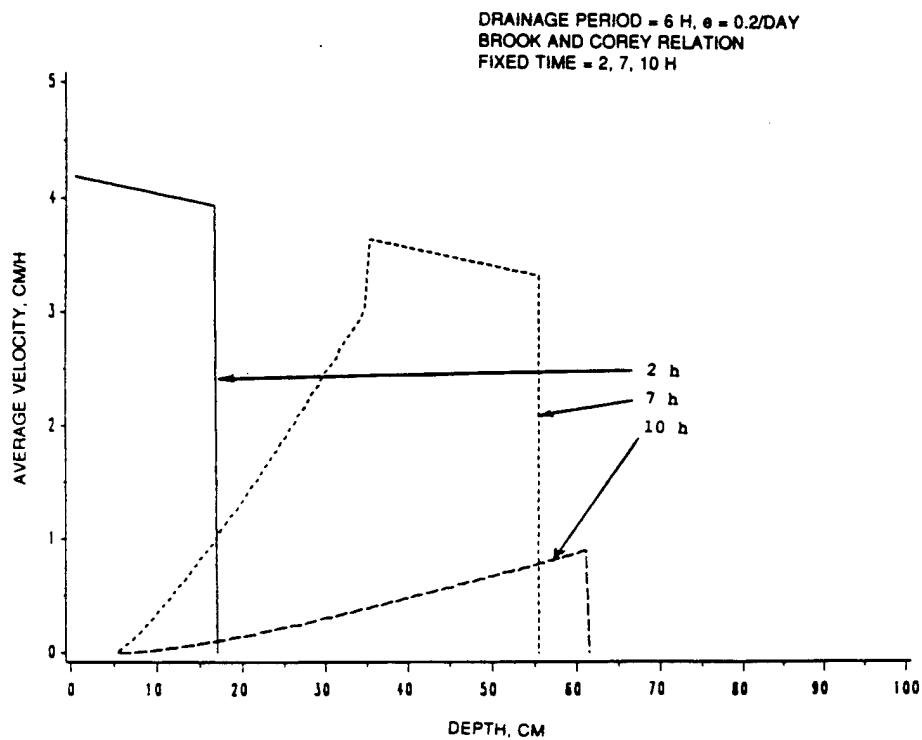


Fig. 10. Average velocity as a function of depth for fixed values of time

### An example of application

A wetting event with moisture applied at the ground surface was considered, with  $K(\theta)$  given by Eq. (4). The soil was Glendale clay loam, investigated by Sisson et al. (1980), with the following properties:  $\theta_s = 0.52$ ,  $\theta_0 = 0.246$ ,  $K_s = 1$  m/day, and  $a = 4.25$ . The moisture was applied at the rate of 2 cm/h for 6 hours. These values were used by Charbeneau (1984). The plant-root extraction  $e(t)$  was considered constant but values of  $e = 0.1, 0.2, 0.3, 0.4$ , and  $0.5$ /day were considered. It should be emphasized that these values were used to illustrate the procedure presented in the paper. If  $n = 0.52$ , then  $e = 0.1$ /day would correspond to  $r(t) = 0.052$ /day. For one meter of soil column, this would translate into 5.2 mm of plant-root extraction for a day. Likewise,  $e = 0.5$ /day would yield  $r(t) = 0.25$ /day or 25 mm/day. This rate is clearly high but the objective here was to intentionally show the modulation of soil moisture profile by the plant-root extraction.

The kinematic wave model was applied to compute  $\theta(z, t)$ ,  $q(z, t)$ , and  $u(z, t)$ . Then  $\theta(t)$ ,  $u(t)$  and  $q(t)$  were obtained at selected values of  $z$ . Likewise,  $\theta(z)$  and  $q(z)$  were computed at selected values of  $t$ . For a sample case of  $e = 0.2$ /day, computations are illustrated. Figure 5 shows  $\theta(t)$  at  $z = 10, 20$ , and  $30$  cm, and Fig. 6 shows  $\theta(z)$  at  $t = 2, 7$  and  $10$  h. The moisture profile has realistic appearance. The moisture flux is plotted as a function of  $t$  in Fig. 7, and as a function of  $z$  in Fig. 8. The average velocity is plotted as a function of  $t$  in Fig. 9, and as function of  $z$  in Fig. 10. Both  $q$  and  $u$  appear to be realistic in their variation. The effect of increasing  $e$  was to compress domain  $D_2$ . In other words, after the moisture flux was ended at the ground surface, the moisture profile returned to its initial state more quickly where the moisture extraction rate was higher. For higher  $e$ , the characteristics in domain  $D_1$  were more curved.

### Conclusions

The kinematic wave model for soil moisture movement has been formulated, and its solution domain involves three free boundaries. Analytical solutions are tractable for the case when the upstream boundary condition is independent of time. For a time-dependent boundary

condition, numerical solutions are the only resort. In this model, the advancing front of water or wetting front is necessarily an advancing shock wave. It is plausible to assume that the moisture content at the wetting front is  $\theta_0$ . Since the kinematic wave theory cannot account for this assumption, the diffusion wave model has to be employed in that case.

*Acknowledgements.* This study was supported in part by Army Research Office under the project "A Continuum Model for Stream-flow Synthesis". Grant No. DAALO3-89-G-0116.

### References

- Brooks RH, Corey AT (1964) Hydraulic properties of porous media. Hydrology Paper 3, Colorado State University, Fort Collins, Colorado
- Charbeneau RJ (1984) Kinematic models for soil moisture and solute transport. Water Resour Res 20:699-706
- Charbeneau RJ, Weaver JW, Smith VA (1989) Kinematic modeling of multiphase solute transport in the vadose zone. EPA Report EPA/600/2-89/035, RS Kerr Environmental Research Laboratory, U.S. Environmental Protection Agency, Ada, Oklahoma
- Germann P (1985) Kinematic wave approach to infiltration and drainage into and from soil macropores. Trans ASAE 28:745-749
- Germann P, Beven K (1985) Kinematic wave approximation to infiltration into soils with sorbing macropores. Water Resour Res 21:990-996
- Germann PF, Beven K (1986) A distribution function approach to waterflow in soil macropores based on kinematic wave theory. J Hydrol 83:173-183
- Germann PF, Smith MS, Thomas GW (1987) Kinematic wave approximation to the transport of *Escherichia coli* in the vadose zone. Water Resour Res 23:1281-1287
- Hsu R, Liu CL (1990) Use of parameter estimation in determining soil hydraulic properties from unsaturated flow. Water Resour Manag 4:1-19
- Irmay SE (1956) Extension of Darcy law to unsaturated flow through porous media. Proc Darcy Symposium, IASH-IUGG, Dijon, France
- Sisson JB, Ferguson AH, van Genuchten MTh (1980) Simple method for predicting drainage from field plots. Soil Sci Soc Am J 44:1147-1152
- Smith RE (1983) Approximate soil water movement by kinematic characteristics. Soil Sc Am J 47:3-8
- Yamada T, Kobayashi M (1988) Kinematic wave characteristics and new equations of unsaturated infiltration. J Hydrol 102:257-266

## ORIGINAL PAPER

V. P. Singh · V. Aravamuthan · E. S. Joseph

**Errors of kinematic-wave and diffusion-wave approximations for time-independent flows in infiltrating channels**

Received: 1 January 1993

**Abstract** Time-independent (or steady-state) cases of channel flow were treated and errors of the kinematic-wave and diffusion-wave approximations derived for finite flow at the upstream end. The diffusion-wave approximation was found to be in excellent agreement with the dynamic wave representation, with error magnitudes of 0.2% for values of  $KF_0^2 \geq 7.5$ , where  $K$  is the kinematic-wave number and  $F_0$  is the Froude number. Even for small values of  $KF_0^2$  (e.g.,  $KF_0^2 = 0.75$ ), the errors were typically in the range of 1.3 to 3.7%. The approximate analytical diffusion-wave solution performed poorly with error magnitudes greater than 30% even for large values of  $KF_0^2$ . The kinematic-wave approximation was also found to be in good agreement with the dynamic-wave representation with errors of about 1.2% for  $KF_0^2 = 7.5$  and varying from 15 to 44% for  $KF_0^2 = 0.75$ .

In overland flows, the steady state is attained at the outlet for constant rainfall after the depth of flow reaches the equilibrium. The same is true for flow in a channel subject to constant lateral inflow. For a channel receiving a constant inflow of long duration at the upstream boundary, the flow at the downstream end would reach the equilibrium and this frequently occurs in border and furrow irrigation. Despite occurrences of steady state or time-independent flows, they have not received much attention in hydrology (Morris 1978). The steady-state solution aids in understanding the nature of the water-surface profile. It may help determine the condition for use of zero depth in place of zero inflow at the upstream boundary. When the rainfall du-

ration is much greater than the time of equilibrium, the steady-state water surface profiles are very useful.

Mathematical treatment of steady-state flows is based on the shallow water-wave (SWW) theory or its simplifications, including the kinematic-wave (KW) or the diffusion-wave (DW) approximation, in conjunction with appropriate boundary conditions. A comprehensive discussion of steady-state flows using the diffusion-wave (DW) approximation was presented by Govindaraju et al. (1988) including both numerical and analytical results for flux-type boundary conditions. The upstream boundary condition was one of zero inflow. Both the zero depth-gradient and the critical-depth downstream boundary conditions were investigated. For steep slopes, the upstream boundary condition of zero depth was found to be justifiable. It was shown that the critical-depth condition at the downstream boundary was a stringent condition which might give rise to problems for certain ranges of parameter values when seeking a numerical solution. Furthermore, Govindaraju et al. (1988) employed an analytical approximation in the form of a cubic approximation of the DW model for the zero depth-gradient downstream boundary condition. The cubic approximation was found to be accurate when  $F_0^2 K$  was sufficiently small, with  $F_0$  being the Froude number and  $K$  the kinematic wave number.

Parlange et al. (1989) improved the approximation of Govindaraju et al. (1988) by using a Taylor series approximation, and showed that the improved approximation and the earlier approximation would provide the upper and lower bounds of the numerical solution. Most studies dealing with evaluating the adequacy of the kinematic-wave (KW) or diffusion-wave (DW) approximation have dealt with space-time dependent flows. Criteria for judging the adequacy of these approximations have been derived as point values either in terms of  $K$  or  $KF_0^2$  for given flow situations, but they do not relate to errors in time and/or space. Moreover, an explicit treatment of steady-state flows has not been included in these studies.

Pearson (1989) examined the criteria for using the KW approximation to the St. Venant (SV) equations for shallow water flow. For steady-state one-dimensional flow

V. P. Singh (✉) · V. Aravamuthan  
Department of Civil and Environmental Engineering,  
Louisiana State University,  
Baton Rouge, LA 70803-6405, USA

E. S. Joseph  
Department of Civil Engineering, Southern University,  
Baton Rouge, LA 70813, USA

over a plane he showed that for the condition of zero flow at the upstream boundary, the assumed steady-state upstream depth is generally nonzero, but is implicitly assumed to be zero in the kinematic-wave approximation. By plotting contours of dimensionless steady-state upstream depth over a 2-parameter plane ( $F_0, KF_0^2$ ) he obtained a new criterion as  $K > 3 + 5/F_0^2$  for kinematic-wave modeling.

Parlange et al. (1990) were probably the first to undertake an investigation of errors in the KW and DW approximations by comparing their predictions with the numerical solution of the St. Venant (SV) equations under steady state conditions. It was shown that the two approximations could have significant errors even for critical flow and fairly large values of the kinematic wave number. When the KW approximation was inaccurate, the improvement by the DW approximation was only modest. Parlange et al. (1990) then proposed a more accurate approximation when the kinematic wave number was large. They suggested splitting the solution of the SV equations in two regions, one near the downstream end of the plane and the other covering most of the plane.

However, no explicit relations as a function of space between these criteria and the errors resulting from the KW or DW approximation have been derived as yet. Also, these criteria did not include the effect of infiltration although this is vital for surface irrigation. As a result, the actual error of these approximations as a function of space is usually not known. Furthermore, it is not evident in hydrologic modeling if the KW and DW approximations are valid for the entire length of the channel or a portion thereof, or for infiltrating channels.

The objective of this study was to derive, under simplified conditions, these errors as a function of space for the KW and DW approximations for time-independent flows in infiltrating channels.

### Shallow water-wave (SWW) theory for time-independent flows

#### Governing equations

The SWW theory for time-independent flows can be described by the St. Venant (SV) equations. For a time-independent flow in an infiltrating channel of length  $L$ , these equations can be written in one-dimensional form on a unit width basis as:

Continuity equation,

$$\frac{d}{dx}(uh) = -f \quad (1)$$

and momentum equation,

$$\frac{d}{dx}\left(\frac{1}{2}u^2 + gh\right) = g(S_0 - S_f) \quad (2)$$

where  $h$  is depth of flow ( $L$ ),  $u$  is local mean velocity ( $L/T$ ),  $f$  is uniform infiltration rate ( $L/T$ ),  $g$  is accelera-

tion due to gravity ( $L/T^2$ ),  $x$  is space coordinate in the direction of flow ( $L$ ),  $S_0$  is bed slope, and  $S_f$  is frictional slope. Note  $Q = uh$  is discharge ( $L^3/(TL)$ ) per unit width, and Eq. (2) neglects the effect of momentum exchange between longitudinal flow and infiltration. This amounts to assuming that infiltration occurs in the vertical direction only.  $S_f$  can be approximated as

$$S_f = \beta \frac{u^2}{h} \quad (3)$$

where  $\beta (T^2/L)$  is some resistance parameter. If the Chezy relation is used then  $\beta = g/C^2$ , where  $C$  is Chezy's resistance parameter.

Equations (1) and (2) are the governing equations for the dynamic wave (DYW) representation for time-independent flows. The KW approximation is based on Eq. (1) and Eq. (2) with the left side deleted,

$$g(S_0 - S_f) \quad \text{or} \quad S_0 = S_f \quad (4)$$

which can be expressed as Eq. (3). The DW approximation uses Eq. (1) and Eq. (2) with the convective acceleration term deleted,

$$\frac{dh}{dx} = S_0 - S_f \quad (5)$$

It is useful to express the SV equations in dimensionless form. To that end, the following normalizing quantities are defined:  $Q_0$  = discharge per unit width ( $L^2/T$ ) of the channel at the upstream boundary;  $H_0$  = normal depth ( $L$ ) of flow corresponding to  $Q_0$  at the upstream boundary;  $U_0$  = normal velocity ( $L/T$ ) for  $Q_0 (= Q_0/H_0)$ ;  $x_0$  = normalizing distance ( $L$ ) computed as  $Q_0/\bar{f}$ , where  $\bar{f}$  is the average rate of infiltration during the period of irrigation obtained as  $\bar{f} = \int_0^T f(w) dw / T$ ,  $f(t)$  = infiltration rate ( $L/T$ ),  $T$  = duration of irrigation,  $T_0$  = normalizing time ( $T$ ) computed as  $T_0 = H_0/\bar{f}$ , and  $F_0$  = normalizing Froude number  $= U_0/(gH_0)^{0.5}$ . It should be noted that the quantities qualified as "normal" correspond to the normal flow, whereas those qualified as "normalizing" are employed to nondimensionalize the flow variables. With the use of the above normalizing quantities, the following dimensionless quantities can be defined:

$$x_* = \frac{x}{x_0}, \quad h_* = \frac{h}{H_0}, \quad u_* = \frac{u}{U_0} \quad (6)$$

$$Q_* = \frac{Q}{Q_0} = \frac{uh}{Q_0}, \quad f_* = \frac{f}{\bar{f}}, \quad F_* = \frac{F}{F_0} = \frac{u_*}{(h_*)^{0.5}} \quad (7)$$

Recall that the Froude number  $F$  is

$$F = \text{Froude number} = \frac{u}{(gh)^{0.5}} \quad (8)$$

and the kinematic wave number  $K$  is

$$K = \frac{S_0 L}{F_0^2 H_0} \quad (9)$$

With the introduction of the above normalizing quantities, Eq. (1) becomes

$$\frac{d}{dx_*} (u_* h_*) = -f_* \quad (10)$$

and Eq. (2) becomes

$$u_* \frac{du_*}{dx_*} + \frac{1}{F_0^2} \frac{dh_*}{dx_*} = K \left( 1 - \frac{u_*^2}{h_*} \right) \quad (11)$$

Equations (10) and (11) are the governing equations for the DYW representation for time-independent flows. The KW approximation is based on Eq. (10) and Eq. (11) with the left side deleted,

$$K \left( 1 - \frac{u_*^2}{h_*} \right) = 0 \quad \text{or} \quad u_*^2 = h_* \quad (12)$$

This is actually the formal limit of Eq. (11) when  $1/KF_0^2 \rightarrow 0$ . The DW approximation uses Eq. (10) and Eq. (11) with the convective-acceleration term deleted,

$$\frac{1}{F_0^2} \frac{dh_*}{dx_*} = K \left( 1 - \frac{u_*^2}{h_*} \right) \quad (13)$$

This can be deduced from Eq. (11) by letting  $F_0^2 \rightarrow 0$  for fixed  $KF_0^2$ .

#### Boundary conditions

The boundary condition can be specified at the upstream boundary as follows:

$$h(0) = h_0, \quad u(0) = u_0, \quad Q(0) = Q_0 \quad (14)$$

In dimensionless terms,

$$h_*(0) = h_{0*}, \quad u_*(0) = u_{0*}, \quad Q_*(0) = Q_{0*} \quad (15)$$

#### Definition of error

The relative error  $E$  can be defined by

$$E_* = \frac{S_K - S_D}{S_D} \quad (16)$$

where  $S_K$  is the dimensionless solution from KW or DW approximation and  $S_D$  is the dimensionless solution from DYW representation. The solution can be either in terms of depth ( $h_*$ ), velocity ( $u_*$ ), or discharge ( $Q_*$ ). Thus,

$$E = \frac{u_K - u_D}{u_D}, \quad E = \frac{h_K - h_D}{h_D}, \quad E = \frac{Q_K - Q_D}{Q_D} \quad (17)$$

where the subscripts  $K$  and  $D$  correspond to the KW (or DW) and DYW solutions, respectively.

The differential equation for error can be obtained by differentiating Eq. (16) with respect to  $x_*$  as

$$\frac{dE}{dx_*} = \frac{(E+1)}{S_K} \frac{dS_K}{dx_*} - \frac{(E+1)^2}{S_K} \frac{dS_D}{dx_*} \quad (18)$$

Note that

$$S_D = \frac{S_K}{E+1} \quad (19)$$

Equation (18) was used to define the error. The differential equation for error can, however, be defined without explicitly knowing  $S_D$  so long as  $S_K$  is known, as seen from Eq. (19).

For the above-specified boundary condition, twelve cases involving  $F_0 = 0.1, 0.5, 1.0$ ; and  $K = 3, 5, 10$  and  $30$ , were considered for computing errors. The KW, DW and DYW solutions were computed in terms of depth, velocity, and discharge for all of these cases.

#### Hydrodynamic solutions

##### Kinematic-wave solution

Equation (10), subject to the upstream boundary condition given by Eq. (15), has the solution:

$$u_* h_* = Q_* = -f_* x_* + a, \quad a = h_{0*} u_{0*} = Q_{0*} = 1 \quad (20)$$

where  $a$  is the dimensionless discharge at the upstream boundary which equals one. With introduction of Eq. (12),

$$u_* = (a - f_* x_*)^{1/3} = (1 - f_* x_*)^{1/3} \quad (21)$$

which is the KW solution. When expressed in terms of dimensionless depth, it becomes

$$h_* = (a - f_* x_*)^{2/3} = (1 - f_* x_*)^{2/3} \quad (22)$$

Equations (21) and (22) show that the flow will advance as far as  $X_* = a/f_* = 1/f_*$ , and clearly depends on the upstream condition and the rate of infiltration.

The KW solution (depth, velocity, and discharge) was computed for all 12 different cases involving values of the Froude number ( $F_0 = 0.1, 0.5$ , and  $1.0$ ), kinematic wave number ( $K = 3, 5, 10$ , and  $30$ ), lateral inflow  $q_* = 0$ , infiltration rate  $f_* = 0.5$ , and dimensionless upstream discharge ( $a = 1.0$ ). The solution in terms of flow depth for a sample case ( $F_0 = 0.5$ ) is shown in Fig. 1. The KW solution is not dependent on  $K$  or  $F_0$ . The depth decreases with the longitudinal distance. This is due to the fact that the total infiltration increases from upstream to downstream.

##### Diffusion-wave solution

Equation (10), subject to the condition in Eq. (15), has the solution given by Eq. (20). Substitution for  $h_*$  from Eq. (20) into Eq. (13) yields

$$\frac{d}{dx_*} \left( \frac{a - f_* x_*}{u_*} \right) = K F_0^2 \left( 1 - \frac{u_*^3}{(a - f_* x_*)} \right) \quad (23)$$

Differentiation and simplification of Eq. (23) produce the DW equation in terms of  $u_*$ .

Kinematic wave approximation : Froude number = 0.50

Upstream boundary condition : Constant discharge = 1

Lateral inflow  $q = 0.00$  Infiltration  $F = 0.50$

$\bigcirc\bigcirc$   $K = 3.00$   $\triangle\triangle$   $K = 5.00$   $++$   $K = 10.00$   $\times\times$   $K = 30.00$

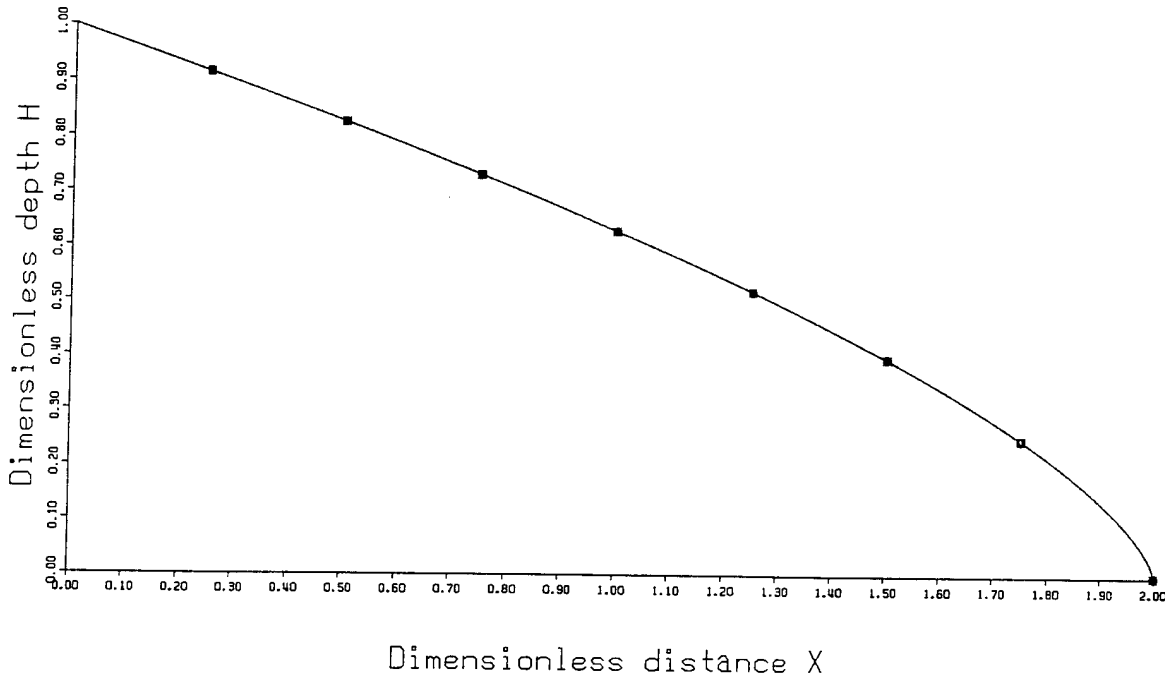


Fig. 1 Dimensionless flow depth by the kinematic-wave approximation as a function of dimensionless distance when the upstream discharge is 1.0, Froude number=0.5, and  $K$  is variable

$$\frac{du_*}{dx_*} = \frac{K F_0^2 u_*^5 - K F_0^2 u_*^2 (1 - f_* x_*) - f_* u_* (1 - f_* x_*)}{(1 - f_* x_*)^2} \quad (24)$$

Its analytical solution is not tractable.

The DW approximation can also be expressed in terms of  $h_*$  as

$$\frac{dh_*}{dx_*} = K F_0^2 \left( 1 - \frac{(1 - f_* x_*)^2}{h_*^3} \right) \quad (25)$$

Equation (25) shows that the depth gradient becomes zero when

$$h_* = (1 - f_* x_*)^{2/3} \quad (26)$$

which is the KW solution given by Eq. (22). When  $f_* x_* = 1$ , the depth gradient equals

$$\frac{dh_*}{dx_*} = K F_0^2 \quad (27)$$

An attempt was made to integrate Eq. (25) by prescribing the boundary condition at the upstream end, but this resulted in a solution which was not realistic. This can be attributed to the highly nonlinear nature of Eq. (25) and the presence of subcritical flow. A viable solution can be

obtained by prescribing a downstream boundary condition and marching the solution from downstream to upstream.

A solution could not be obtained for the downstream depth  $h_* = 0.0$ . A very small but finite depth  $h_* = 0.04$  was prescribed at the downstream end. By employing this procedure, the diffusion wave solution (dimensionless head, velocity and discharge) was computed for all 12 cases involving various values of  $F_0$  and  $K$ . For a sample case ( $F_0 = 0.5$ ), the solution in terms of dimensionless depth is shown in Fig. 2. As can be seen from the figure for a constant downstream depth of  $h_* = 0.04$ , the upstream depth varied from 0.85 for  $K = 3$  to 0.98 for  $K = 30$ . The depth decreased from upstream to downstream due to infiltration. The infiltration depth was zero at the upstream end and increased to 0.5 at the downstream end.

#### Approximate diffusion-wave solution

An approximate analytical solution of Eq. (25) can be obtained following Parlange et al. (1989). To that end Eq. (25) can be written as

$$\varepsilon h_*^3 \frac{dh_*}{dx_*} - h_*^3 = (1 - f_* x_*)^2 \quad (28)$$

where  $\varepsilon = 1/KF_0^2$ .

Using the transformation  $z_* = 1 - f_* x_*$ , Eq. (28) can be written as

Diffusion wave approximation : Froude number = 0.50

Upstream boundary condition : Constant discharge = 1

Lateral inflow  $q = 0.00$  Infiltration  $F = 0.50$

○ K = 3.00    △ K = 5.00    + K = 10.00    × K = 30.00

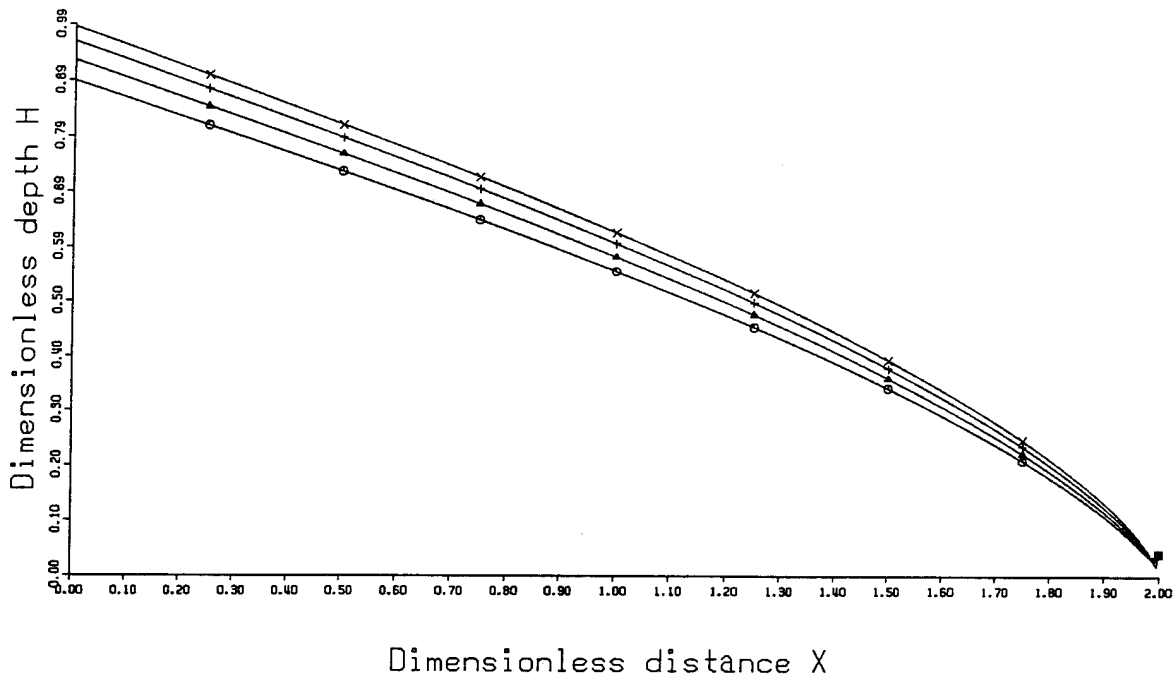


**Fig. 2** Dimensionless flow depth by the diffusion-wave approximation as a function of dimensionless distance when the upstream discharge is 1.0, Froude number=0.5, and  $K$  is variable

$$f_* \epsilon h_*^3 \frac{dh_*}{dz_*} + h_*^3 = z_*^2 \quad (29)$$

Taking a Taylor-series approximation for  $h_*$  near  $z_*=0$

$$h_* = h_{*0} + \frac{dh_*}{dz_*} z_* + \text{HOT} \quad (30)$$

where HOT represents higher order terms, and  $h_{*0} = h_*(0)$ . From Eq. (29) at  $z_*=0$ ,  $dh_*/dz_* = -1/(f_* \epsilon)$ . Equation (30) now becomes

$$h_* = h_{*0} - \frac{z_*}{f_* \epsilon} \quad (31)$$

This is a good approximation of Eq. (29) near  $z_*=0$  but clearly a poor approximation when  $z_*$  approaches 1. Equation (29) can be written as

$$\frac{\epsilon f_* h_*}{3} \frac{dh_*^3}{dz_*} + h_*^3 = z_*^2 \quad (32)$$

Substitution of Eq. (31) in Eq. (32) to replace the linear term yields

$$\frac{dh_*^3}{dz_*} + \frac{3h_*^3}{(f_* \epsilon h_{*0} - z_*)} - \frac{3z_*^2}{(f_* \epsilon h_{*0} - z_*)} = 0 \quad (33)$$

This is a linear differential equation and has an analytical solution. Let  $y = h_*^3$ . Equation (33) can be written as

$$\frac{dy}{dz_*} + \frac{3y}{(f_* \epsilon h_{*0} - z_*)} - \frac{3z_*^2}{(f_* \epsilon h_{*0} - z_*)} = 0 \quad (34)$$

Its analytical solution is

$$c (f_* \epsilon h_{*0} - z_*)^3 + f_*^2 \epsilon^2 h_{*0}^2 + 3z_*^2 - 3f_* \epsilon h_{*0} z_* = h_*^3$$

where  $c$  is the constant of integration. Its value can be found by using the condition  $h_* = h_{*0}$  at  $z_*=0$

$$c = \frac{h_{*0} - f_*^2 \epsilon^2}{f_*^3 \epsilon^3 h_{*0}} \quad (35)$$

Substituting Eq. (35) into Eq. (34) yields the solution

$$\frac{(h_{*0} - f_*^2 \epsilon^2)}{f_*^3 \epsilon^3 h_{*0}} (f_* \epsilon h_{*0} - z_*)^3 + f_*^2 \epsilon^2 h_{*0}^2 + 3z_*^2 - 3f_* \epsilon h_{*0} z_* = h_*^3 \quad (36)$$

The value of  $h_{*0}$  is found by substituting  $h_* = h_{*1}$  at  $z_*=1$ . Carrying out the above substitution and some algebraic manipulation yields

$$f_*^3 \epsilon^3 h_{*0}^4 - 3f_*^2 \epsilon^2 h_{*0}^3 + 3f_* \epsilon h_{*0}^2 + (-h_{*1}^2 f_*^3 \epsilon^3 - 1)h_{*0} + f_*^2 \epsilon^2 = 0 \quad (37)$$

Diffusion wave approximation : Froude number = 0.50  
 Upstream boundary condition : Constant discharge = 1  
 Analytical solution  
 Lateral inflow  $q = 0.00$  Infiltration  $F = 0.50$   
 $\bigcirc-\bigcirc$   $K = 10.00$   $\triangle-\triangle$   $K = 30.00$

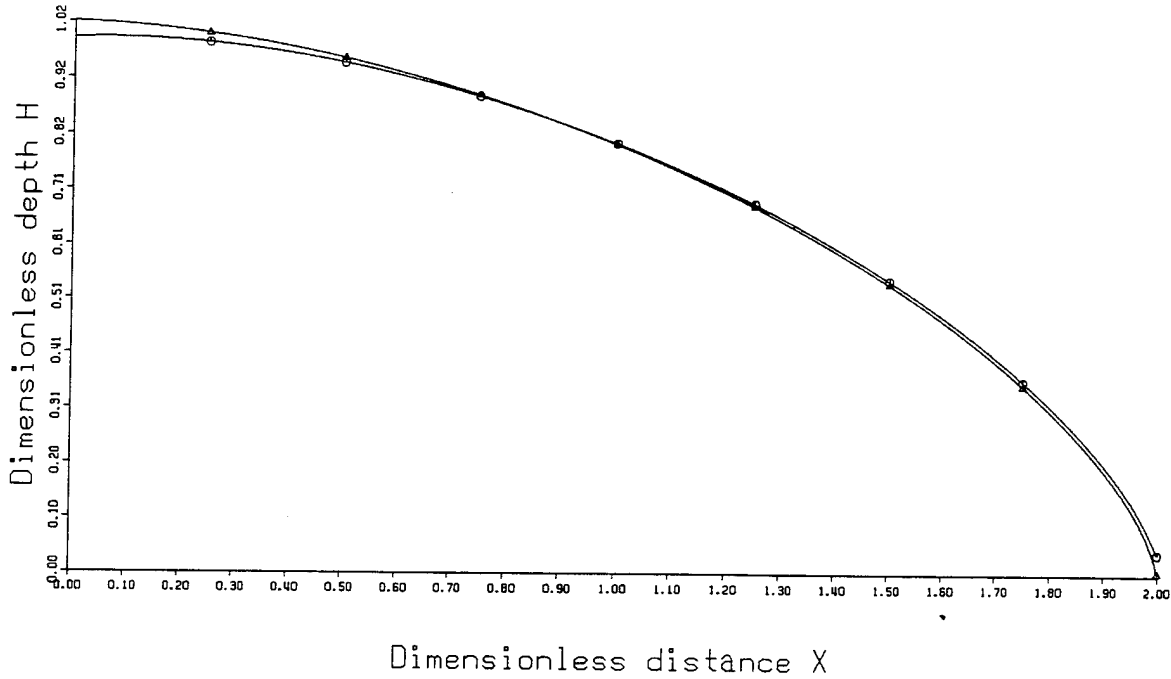


Fig. 3 Dimensionless flow depth by approximate analytical diffusion-wave solution as a function of dimensionless distance when the upstream discharge is 1.0, Froude number=0.5, and  $K=10, 30$

For a given value of  $h_{1*}$ , the above equation must be solved to obtain the value of  $h_{*0}$ .

This is an explicit solution, for all quantities on the right hand side are known. It was found that Eq. (37) yielded positive real roots only for large values of  $KF_0^2$ . The solution in terms of dimensionless depth for two values of  $K$  ( $K=10$  and  $30$ ) is shown in Fig. 3.

#### Dynamic-wave solution

Equation (10), subject to Eq. (15), has the solution given by Eq. (20). Substitution for  $h_*$  from Eq. (15) in Eq. (11) leads to

$$u_* \frac{du_*}{dx_*} + \frac{1}{F_0^2} \left[ \frac{d}{dx_*} \left( \frac{1-f_* x_*}{u_*} \right) \right] = K \left[ 1 - \frac{u_*^3}{1-f_* x_*} \right]. \quad (38)$$

Carrying out the required differentiation and simplifying lead to

$$\frac{du_*}{dx_*} = \frac{KF_0^2 u_*^2 (1-f_* x_*) - KF_0^2 u_*^5 + f_* u_* (1-f_* x_*)}{(1-f_* x_*) [F_0^2 u_*^3 - (1-f_* x_*)]}. \quad (39)$$

Similarly, in terms of  $h_*$ , Eq. (11) becomes

$$\frac{dh_*}{dx_*} = \frac{K F_0^2 h_*^3 - K F_0^2 (1-f_* x_*)^2 + F_0^2 h_* f_* (1-f_* x_*)}{h_*^3 - F_0^2 (1-f_* x_*)^2}. \quad (40)$$

It is seen from Eq. (30) that the depth gradient becomes infinite when

$$h_* = [F_0 (1-f_* x_*)]^{2/3} \quad (41)$$

and is given by Eq. (27) when  $a = f_* x_* = 1$ .

The procedure outlined in section 2 was used to integrate Eq. (40) to get the value of  $h_*$  for different values of  $x_*$  for all 12 different cases. For a sample case ( $F_0=0.5$ ), the solution in terms of the dimensionless depth is shown in Fig. 4. As can be seen from the figure, for a constant downstream depth of  $h_* = 0.04$ , the upstream depth varied from 0.88 for  $K=3$  to 0.98 for  $K=30$ . The depth decreased from upstream to downstream due to infiltration which was zero at the upstream end and increased to 0.5 at the downstream end.

#### Determination of error

##### Error in KW approximation

Equation (18) is the error differential equation with  $S$  specified by the flow depth. For the KW approximation,  $h_*$  is explicitly given by Eq. (22), and  $h_D$  by the solution of Eq.

Dynamic wave approximation : Froude number = 0.50

Upstream boundary condition : Constant discharge = 1

Lateral inflow  $q = 0.00$  Infiltration  $F = 0.50$

$\bigcirc\bigcirc$   $K = 3.00$   $\triangle\triangle$   $K = 5.00$   $++$   $K = 10.00$   $\times\times$   $K = 30.00$

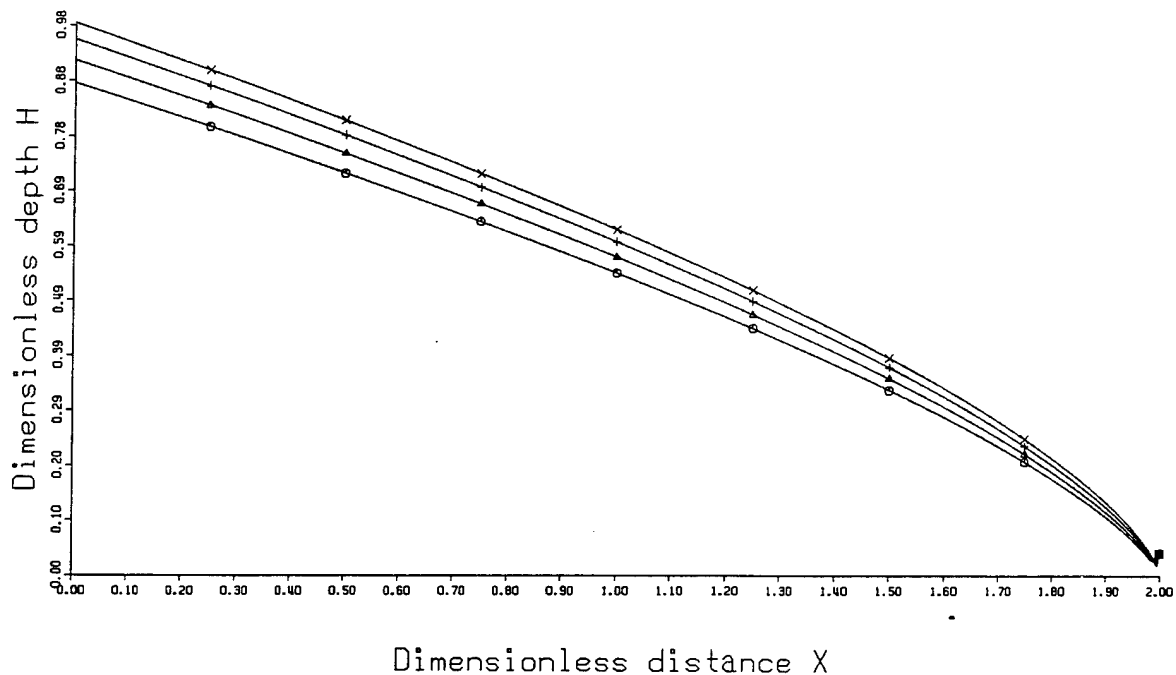


Fig. 4 Dimensionless flow depth by the dynamic-wave approximation as a function of dimensionless distance when the upstream discharge is 1.0, Froude number=0.5, and  $K$  is variable

(40). Substituting for  $h_D$  and  $h_K$  in Eq. (18) leads to the following error differential equation:

$$\frac{dE}{dx_*} = \frac{(E+1)}{h_K} \left[ \frac{dh_K}{dx_*} - (E+1) \frac{dh_D}{dx_*} \right] \quad (42)$$

To that end,  $dh_K/dx_*$  is obtained by differentiating Eq. (22):

$$\frac{dh_K}{dx_*} = -\frac{2f_*}{3} (1-f_* x_*)^{-1/3} \quad (43)$$

and  $dh_D/dx_*$  is given by Eq. (40). Substituting Eqs. (22), (40), and (43) into Eq. (42) yields the following differential equation for error in the KW solution:

$$\frac{dE}{dx_*} = \frac{(E+1)}{(1-f_* x_*)^{2/3}} \left[ \frac{-2f_*}{3(1-f_* x_*)^{1/3}} \right] - \frac{(E+1)^2}{(1-f_* x_*)^{2/3}} \frac{K F_0^2 h_D^3 - K F_0^2 (1-f_* x_*)^2 + F_0^2 h_D f_* (1-f_* x_*)}{h_D^3 - F_0^2 (1-f_* x_*)^2} \quad (44)$$

Note that  $h_D$  is expressed in terms of  $h_K$  through Eq. (19). Upon simplifying Eq. (44),

$$\frac{dE}{dx_*} = \frac{-2f_* (E+1)}{3 h_K^{3/2}} - \frac{(E+1)^2}{h_K} \left[ \frac{K F_0^2 - K F_0^2 (E+1)^3 + f_* F_0^2 h_K^{-1/2}}{1 - F_0^2 (E+1)^3} \right] \quad (45)$$

where  $h_K = (1-f_* x_*)^{2/3}$ . Equation (45) specifies error in the KW solution as a function of distance.

An explicit solution for error in the KW approximation is not tractable. However, a numerical solution is relatively simple. The longitudinal variation of error in depth for the case  $F_0=0.5$  is shown in Fig. 5. An analysis of the error profile shows that the KW approximation is an excellent approximation for large values of  $K F_0^2$  ( $K F_0^2 \geq 7.5$ ). The error profile is almost flat for  $K F_0^2 = 7.5$  with error magnitudes of 1.2%. The error varied from 1.5% to 44% for  $K F_0^2 = 0.75$ . This indicates that the KW approximation is a poor approximation for small values of  $K F_0^2$ . It is also observed that the error becomes very large at the downstream end. This is due to the fact that the KW approximation require that the depth be zero at the downstream end, whereas a small but finite depth is required for the DYW approximation.

#### Error in DW approximation

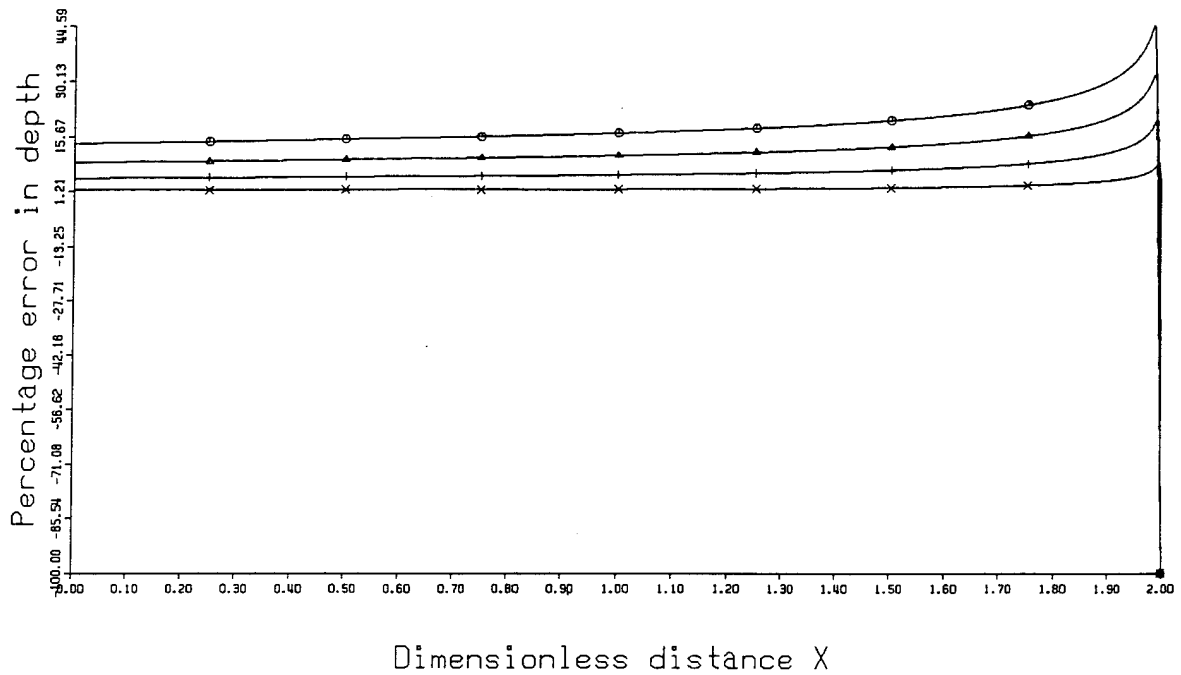
The error differential equation for DW approximation can be obtained by substituting Eqs. (25) and (40) in Eq. (42).

Error in kinematic wave approximation : Froude number = 0.50

Upstream boundary condition : Constant discharge = 1

Lateral inflow  $q = 0.00$  Infiltration  $F = 0.50$

$\bigcirc\bigcirc$   $K = 3.00$   $\triangle\triangle$   $K = 5.00$   $++$   $K = 10.00$   $\times\times$   $K = 30.00$



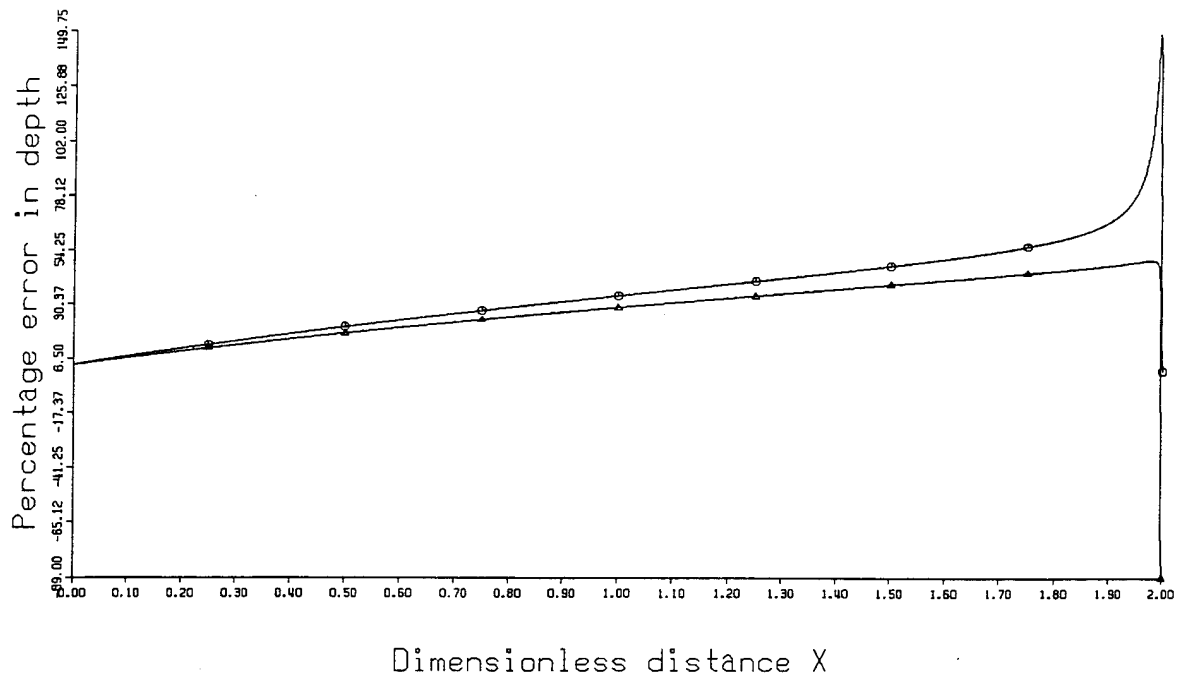
Error in diffusion wave approximation : Froude number = 0.50

Upstream boundary condition : Constant discharge = 1

Analytical solution

Lateral inflow  $q = 0.00$  Infiltration  $F = 0.50$

$\bigcirc\bigcirc$   $K = 10.00$   $\triangle\triangle$   $K = 30.00$



Error in diffusion wave approximation : Froude number = 0.50

Upstream boundary condition : Constant discharge = 1

Lateral inflow  $q = 0.00$  Infiltration  $F = 0.50$

$\bigcirc-\bigcirc$   $K = 3.00$   $\triangle-\triangle$   $K = 5.00$   $++$   $K = 10.00$   $\times-\times$   $K = 30.00$

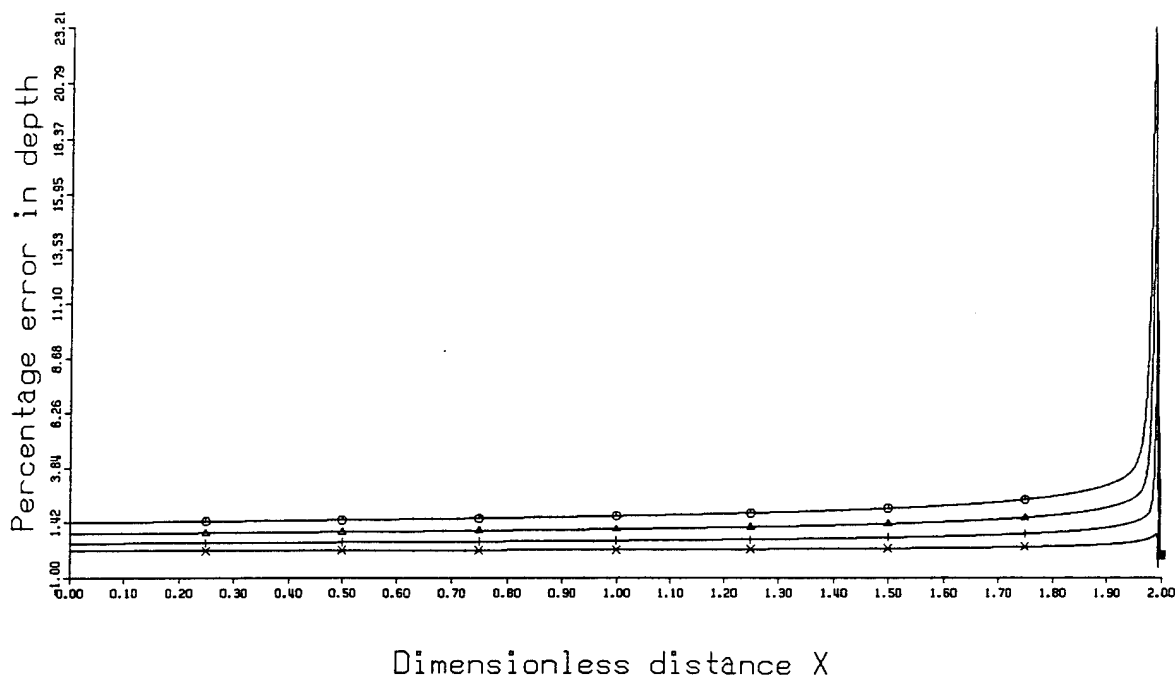


Fig. 7 Error in the flow depth by the analytical diffusion-wave solution as a function of dimensionless distance when the upstream discharge is 1.0, Froude number=0.5, and  $K$  is variable

With these substitutions we obtain

$$\frac{dE}{dx_*} = \frac{(E+1)}{h_K} \left[ \frac{K F_0^2 h_K^3 - K F_0^2 (1-f_* x_*)^2}{h_K^3} \right] - \frac{(E+1)^2}{h_K} \left[ \frac{K F_0^2 h_D^3 - K F_0^2 (1-f_* x_*)^2 + F_0^2 h_D f_* (1-f_* x_*)}{h_D^3 - F_0^2 (1-f_* x_*)^2} \right] \quad (46)$$

On simplifying,

$$\frac{dE}{dx_*} = \left[ \frac{K F_0^2 h_K^3 - K F_0^2 (f_* x_*)^2}{h_K^4} \right] (E+1) - \frac{(E+1)^2}{h_K} \left[ \frac{K F_0^2 h_K^3 + F_0^2 h_K f_* (1-f_* x_*) (E+1)^2 - K F_0^2 (1-f_* x_*)^2 (E+1)^3}{h_K^3 - F_0^2 (1-f_* x_*)^2 (E+1)^3} \right] \quad (47)$$

The longitudinal variation of error in depth for the case  $F_0=0.5$  is shown in Fig. 6. An analysis of the error profile

Fig. 5 Error in the flow depth by the kinematic-wave approximation as a function of dimensionless distance when the upstream discharge is 1.0, Froude number=0.5, and  $K$  is variable

Fig. 6 Error in the flow depth by the diffusion-wave approximation as a function of dimensionless distance when the upstream discharge is 1.0, Froude number=0.5, and  $K$  is variable

shows that the DW approximation is an excellent approximation for large values of  $K F_0^2$  ( $K F_0^2 \geq 7.5$ ). The error profile is almost flat for  $K F_0^2 = 7.5$  with error magnitudes of 0.8%. The error varied from 1.42% to 6.0% for  $K F_0^2 = 0.75$ . As can be seen from the figure, the error magnitude becomes large ( $\approx 23\%$ ) near the downstream end of the channel ( $1.99 < x_* < 2.0$ ). This indicates that the DW approximation is valid over a large range of  $K F_0^2$  and in most of the channel reach.

#### Error in approximate DW solution

Equation (18) is the error differential equation with  $S$  specified by the flow depth. For the approximate analytical solution,  $h_K$  is given by Eq. (36). Substitution for  $h_D$  and  $h_K$  in Eq. (18) gives the differential equation for error.

To that end,  $dh_K/dx_*$  is obtained by differentiating Eq. (36):

$$\frac{dh_K}{dx_*} = \frac{f_*}{h_*(f_* \varepsilon h_{*0} + f_* x_* - 1)} - \frac{f_*(1 - f_* x_*)^2}{h_*^2(f_* \varepsilon h_{*0} + f_* x_* - 1)} \quad (48)$$

and  $dh_D/dx_*$  is given by Eq. (39).

Substituting Eqs. (36), (40), and (48) into Eq. (42) yields the following differential equation for error in the approximate analytical solution.

$$\frac{dE}{dx_*} = \frac{(E+1)}{h_K^3} \left[ \frac{f_* h_K - f_*(1 - f_* x_*)^2}{f_* \varepsilon h_{*0} + f_* x_* - 1} \right] - \frac{(E+1)^2}{h_K} \left[ \frac{K F_0^2 h_K^3 - K F_0^2 (1 - f_* x_*)^2 (E+1)^3 + F_0^2 f_* h_K (1 - f_* x_*) (E+1)^2}{[h_K^3 - F_0^2 (1 - f_* x_*)^2 (E+1)^3]} \right] \quad (49)$$

where  $h_K$  is given by Eq. (36). The longitudinal variation of error is shown in Fig. 7. The magnitude of error varied from about 6.4% at the upstream end to greater than 30% at the downstream end. This shows that the approximate analytical diffusion-wave solution is not suitable.

## Conclusions

The following conclusions can be drawn from this study:

(1) When the upstream condition of finite discharge and depth is known, the governing differential equation cannot be integrated directly from upstream to downstream. An iterative procedure must be followed by which the downstream depth,  $K$  and  $F_0$  are varied until the upstream depth agrees with the given condition. (2) For upstream boundary conditions of finite discharge and depth, the KW approximation was in excellent agreement with the DYW representation for large values of  $K F_0^2$ . The error profiles were flat [almost a constant value of error ( $\approx 1.2\%$ )] for  $K F_0^2 = 7.5$  and curved downwards for smaller values of  $K F_0^2$  with errors varying between 18% and 44% for  $K F_0^2 = 0.75$ . The KW approximation is a good approximation for large values of  $K F_0^2$ , but a poor approximation for small values of  $K F_0^2$ . (3) For upstream boundary conditions of finite discharge and depth, the DW approximation was in excellent agreement with the DYW representation for large values of  $K F_0^2$  in the region  $0.0 \leq x_* \leq 1.98$ . The error profiles were flat [almost a constant value of error ( $\approx 0.8\%$ )] for  $K F_0^2 = 7.5$  and  $\approx 1.4\%$  for  $K F_0^2 = 0.75$ . The DW approximation was found to be a good approximation for the range of values of  $K F_0^2$  considered ( $0.75 \leq K F_0^2 \leq 7.5$ ) and in the region  $0.0 \leq x_* \leq 1.98$ . (4) The approximate analytical solution performed poorly for larger values of  $K F_0^2$  and a vi-

able solution could not be obtained for small values of  $K F_0^2$ .

**Abbreviations:**  $C$ =Chezy's resistance parameter ( $L^{0.5}/T$ );  $f$ =rate of infiltration ( $L/T$ );  $\bar{f}$ =average rate of infiltration ( $L/T$ );  $F$ =Froude number;  $F_0$ =normalizing Froude number;  $F_*$ =Froude number in dimensionless domain;  $g$ =acceleration due to gravity ( $L/T^2$ );  $h$ =flow depth ( $L$ );  $h_*$ =dimensionless flow depth;  $H_0$ =normal depth of flow ( $L$ );  $K$ =kinematic wave number;  $L$ =length of the channel ( $L$ );  $Q$ =discharge per unit width ( $L^3/(TL)$ );  $Q_0$ =normal discharge ( $L^3/(TL)$ );  $Q_*$ =dimensional discharge;  $S_f$ =frictional slope;  $S_0$ =bed slope;  $T$ =duration of irrigation ( $T$ );  $T_0$ =normalizing time ( $T$ );  $u$ =flow velocity ( $L/T$ );  $U_0$ =normal velocity ( $L/T$ );  $u_*$ =dimensionless velocity;  $x$ =distance measured from the upstream boundary ( $L$ );  $x_0$ =normalizing distance ( $L$ );  $x_*$ =dimensionless distance;  $\beta$ =resistance parameter ( $T^2/L$ ).

**Acknowledgements** This study was supported in part by funds provided by the Army Research Office, Department of the Army, under the project "A Continuum Model for Streamflow Synthesis," Grant No. DAAL03-89-G-0116.

## References

- Govindaraju RS, Jones SE, Kavvas ML (1988) On the diffusion wave model for overland flow. 2. Steady state analysis. *Water Res Res* 24: 745-754
- Morris M (1978) The effect of the small-slope approximation and lower boundary condition on the solutions of the Saint Venant equations. *J Hydrol* 40: 31-47
- Parlange JY, Hogarth W, Sander G, Rose C, Haverkamp R, Surin A, Brutsaert W (1990) Asymptotic expansion for steady-state overland flow. *Water Res Res* 26: 579-583
- Parlange JY, Hogarth W, Sander G, Surin A, Haverkamp R (1989) Comment on "On the diffusion wave model for overland flow." 2. Steady state analysis. In: Govindaraju RS, Jones SE, Kavvas ML (1988) *Water Res Res* 25: 1923-1924
- Pearson CP (1989) One-dimensional flow over a plane: criteria for kinematic wave modeling. *J Hydrol* 111: 39-48

## Accuracy of hydrodynamic models of flood-discharge determinations

V.P.Singh & V.Aravamuthan

*Department of Civil Engineering, Louisiana State University, Baton Rouge, La., USA*

E.S.Joseph

*Department of Civil Engineering, Southern University, Baton Rouge, La., USA*

**ABSTRACT:** Hydrodynamic models employed for computing flood discharges are based on the shallow water-wave theory that is described by the St. Venant (SV) equations. These models are derived from either the kinematic-wave (KW) approximation, the diffusion-wave (DW) approximation or the dynamic-wave (DYW) representation of the SW equations. In the studies reported to date, different types of criteria have been established to evaluate the adequacy of the KW and DW approximations, but no explicit relations either in time or in space between these criteria and the errors resulting from these approximations have been derived yet. Furthermore, when doing hydrologic modeling, it is not evident if the KW and DW approximations are valid on one hand for the entire hydrograph or a portion thereof, and on the other hand for the entire channel length or a portion thereof. In other words, most of these criteria take on fixed point-values for a given rainfall-runoff event. This paper attempts to derive, under simplified conditions, error equations for the KW and DW approximations for space-independent as well as for time-independent flows, which provide a continuous description of error in the flow-discharge hydrograph. For space-independent flows, a dimensionless parameter  $\gamma$  is defined which reflects the effect of initial depth of flow, channel-bed slope, lateral inflow, and channel roughness. For time-independent flows, the dimensionless parameter is the product of the kinematic wave number and the square of the Froude number. The kinematic wave, diffusion wave and dynamic wave solutions are parameterized through these parameters. By comparing the kinematic wave and diffusion wave solutions with the dynamic wave solution, equations are derived in terms of these parameters for the error in the kinematic wave and diffusion wave approximations.

### 1 INTRODUCTION

Physically-based models of overland flow, channel flow, surface irrigation, and many other phenomena involving unsteady, free surface open channel flows are based on the shallow water wave (SWW) theory. These models are based either on the kinematic wave (KW) approximation (Lighthill and Whitham, 1955), diffusion wave approximation (DW), or dynamic wave (DYW) representation. Lighthill and Whitham (1955) showed that at the Froude numbers less than one (appropriate to flood waves) the dynamic waves are rapidly attenuated and the kinematic waves become dominant. Using a dimensionless form of the St. Venant (SV) equations, Woolhiser and Liggett (1967) obtained what is now referred to as the kinematic wave number,  $K$ , as a criterion for evaluating the adequacy of the KW approximation. For  $K$  greater than 20, the KW approximation was considered to be an accurate representation of the SV

equations in modeling of overland flow. However, no relation between  $K$  and the error in the KW approximation was suggested. Morris and Woolhiser (1980) modified the above criterion with an explicit inclusion of Froude number,  $F_0$ , and showed, based on numerical experimentation, that  $F_0^2 K \geq 5$  was a better indicator of the adequacy of the KW approximation. A relation between this criterion and the error resulting from the KW approximation was not derived, however.

Using a linear perturbation analysis, Ponce and Simons (1977) derived properties of the KW and DW approximations as well as DYW representations in modeling of open channel flows. They derived a spectrum showing the regions of the validity of the KW and DW approximations. Menendez and Norscini (1982) extended the work of Ponce and Simons by including the phase lag between the depth and velocity of flow. Their results were, however, similar to those of Ponce and Simons (1977). In

another but similar study, Ponce, et al. (1978), based on propagation characteristics of sinusoidal perturbation, derived criteria to evaluate the adequacy of the KW and DW approximations. Daluz Viera (1983) compared solutions of the SV equations with those of the KW and DW approximations for a range of  $F_0$  and  $K$ , and defined the regions of validity of these approximations in the  $K$ - $F_0$  space.

Fread (1985) developed criteria for defining the range of application of the KW and DW approximations. These were based on an analysis of the magnitude of the normalized errors in the momentum equation due to omission of certain terms. In a comprehensive study, Ferrick (1985) defined a group of dimensionless scaling parameters to establish the spectrum of river waves, with continuous transitions between wave types and subtypes. With the aid of these parameters he was able to discern when the KW and DW approximations would be valid.

In most of these studies, different types of criteria have clearly been established to evaluate the adequacy of the KW and/or DW approximations, but no explicit relations either in time or space between these criteria and the errors resulting from these approximations have been derived yet. Furthermore, when doing hydrologic modeling it is not evident if the KW and DW approximations are valid for the entire flood hydrograph or a portion thereof. In other words, most of these criteria take on fixed point values for a given event. The objective of this study is to derive, under simplified conditions, error equations for the KW and DW approximations for space-independent as well as time-independent flows, which specify errors as a function of time.

## 2 SHALLOW WATER-WAVE (SWW) THEORY

The SWW theory can be described by some form of the SV equations. For flow over an infiltrating plane subject to uniform rainfall, these equations can be written in one-dimensional form on a unit width basis as

continuity equation,

$$\frac{\partial h}{\partial t} + \frac{\partial}{\partial x} (uh) = q - f \quad (1)$$

momentum equation,

$$\frac{\partial u}{\partial t} + \frac{\partial}{\partial x} \left( \frac{1}{2} u^2 + gh \right) = (g(S_0 - S_f) - \frac{qu}{h}) \quad (2)$$

where  $h$  is the depth of flow (L),  $u$  is local mean velocity (L/T),  $q$  is uniform

rainfall intensity (L/T),  $f$  is uniform infiltration rate (L/T),  $g$  is acceleration due to gravity,  $x$  is space coordinate in the direction of flow (L),  $t$  is time (T),  $S_0$  is bed slope, and  $S_f$  is frictional slope. Note  $Q = uh$  is discharge (L<sup>3</sup>/TL) per unit width.  $S_f$  can be approximated as

$$S_f = \beta \frac{u^2}{h} \quad (3)$$

where  $\beta$  is some resistance parameter. If the Chezy relation is used for representing the friction then  $\beta = g/C^2$ , where  $C$  is Chezy's resistance parameter.

The DYW representation employs the full form of equations (1) and (2). The KW approximation is based on equation (1) and equation (2) with the left side omitted,

$$g(S_0 - S_f) - \frac{qu}{h} = 0 \quad (4)$$

The DW approximation uses equation (1) and equation (2) with local and convective acceleration deleted,

$$g \frac{\partial h}{\partial x} = g(S_0 - S_f) - \frac{qu}{h} \quad (5)$$

Analytical solutions of the SV equations or their variants in the KW and DW approximations are tractable only for simple cases. To that end, both space-independent and time-independent cases are considered in this study. In the first case, the water surface is flat.

## 3 SPACE-INDEPENDENT FLOWS

### 3.1 Governing Equations

For space-independent (or uniform) flows, equation (1) takes the form

$$\frac{dh}{dt} = q - f \quad (6)$$

and equation (2) becomes

$$\frac{du}{dt} = g(S_0 - S_f) - \frac{qu}{h} \quad (7)$$

Equations (6) and (7) are the governing equations for the DYW representation for spatially uniform flows. The KW approximation is based on equation (6) and equation (7) with the left side dropped,

$$g(S_0 - S_f) - \frac{qu}{h} = 0 \quad (8)$$

The DW approximation uses equation (6) as well as equation (8). Therefore, for spatially uniform flows, the KW

approximation is identical to the DW approximation. Equation (8) can also be approximated by neglecting the momentum exchange between lateral inflow and longitudinal channel flow as

$$S_0 = S_f \quad (9)$$

which can be expressed as equation (3). Similarly, equation (7) can be written as

$$\frac{du}{dt} = g(S_0 - S_f) \quad (10)$$

Depending upon the presence or absence of  $f$ , equation (6) can also be simplified. If  $f = 0$ , then

$$\frac{dh}{dt} = q \quad (11)$$

### 3.2 Types of Scenarios

Depending upon the presence of lateral inflow and infiltration, four different scenarios can be considered: (1)  $f = 0$ ,  $q = q_0 = \text{constant}$ ; this includes the case  $q = 0$ . (2)  $q = q_0 = \text{constant}$ , and  $f = f_0 = \text{constant}$ ; and this includes the case  $q = f = 0$ . (3)  $q - f = 0$ ,  $q = q_0 = \text{constant}$ ; this includes the case  $q = f = 0$ . (4)  $q = 0$ ,  $f = f_0 = \text{constant}$ ; this includes the case  $f = 0$ . It may be noted that the scenario with  $q = 0$  in equation (11) or  $(q - f) = 0$  in equation (6) applies to the recession hydrograph. The same applies if  $(q - f) < 0$ .

### 3.3 Initial Conditions

Two types of initial conditions ( $t = 0$ ) can be assumed:

$$(1) \quad h(0) = h_0, \quad u(0) = u_0, \quad (12)$$

$$(2) \quad u(0) = 0, \quad h(0) = 0 \quad (13)$$

### 3.4 Scenarios for Determination of Error

Error equations have been derived by Singh (1992a, 1992b) for the KW and DW approximations under the above-mentioned conditions for four different scenarios. Treated together, eighteen cases result and are summarized in Table 1.

## 4 TIME-INDEPENDENT FLOWS

### 4.1 Governing Equations

For time-independent flow, equation (1) takes the form

$$\frac{d}{dx} (uh) = q - f \quad (14)$$

and equation (2) becomes

$$\frac{d}{dx} \left( \frac{1}{2} u^2 + gh \right) = g(S_0 - S_f) - \frac{qu}{h} \quad (15)$$

Equations (14) and (15) are the governing equations for the DYW representation for time-independent flows. The KW approximation is based on equation (14) and equation (15), with the left side deleted, leading to equation (8). The DW approximation uses equation (14) and equation (15) with convective acceleration deleted,

$$g \frac{dh}{dx} = g(S_0 - S_f) - \frac{qu}{h} \quad (16)$$

Equations (15) and (16) can also be approximated by neglecting the momentum-exchange between lateral inflow and longitudinal channel flow respectively as

$$\frac{d}{dx} \left( \frac{1}{2} u^2 + gh \right) = g(S_0 - S_f) \quad (17)$$

and

$$\frac{dh}{dx} = S_0 - S_f \quad (18)$$

Depending upon the presence of  $f$ , equation (14) can also be simplified. If  $f = 0$ , then

$$\frac{d(uh)}{dx} = q \quad (19)$$

### 4.2 Types of Scenarios

Depending upon the presence of lateral inflow and infiltration, four different scenarios can be considered as in the preceding section. It may be noted that the scenario with  $q = 0$  in equation (19) or  $q - f = 0$  in equation (14) applies to the case of losing flow. This same would apply if  $q - f < 0$ .

### 4.3 Boundary Conditions

Two types of conditions at the upstream boundary ( $x = 0$ ) can be assumed:

$$(1) \quad h(0) = h_0, \quad u(0) = u_0, \quad (20)$$

$$(2) \quad u(0) = 0, \quad h(0) = h_0 \quad (21)$$

Depending upon the type of flow, the boundary conditions may have to be specified at the upstream boundary as well as the downstream boundary or at the upstream boundary alone.

The upstream boundary condition, given by equation (21), influences both

Table 1. List of cases for error analysis for space-independent flows.

Case No.	Scenario No.	Governing Eqs			Initial Conditions	Lateral Inflow $q$	Lateral Outflow $f$
		KW/DW Approximations	DYW Representation				
1	1	Eqs. (11) and (8)	Eqs. (11) and (7)		Eq. (12)	$q = \text{constant}$	$f = 0$
2	1	Eqs. (11) and (8)	Eqs. (11) and (7)		Eq. (13)	$q = \text{constant}$	$f = 0$
3	1	Eqs. (11) and (9)	Eqs. (11) and (7)		Eq. (12)	$q = \text{constant}$	$f = 0$
4	1	Eqs. (11) and (9)	Eqs. (11) and (7)		Eq. (13)	$q = \text{constant}$	$f = 0$
5	1	Eqs. (11) and (9)	Eqs. (11) and (10)		Eq. (12)	$q = \text{constant}$	$f = 0$
6	1	Eqs. (11) and (9)	Eqs. (11) and (10)		Eq. (13)	$q = \text{constant}$	$f = 0$
7	2	Eqs. (6) and (8)	Eqs. (6) and (7)		Eq. (12)	$q = \text{constant}$	$f = \text{constant}$
8	2	Eqs. (6) and (8)	Eqs. (6) and (7)		Eq. (13)	$q = \text{constant}$	$f = \text{constant}$
9	2	Eqs. (6) and (9)	Eqs. (6) and (7)		Eq. (12)	$q = \text{constant}$	$f = \text{constant}$
10	2	Eqs. (6) and (9)	Eqs. (6) and (7)		Eq. (13)	$q = \text{constant}$	$f = \text{constant}$
11	2	Eqs. (6) and (9)	Eqs. (6) and (10)		Eq. (12)	$q = \text{constant}$	$f = \text{constant}$
12	2	Eqs. (6) and (9)	Eqs. (6) and (10)		Eq. (13)	$q = \text{constant}$	$f = \text{constant}$
13	3	Eqs. (11) with $q = 0$ and (8)	Eqs. (11) with $q = 0$ and (7)		Eq. (12)	$q = 0$	$f = 0$
14	3	Eqs. (11) with $q = 0$ and (9)	Eqs. (11) with $q = 0$ and (7)		Eq. (12)	$q = 0$	$f = 0$
15	3	Eqs. (11) with $q = 0$ and (9)	Eqs. (11) with $q = 0$ and (10)		Eq. (12)	$q = 0$	$f = 0$
16	4	Eqs. (6) with $q = 0$ and (8)	Eqs. (6) with $q = 0$ and (7)		Eq. (12)	$q = 0$	$f = \text{constant}$
17	4	Eqs. (6) with $q = 0$ and (9)	Eqs. (6) with $q = 0$ and (9)		Eq. (12)	$q = 0$	$f = \text{constant}$
18	4	Eqs. (6) with $q = 0$ and (9)	Eqs. (6) with $q = 0$ and (10)		Eq. (12)	$q = 0$	$f = \text{constant}$

the supercritical and subcritical flow outside zone A of the characteristic solution domain. The downstream boundary condition ( $x = L$ ) can be of two types:

- (1) Critical flow downstream boundary condition:

$$u(L) = [gh(L)]^{0.5} \quad (22)$$

where  $L$  is the channel length. This occurs when the channel ends at the steep bank of a river. For supercritical slow

$$u(L) > [h(L)g]^{0.5} \quad (23)$$

- (2) Zero-depth gradient downstream boundary condition:

$$\frac{dh(L)}{dx} = 0 \quad (24)$$

#### 4.4 Scenarios for Determination of Error

Error equations have been derived by Singh and Aravamuthan (1992a, 1992b, 1992c) for the KW and DW approximations under the above-mentioned conditions for four different scenarios. Taken together, these will give rise to 21 cases that are summarized in Table 2.

### 5 DEFINITION OF ERROR

The relative error  $E$  is defined as

$$E = \frac{S_K - S_D}{S_D} \quad (25)$$

where  $S_K$  is the solution from the KW or DW approximation, and  $S_D$  is the solution from the DYW representation. The solution can be either in terms of depth ( $h$ ), velocity ( $u$ ), or discharge ( $Q$ ), i.e.,  $S(u, h, Q)$ . Subscripts  $K$  and  $D$  correspond to the KW (or DW) and DYW solutions, respectively. The differential equation of  $E$  can be obtained by differentiating equation (25) as

$$\frac{dE}{dx} = \frac{(E+1)}{S_K} \frac{dS_K}{dx} - \frac{(E+1)}{S_D} \frac{dS_D}{dx} \quad (26)$$

The differential equation for error can, however, be defined without explicitly knowing  $S_D$ , so long as  $S_K$  is explicitly known.

### 6 ERROR EQUATIONS FOR SPACE-INDEPENDENT FLOWS

We consider the case where  $f = 0$ , and  $q = q_0$ .

#### 6.1 Kinematic Wave and Diffusion Wave Solution

Equation (11), subject to equation (12), has the solution:

$$h = h_0 + q_0 t \quad (27)$$

From the kinematic wave approximation,

$$u = \left(\frac{S_0}{\beta}\right)^{0.5} h^{0.5} \quad (28)$$

It is convenient to define a dimensionless time  $\tau$  as

$$\tau = \frac{h}{h_0} = \frac{h_0 + q_0 t}{h_0}, \quad h_0 \neq 0, \quad \tau \geq 1 \quad (29)$$

Equation (14) can be expressed in dimensionless form as

$$h_* = \frac{h}{h_0} = \tau$$

Equation (34) can be expressed in dimensionless form as

$$v = \frac{u}{U} = \tau^{0.5}, \quad U = \left(\frac{S_0 h_0}{\beta}\right)^{0.5} \quad (30)$$

The kinematic wave (KW) or diffusion wave (DW) solution is given by equations (33) and (34). The velocity increases parabolically with  $\tau$ .

#### 6.2 Dynamic Wave Solution

Equation (11) has the solution given by equation (27). Equation (2) can be expressed in dimensionless terms as

$$\frac{dv}{d\tau} = \frac{\gamma^{0.5}}{2} - \frac{\gamma^{0.5}}{2} \frac{v^2}{\tau}, \quad \gamma = \frac{4g^2 \beta S_0 h_0}{q_0^2} \quad (31)$$

Equation (31) is a special case of the Riccati equation. When  $\tau = 1$ ,  $v = 1$ , and  $dv/d\tau = 0$ . With these initial conditions in hand, equation (31) was solved by using the 4th order Runge-Kutta method. For a fixed  $\gamma$ ,  $v$  increases with increasing  $\tau$ , and for a fixed  $\tau$ , it increases with  $\gamma$ . However, for  $\gamma \geq 1.5$ ,  $v$  is not very sensitive to  $\gamma$ .

#### 6.3 Error in KW and DW Approximations

By making use of equations (30) and (31) in equation (26), one obtains the error differential equation:

$$\begin{aligned} \frac{dE}{d\tau} = & C_0(\tau) + C_1(\gamma, \tau) E \\ & + C_2(\gamma, \tau) E^2 \end{aligned} \quad (32a)$$

Table 2. List of cases for error analysis for time-independent flows.

Case No.	Scenario No.	Governing Eqs.			Boundary Conditions				Lateral Inflow $q$	Infiltration $f$
		KW Approximation	DW Approximation	DYW Approximation	Upstream	Down-stream (critical depth)	Down-stream (zero-depth gradient)			
1	1	Eqs. (14) and (16)	Eqs. (14) and (16)	Eqs. (14) and (15)	Eq. (20)	N.A.	N.A.	$q_0$	$f_0$	
2	1	Eqs. (14) and (4)	Eqs. (14) and (16)	Eqs. (14) and (15)	Eq. (21)	N.A.	Eq. (24)	$q_0$	0	
3	1	Eqs. (14) and (9)	Eqs. (14) and (16)	Eqs. (14) and (15)	Eq. (21)	Eq. (24)	N.A.	$q_0$	0	
4	2	Eqs. (14) and (9)	Eqs. (14) and (16)	Eqs. (14) and (15)	Eq. (20)	N.A.	N.A.	$q_0$	0	
5	2	Eqs. (14) and (9)	Eqs. (14) and (16)	Eqs. (14) and (15)	Eq. (21)	N.A.	Eq. (24)	$q_0$	0	
6	2	Eqs. (14) and (9)	Eqs. (14) and (16)	Eqs. (14) and (15)	Eq. (21)	Eq. (24)	N.A.	$q_0$	0	
7	3	Eqs. (14) and (9)	Eqs. (14) and (18)	Eqs. (14) and (17)	Eq. (20)	N.A.	N.A.	$q_0$	0	
8	3	Eqs. (14) and (9)	Eqs. (14) and (18)	Eqs. (14) and (17)	Eq. (21)	N.A.	Eq. (24)	$q_0$	0	
9	3	Eqs. (14) and (9)	Eqs. (14) and (18)	Eqs. (14) and (17)	Eq. (21)	Eq. (24)	N.A.	$q_0$	0	
10	4	Eqs. (14) and (4)	Eqs. (14) and (16)	Eqs. (14) and (15)	Eq. (20)	N.A.	N.A.	$q_0$	$f_0$	
11	4	Eqs. (14) and (4)	Eqs. (14) and (16)	Eqs. (14) and (15)	Eq. (21)	N.A.	Eq. (24)	$q_0$	$f_0$	
12	4	Eqs. (14) and (4)	Eqs. (14) and (16)	Eqs. (14) and (15)	Eq. (21)	Eq. (24)	N.A.	$q_0$	$f_0$	
13	5	Eqs. (14) and (4)	Eqs. (14) and (16)	Eqs. (14) and (15)	Eq. (20)	N.A.	N.A.	$q_0$	$f_0$	
14	5	Eqs. (14) and (9)	Eqs. (14) and (16)	Eqs. (14) and (15)	Eq. (21)	N.A.	Eq. (24)	$q_0$	$f_0$	
15	5	Eqs. (14) and (9)	Eqs. (14) and (17)	Eqs. (14) and (15)	Eq. (21)	N.A.	N.A.	$q_0$	$f_0$	
16	6	Eqs. (14) and (9)	Eqs. (14) and (20)	Eqs. (14) and (17)	Eq. (21)	Eq. (22)	N.A.	$q_0$	$f_0$	
17	6	Eqs. (14) and (9)	Eqs. (14) and (20)	Eqs. (14) and (17)	Eq. (21)	N.A.	N.A.	$q_0$	$f_0$	
18	6	Eqs. (14) and (9)	Eqs. (14) and (20)	Eqs. (14) and (17)	Eq. (21)	N.A.	Eq. (24)	$q_0$	$f_0$	
19	7	Eqs. (14) and (4)	Eqs. (14) and (17)	Eqs. (14) and (15)	Eq. (20)	N.A.	N.A.	0	$f_0$	
20	7	Eqs. (14) and (9)	Eqs. (14) and (17)	Eqs. (14) and (15)	Eq. (20)	N.A.	N.A.	0	$f_0$	
21	7	Eqs. (14) and (9)	Eqs. (14) and (17)	Eqs. (14) and (17)	Eq. (20)	N.A.	N.A.	0	$f_0$	

$$E(1) = 0, \tau \geq 1$$

(32b)

## 7 ERROR EQUATIONS FOR TIME-INDEPENDENT FLOWS: NON-ZERO VELOCITY AT THE UPSTREAM BOUNDARY

where

$$C_0(\tau) = \frac{1}{2\tau} \quad (33)$$

$$C_1(\gamma, \tau) = \frac{1}{2\tau} (1 - 2\Gamma \tau^{0.5}) \quad (34)$$

$$C_2(\gamma, \tau) = -\frac{\Gamma}{2\tau^{0.5}} \quad (35)$$

Equation (32) is a Riccati equation and has to be solved numerically; it also holds for error in discharge. The distribution of error with  $\tau$  is shown in Figure 1. The distribution is highly skewed, with a sharp rise and gradual decline over an extended range of  $\tau$ . For a fixed  $\tau$ , the error increases with decreasing  $\gamma$ .

### 7.1 Kinematic Wave Solution

Equation (1) takes the form

$$\frac{d(uh)}{dx} = q_0 \quad (36)$$

which has the solution

$$uh = a + q_0 x \quad (37)$$

where  $a$  is constant of integration. The KW approximation is given by equation (28). If

$$H = \left(\frac{\beta}{S_0}\right)^{1/3} (u_0 h_0)^{2/3} \quad (38)$$

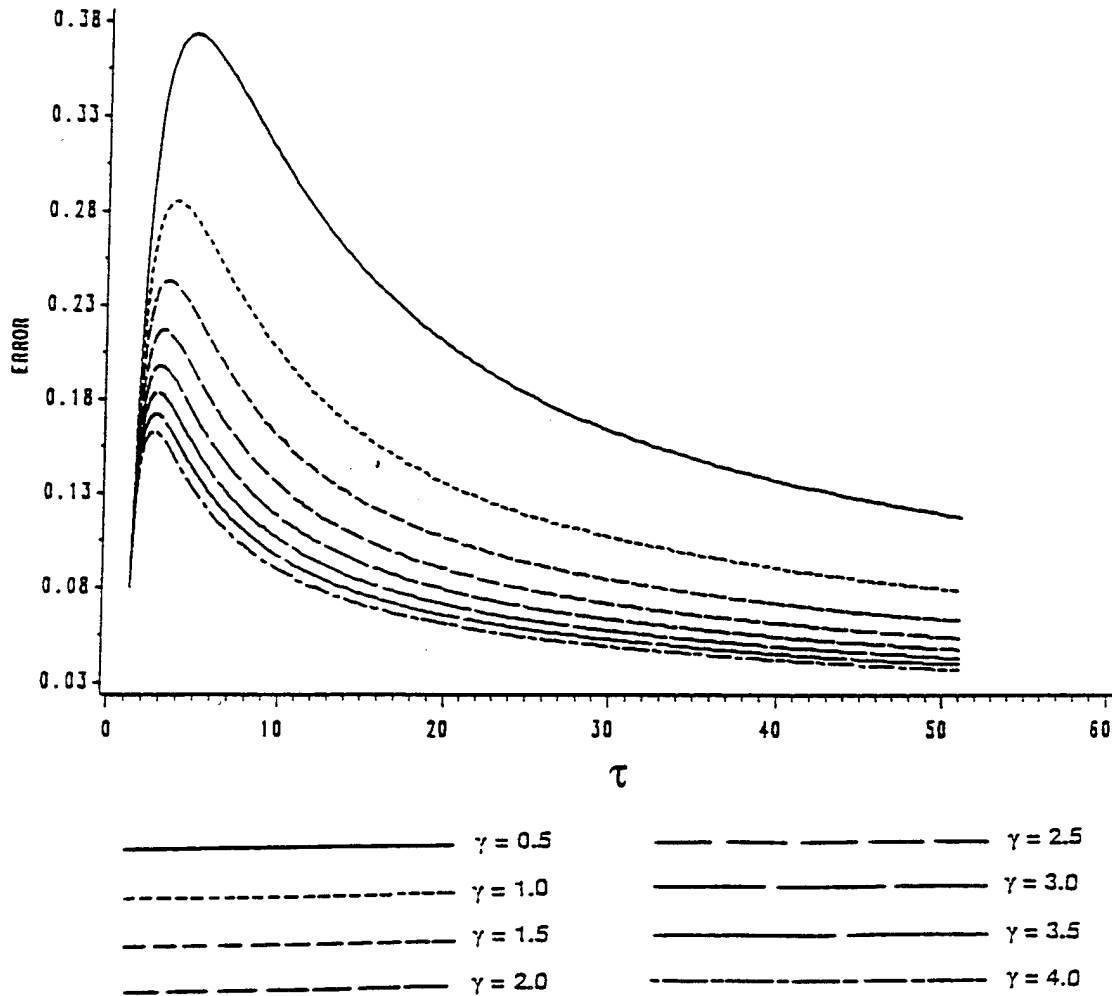


Figure 1. Error in the KW or DW approximation as a function of dimensionless time for space-independent flows.

Diffusion wave approximation : Froude number = 1.00  
 Upstream boundary conditions: Discharge AA = 0.00 Depth H = 1.03  
 Lateral inflow q = 1.00 Infiltration F = 0.00

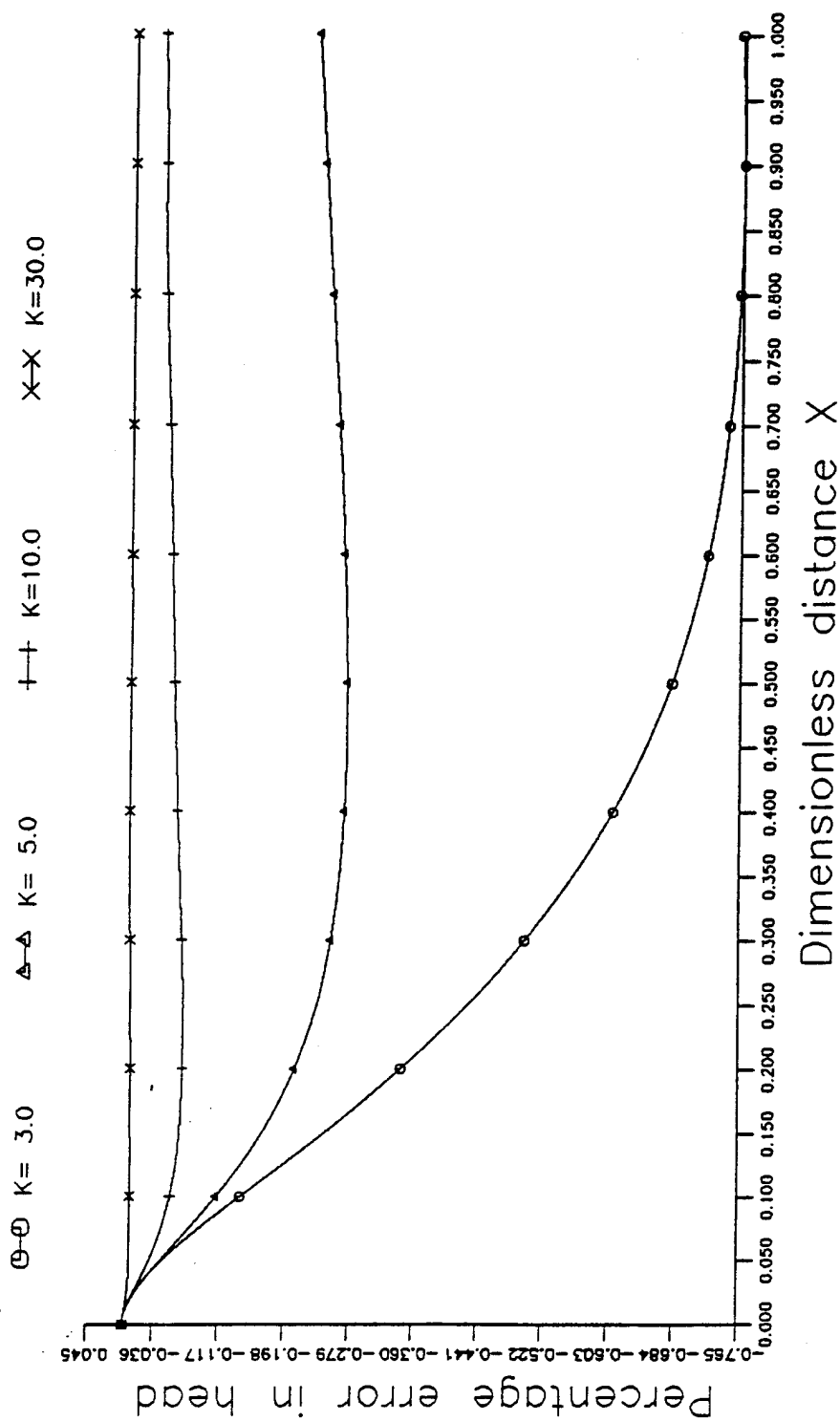


Figure 2. Error in the KW approximation as a function of dimensionless distance for time-independent flows.

Kinematic wave approximation : Froude number = 1.00  
 Upstream boundary conditions: Discharge AA = 0.00 Depth H = 1.03  
 Lateral inflow q = 1.00 Infiltration F = 0.00

○-○ K= 3.0      ▲-▲ K= 5.0      +--+ K=10.0      X-X K=30.0

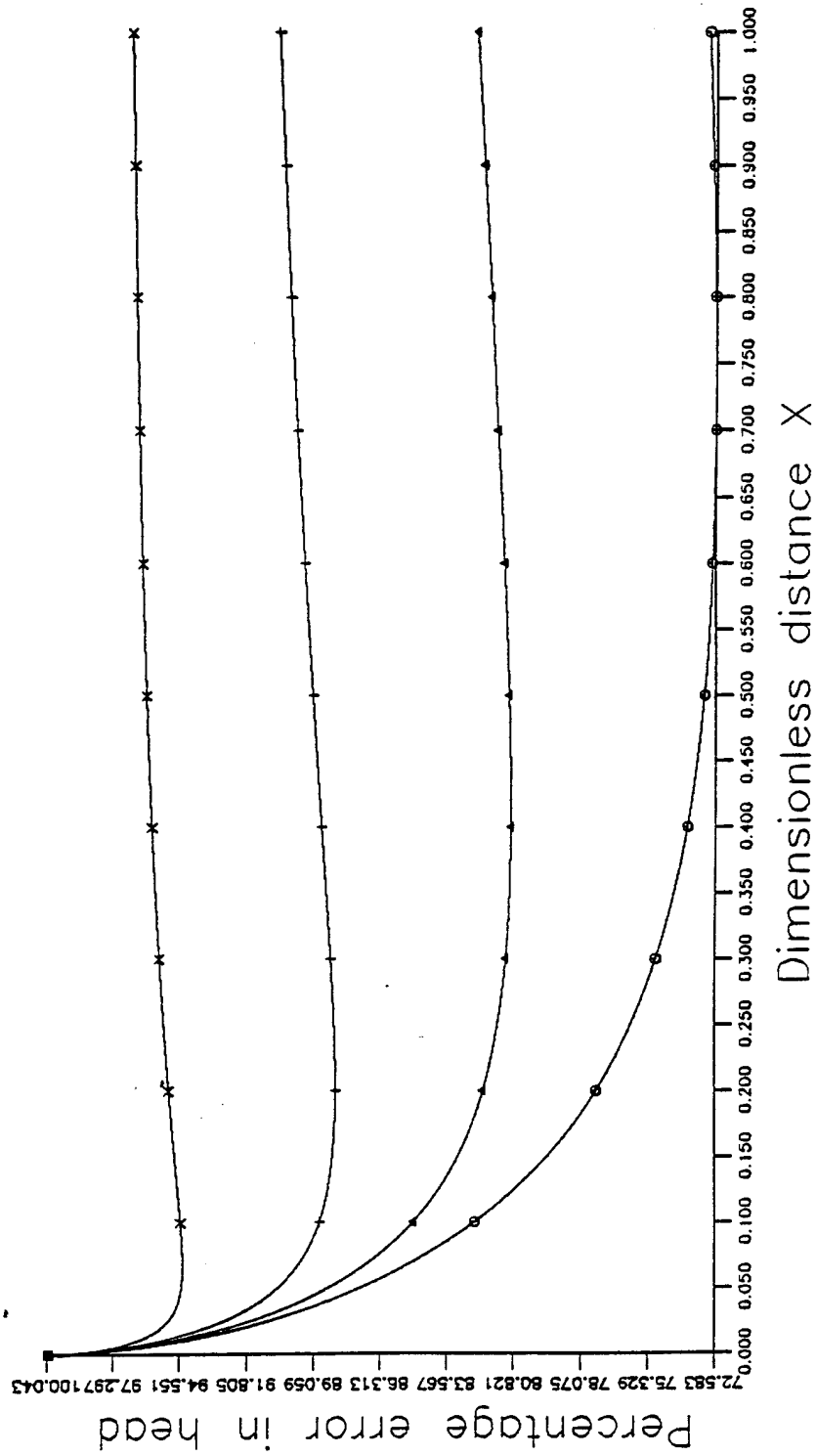


Figure 3. Error in the DW approximation as a function of dimensionless distance for time-independent flows.

then

$$h_* = \frac{h}{H} = \left( \frac{q_0 x + a}{u_0 h_0} \right)^{2/3} \quad (39)$$

## 7.2 Diffusion Wave Solution

Equation (1) has the solution given by equation (37). Equation (2) reduces to

$$\frac{dh}{dx} = S_0 - \beta \frac{u^2}{h} \quad (40)$$

With the upstream boundary condition given by equation (20), equation (40) can be written in terms of  $h$  as

$$\frac{dh}{dx} = S_0 - \beta \frac{(q_0 x + a)^2}{h^3} \quad (41)$$

## 7.3 Dynamic Wave Solution

Equation (1) has the solution given by equation (44). Equation (2) reduces to

$$\frac{d}{dx} \left( \frac{1}{2} u^2 + gh \right) = gS_0 - g\beta \frac{u^2}{h} \quad (42)$$

which can be expressed in terms of  $h$  as

$$\frac{dh}{dx} = \frac{1}{gh^3 - (q_0 x + a)^2} [gS_0 h^3 - q_0(q_0 x + a)h - \beta(q_0 x + a)^2] \quad (43)$$

## 7.4 Errors of KW and DW Approximations

The DW approximation gave good results for the entire channel reach with error less than 1%. The error decreased with increasing values of  $KF_0^2$ , as shown in Figure 2. The KW approximation gave adequate results (error < 10%) in the region ( $0.1 \leq x \leq 1.0$ ) for  $F_0^2$  values greater than 30, as shown in Figure 3.

## 8 ERROR EQUATIONS FOR TIME-INDEPENDENT FLOWS: ZERO DEPTH-GRADIENT DOWN-STREAM BOUNDARY

Following the procedure of Section 7, error equations were derived for the case of the zero-depth gradient downstream boundary condition. The DW approximations gave adequate results in the region ( $0.1 \leq x \leq 1.0$ ) and for  $KF_0^2$  values greater than 30. For larger values of  $KF_0^2$ , the errors were less than 1% in the region ( $0.1 \leq x \leq 1.0$ ) and increased to about 21% at the upstream end of the channel. The KW approximation gave reasonable results (errors < 10.1) for  $KF_0^2$  greater than 30 and in the region  $0.1 \leq x \leq 1.0$ .

## 9 ERROR EQUATIONS FOR TIME-INDEPENDENT FLOWS: CRITICAL FLOW-DEPTH DOWN-STREAM BOUNDARY CONDITION

The error equations for the critical depth downstream boundary condition were obtained following the procedure of Section 7. For the DW and KW approximations, the errors obtained were almost of the same magnitude as of those obtained using the zero depth gradient downstream condition in the region  $0.1 \leq x \leq 1.0$ .

## 10 CONCLUSIONS

For space-independent flows, the kinematic-wave and diffusion-wave approximations are sufficiently accurate when the dimensionless parameter  $\gamma \geq 3$ . This parameter reflects the effect of initial flow depth, bed slope, lateral inflow, and channel roughness. The error of these approximations declines exponentially when the dimensionless time exceeds 5. The dimensionless time is obtained with the use of initial depth.

For time-independent flows with a constant depth upstream boundary condition and with parameters ( $f = 0.0$ ,  $a = 0.0$ ,  $H = 1.03$ ,  $F_0 = 1.0$ ), the DW approximation was quite accurate, with errors in depths of less than 1%. The errors decreased with an increase in the value of  $KF_0^2$ . The KW approximation was accurate with errors of less than 10% in the region ( $0.1 \leq x \leq 1.0$ ) and for  $KF_0^2$  values greater than 30. For smaller values of  $KF_0^2$ , the KW approximation was not adequate.

## ACKNOWLEDGMENT

This study was supported in part by Army Research Office under the project "A Continuum Model for Streamflow Synthesis," Grant No. DAAL03-89-G-0116.

## REFERENCES

- Daluz Viera, J. H., 1983. Conditions governing the use of approximations for the Saint Venant equations for shallow water flow. *Journal of Hydrology*, Vol. 60, pp. 43-58.
- Ferrick, M. G., 1985. Analysis of river wave types. *Water Resources Research*, Vol. 21, No. 2, pp. 209-220.
- Fread, D. L., 1985. Applicability criteria for kinematic and diffusion routing models. Laboratory of Hydrology, National Weather Service, NOAA, U.S. Department of Commerce, Silver Spring, Maryland.
- Lighthill, M. J. and Whitham, G. B., 1955. On kinematic waves: 1. flood

- movement in long rivers. Proceedings, Royal Society, London, Series A, Vol. 229, pp. 281-316.
- Menendez, A. N. and Norscini, R., 1982. Spectrum of shallow water waves: an analysis. Journal of the Hydraulics Division, ASCE, Vol. 108, No. HY1, pp. 75-93.
- Morris, E. M. and Woolhiser, D. A., 1980. Unsteady, one dimensional flow over a plane: partial equilibrium and recession hydrographs. Water Resources Research, Vol. 16, No. 2, pp. 355-360.
- Ponce, V. M., Li, R. M. and Simons, D. B., 1978. Applicability of kinematic and diffusion models. Journal of the Hydraulics Division, ASCE, Vol. 104, No. HY3, pp. 353-360.
- Ponce, V. M. and Simons, D. B., 1977. Shallow wave propagation in open channel flow. Journal of the Hydraulics Division, ASCE, Vol. 103, No. HY12, pp. 1461-1475.
- Singh, V. P., 1992a. Errors in kinematic wave and diffusion wave approximations for space-independent flows: 1. Cases 1 to 9. Water Resources Report WRR 17, Department of Civil Engineering, Louisiana State University, Baton Rouge, Louisiana.
- Singh, V. P., 1992b. Errors in kinematic wave and diffusion wave approximations for space-independent flows: 2. Cases 10 to 19. Water Resources Report WRR 18, Department of Civil Engineering, Louisiana State University, Baton Rouge, Louisiana.
- Singh, V. P. and Aravamuthan, V., 1992a. Errors in kinematic wave and diffusion wave approximations for time-independent flows: Cases 1 to 7. Technical Report WRR20, Department of Civil Engineering, Louisiana State University, Baton Rouge, Louisiana.
- Singh, V. P. and Aravamuthan, V., 1992b. Errors in kinematic wave and diffusion wave approximations for time-independent flows: Cases 8 to 14. Technical Report WRR21, Department of Civil Engineering, Louisiana State University, Baton Rouge, Louisiana.
- Singh, V. P. and Aravamuthan, V., 1992c. Errors in kinematic wave and diffusion wave approximations for time-independent flows: Cases 15 to 21. Technical Report WRR22, Department of Civil Engineering, Louisiana State University, Baton Rouge, Louisiana.
- Woolhiser, D. A. and Liggett, J. A., 1967. Unsteady one-dimensional flow over a plane - the rising hydrograph. Water Resources Research, Vol. 3, No. 3, pp. 753-771.

[1]

## Muskingum method with variable parameters for flood routing in channels

Wang Guang-Te<sup>a,1</sup> and V. P. Singh<sup>b</sup>

<sup>a</sup> *Institute of Geography, Chinese Academy of Sciences, Beijing 100101, China*

<sup>b</sup> *Department of Civil Engineering, Louisiana State University, Baton Rouge, LA 70803, USA*

(Received 24 August 1990; revised and accepted 27 September 1991)

### ABSTRACT

Wang, G.-T., and Singh, V.P., 1992. Muskingum method with variable parameters for flood routing in channels. *J. Hydrol.*, 134: 57–76.

Three versions of the Muskingum method with variable parameters for flood routing in open channels were derived. The reach travel time was obtained from simplification of the St. Venant equations. The three versions were applied to three example data sets and the results obtained were found to be more accurate than those of the conventional Muskingum method with parameters obtained by trial and error or optimization.

### INTRODUCTION

Since its development around 1934 by McCarthy (1938), the Muskingum method for routing flood waves in rivers and channels has been a subject of many investigations (Singh, 1988). The method represents a river reach as a linear time-invariant system with its inflow  $I$ , outflow  $Q$ , and storage  $w$ , related as

$$w = K[XI + (1 - X)Q] \quad (1)$$

in which  $K$  and  $X$  are parameters.

The Muskingum method, based on eqn. (1) and the water balance equation, can be expressed as

$$Q(i+1) = C_1 I(i+1) + C_2 I(i) + C_3 Q(i), \quad i = 1, 2, \dots \quad (2)$$

where

---

<sup>1</sup> Visiting Scholar, Department of Civil Engineering, Louisiana State University, Baton Rouge, LA 70803, USA.

$$C_1 = \frac{0.5\Delta t - XK}{0.5\Delta t + (1-X)K} \quad (3)$$

$$C_2 = \frac{0.5\Delta t + XK}{0.5\Delta t + (1-X)K} \quad (4)$$

$$C_3 = \frac{-0.5\Delta t + (1-X)K}{0.5\Delta t + (1-X)K} \quad (5)$$

where  $\Delta t$  is the time interval ( $t_{i+1} - t_i$ ) or  $[(i+1) - (i)]$ ,  $Q(i+1)$  is the outflow at the end of the time interval,  $I(i+1)$  is the inflow at the end of the time interval,  $Q(i)$  is the outflow at the beginning of the time interval, and  $I(i)$  is the inflow at the beginning of the time interval.

In the conventional Muskingum method, the parameters  $K$  and  $X$  are considered constant and are determined by calibration using measured inflow and outflow hydrographs. This assumption makes the parameters dependent on the inflow-outflow values used to evaluate them (Dooge, 1973). As a result, the parameter values change from one set of inflow-outflow hydrograph data to another. A more physically realistic approach is to consider the parameters  $K$  and  $X$  to vary in time and space according to the flow variability (Miller and Cunge, 1975). Weinmann and Laurenson (1979) reviewed approximate flood routing methods, with focus on the Muskingum diffusion method. They proposed an inequality for use in routing calculations if negative outflows were to be ignored.

Cunge (1969) derived eqn. (2) using a finite difference approximation of the St. Venant equations with the inertia term neglected, and expressed  $K$  and  $X$  in terms of physical river characteristics

$$K = \frac{\Delta x}{c} = \frac{\Delta x A}{\beta Q} \quad (6)$$

$$X = \frac{1}{2} \left( 1 - \frac{q}{S_0 c \Delta x} \right) \quad (7)$$

where  $\Delta x$  is the reach length (space interval),  $c$  is the flood wave celerity,  $q = Q/B$  is the unit width discharge,  $Q$  is the discharge,  $B$  is the top width,  $S_0$  is the channel bed slope, and  $\beta$  is an exponent.

Koussis (1976, 1978, 1980, 1983) considered the macro form of the continuity equation with no lateral inflow or lateral outflow. By carrying out the discretization in space only, retaining continuous functions for the time derivatives, using a weighting scheme for the time derivative, and assuming linear variation of flow over the time interval  $\Delta t$ , he derived a more general form of the Muskingum method wherein the parameters were discharge-dependent. Koussis was thus able to account for the nonlinear nature of the

flood wave propagation through an explicit consideration of the unsteady-flow loop-shaped storage-discharge relationship. Koussis (1976) was among the first to propose a criterion for space interval or grid size to be used in the Muskingum flood routing. However, he assumed  $X$  to be constant on the grounds that computations were relatively insensitive to this parameter.

In the development of its HEC-1 computer program, the Hydrologic Engineering Center (1982) took  $X = 0.3$  and estimated  $K$  from the mean velocity. In order to make the routed and observed hydrographs comparable,  $K$  was adjusted as necessary. Ponce (1979) considered a simplified form of the Muskingum method by taking  $X = 0$  and  $K/\Delta t = 1$ , where  $\Delta t$  is the time interval. Ponce and Yevjevich (1978) allowed the parameters  $K$  and  $X$  to vary in space and time and computed them for each computational cell using three-point and four-point numerical methods. Ponce and Theurer (1982) calculated the Muskingum parameters based on channel and grid characteristics. Based on numerical experimentation, they found an upper limit to the space step if accuracy was to be preserved.

In this study, the reach travel time  $K$  and the weighting factor  $X$  were derived from a simplified form of the St. Venant equations.  $K$  was a function of storage, discharge and other hydraulic characteristics, that is,  $K = w/[\beta Q^{x(2m+1)(1+x)}]$ , and  $X$  was also a function of discharge and other hydraulic characteristics. The methods of parameter estimation employed here are different from the existing methods. Three versions of the Muskingum method with variable parameters are suggested, in which the parameters were determined either by using a direct search method for inflow-outflow data, or by using physical characteristics of the river reach. These versions were tested using three data sets and were also compared with the conventional Muskingum method.

#### THEORETICAL BASIS FOR VARIABLE PARAMETERS

Unsteady flow in open channels can be represented by the St. Venant equations of continuity

$$\frac{\partial A}{\partial t} + \frac{\partial Q}{\partial x} = 0 \quad (8)$$

and momentum

$$-\frac{\partial Z}{\partial x} = \frac{1}{g} \frac{\partial V}{\partial t} + \frac{V}{g} \frac{\partial V}{\partial x} + \frac{V^2}{C^2 R} \quad (9)$$

where  $A$  is the cross-sectional area of flow,  $V$  is the average velocity of the flow cross-section,  $Q$  is the discharge,  $Q = AV$ ,  $Z$  is the water level,  $g$  is the

gravitational acceleration,  $R$  is the hydraulic radius, and  $C$  is the Chezy's coefficient. For many flow situations, the inertia and acceleration terms can be considered much smaller than friction slope (Henderson, 1967), and can, therefore, be neglected. Equation (9) then reduces to

$$-\frac{\partial Z}{\partial x} = \frac{V^2}{C^2 R} \quad (10)$$

or

$$V = C\sqrt{RS} \quad (11)$$

where  $S$  is the water surface slope.

#### *Average reach travel time*

For shallow wide rectangular channels,  $R \approx h$ , and eqn. (11) becomes

$$V = C\sqrt{RS} = C\sqrt{hS} \quad (12)$$

$$A = PR \approx Ph$$

where  $P$  is the wetted perimeter of the flow cross section, and can be approximated for wide concave channels as

$$P = ah^{m-1} \quad (13)$$

where  $a$  is constant, and  $m$  is exponent with values between 1.2 and 2.0. Therefore

$$A = ah^{m-1} \times h = ah^m \quad (14)$$

Multiplying both sides of eqn. (14) by the reach length,  $L$ , and taking the average values of  $A$  and  $h$  over  $L$  as  $\bar{A}$  and  $\bar{h}$ ,

$$w = L\bar{A} = La(\bar{h})^m \quad (15)$$

By substituting eqn. (12) into eqn. (15) and eliminating  $\bar{h}$ , the following is obtained:

$$w = La \left[ \frac{V^2}{C^2 S} \right] = \frac{KaV^{2m+1}}{(C^2 S)^m} \quad (16)$$

According to hydraulics of open channel flow (Henderson, 1967)

$$Q = PR^{1+\alpha} C(S_0 + S_\Delta)^{1/2} \quad (17a)$$

$$V = CR^\alpha (S_0 + S_\Delta)^{1/2} \quad (17b)$$

where  $S_0$  is the bottom slope of the river,  $S_\Delta = S - S_0$  and  $\alpha$  is an exponent,  $\alpha = 0.5$  for the Chezy formula,  $\alpha = 2/3$  for the Manning formula.

By substituting eqn. (17b) into eqn. (17a) and eliminating  $R$ , the following is obtained:

$$V = P^{-x/(1+x)} C^{1/(1+x)} (S_0 + S_\Delta)^{1/[2(1+x)]} Q^{x/(1+x)} \quad (18)$$

By substituting eqn. (18) into eqn. (16) and simplifying,

$$\begin{aligned} w &= \frac{Ka}{(C^2 S)^m} V^{2m+1} = \frac{Ka}{(C^2 S)^m} \left[ P^{-x/(1+x)} C^{1/(1+x)} (S_0 + S_\Delta)^{1/[2(1+x)]} Q^{x/(1+x)} \right]^{2m+1} \\ &= \frac{Ka}{S^m P^{x(2m+1)/(1+x)}} C^{(1-2mx)/(1+x)} (S_0 + S_\Delta)^{(2m+1)/[2(1+x)]} Q^{x(2m+1)/(1+x)} \end{aligned} \quad (19a)$$

Let

$$\beta_1 = \frac{a C^{(1-2mx)/(1+x)} (S_0 + S_\Delta)^{(2m+1)/[2(1+x)]}}{S^m P^{x(2m+1)/(1+x)}}$$

Then eqn. (19a) reduces to

$$w = \beta_1 K Q^{x(2m+1)/(1+x)} \quad (19b)$$

$$K = \frac{w}{\beta_1 Q^{x(2m+1)/(1+x)}} \quad (20)$$

When  $[x(2m+1)]/(1+x) = 1.0$ , eqn. (20) reduces to eqn. (6) presented by Ponce (1979).

#### *Dimensionless weighting coefficient X*

For the Muskingum method,  $X$  can be represented (Kalinin and Milyukov, 1957) as

$$X = \frac{1}{2} - \frac{l}{2L} \quad (21)$$

where  $l$  is the characteristic length which can be expressed as

$$l = \frac{Q_0}{S_0} \left( \frac{\partial H}{\partial Q_0} \right) = \frac{Q_0}{S_0} \left[ \frac{\partial (H - H_0)}{\partial Q_0} \right] \quad (22)$$

where  $H_0$  is the bottom elevation,  $H$  is the water level, and  $Q_0$  is the steady-flow discharge.

For steady flow, the relationship between the water level and the discharge is

$$H - H_0 = h = b_0 Q_0^\beta \quad (23)$$

where  $h$  is the water depth,  $b_0$  is the constant, and  $\beta$  is an exponent. Taking

the derivative of eqn. (23)

$$\frac{\partial(H-H_0)}{\partial Q_0} = \frac{\partial}{\partial Q_0}[b_0 Q_0^\beta] = b_0 \beta Q_0^{\beta-1} \quad (24)$$

and substituting into eqn. (22) yield

$$l = \frac{Q_0}{S_0} \frac{\partial(H-H)}{\partial Q_0} = \frac{Q_0}{S_0} b_0 \beta Q_0^{\beta-1} = \frac{b_0 \beta}{S_0} Q_0^\beta \quad (25)$$

Substitution of eqn. (25) into eqn. (21) yields

$$X = \frac{1}{2} - \frac{l}{2L} = 0.5 - \frac{b_0 \beta Q_0^\beta}{2LS_0} \quad (26)$$

The relationship between steady-flow discharge  $Q_0$  and unsteady-flow discharge  $Q$  can be expressed (Henderson, 1967) as

$$Q = Q_0 \left(1 + \frac{S_\Delta}{S_0}\right)^{1/2}$$

In general,  $S_0 \gg S_\Delta$ , therefore,  $Q \approx Q_0$ , and eqn. (26) becomes

$$X = 0.5 - \frac{b_0 \beta}{2LS_0} Q^\beta = 0.5 - \alpha_1 Q^\beta \quad (27a)$$

When  $L = \Delta x$ ,  $h = b_0 Q^\beta$ , and  $q/c = \beta h$ , eqn. (27a) becomes

$$X = \frac{1}{2} \left(1 - \frac{q}{C \Delta x S_0}\right) \quad (27b)$$

Equation (27b) is the same as that presented by Ponce (1979) and Koussis (1976).

#### MUSKINGUM METHOD WITH VARIABLE PARAMETERS

Consider an  $(i+1)$ th period. Let  $I(i+1)$  be the inflow,  $Q(i+1)$  the outflow,  $w(i+1)$  the storage, and  $K(i+1)$  the corresponding travel time for that period. Equation (20) can be rewritten as

$$K(i+1) = \frac{\beta_1 w(i+1)}{[Q(i+1)]^{x(2m+1)(1+x)}} \quad (28)$$

In the same way, for the  $i$ th period

$$K(i) = \frac{\beta_1 w(i)}{[(Q(i))]^{x(2m+1)(1+x)}} \quad (29)$$

By dividing eqn. (28) by eqn. (29), the following is obtained:

$$\frac{K(i+1)}{K(i)} = \frac{w(i+1)}{w(i)} \left[ \frac{Q(i)}{Q(i+1)} \right]^{\alpha(2m+1)/(1+\alpha)} = \frac{w(i+1)}{w(i)} \left[ \frac{Q(i)}{Q(i+1)} \right]^{\gamma} \quad (30)$$

where  $\gamma = [\alpha(2m+1)]/(1+\alpha)$ . From the kinematic-wave approximation (Ponce, 1979),

$$Q = \alpha_2 A^{\beta_2}$$

Then

$$\frac{Q(i+1)}{Q(i)} = \left[ \frac{\alpha_2 A(i+1)}{\alpha_2 A(i)} \right]^{\beta_2} = \left[ \frac{LA(i+1)}{LA(i)} \right]^{\beta_2} = \left[ \frac{w(i+1)}{w(i)} \right]^{\beta_2} \quad (31)$$

By substituting eqn. (31) into eqn. (30)

$$\frac{K(i+1)}{K(i)} = \frac{w(i+1)}{w(i)} \left[ \frac{w(i)}{w(i+1)} \right]^{\alpha(2m+1)\beta_2/(1+\alpha)} = \left[ \frac{w(i+1)}{w(i)} \right]^{1 - [\alpha(2m+1)\beta_2/(1+\alpha)]} \quad (32)$$

Three interesting cases result from eqn. (32):

(1) When  $\alpha = 0.5$ ,  $m = 1.5$ ,  $\beta_2 = 0.75$ ,  $[\alpha(2m+1)\beta_2]/[1+\alpha] = 1.0$ , eqn. (32) simplifies to

$$\frac{K(i+1)}{K(i)} = 1.0 \quad (33)$$

Equation (33) expresses that the travel time  $K$  is independent of storage. In other words,  $w(i+1) = K[X(i+1)I(i+1) + [1 - X(i+1)]Q(i+1)]$ .

(2) When  $[\alpha(2m+1)\beta_2]/[1+\alpha] < 1.0$ , for example,  $\alpha = 0.5$ ,  $m = 1.3$ ,  $\beta_2 = 0.75$ ,

$$\frac{\beta_2 \alpha (2m+1)}{1+\alpha} = 0.9$$

$$\frac{K(i+1)}{K(i)} = \left[ \frac{w(i+1)}{w(i)} \right]^{0.10} \quad (34)$$

According to eqn. (34), the travel time  $K$  is directly proportional to storage  $w$ . In practice, when the channel cross-section approximates a rectangular shape and the channel roughness increases with the increase in water level, the average velocity of reach travel decreases with the increase in the water level, and the travel time  $K$  increases with the increase in storage.

(3) When  $[\beta_2 \alpha (2m+1)]/(1+\alpha) > 1.0$ , for instance,  $\alpha = 0.6$ ,  $m = 1.6$ ,  $\beta_2 = 0.75$ ,

$$\frac{\beta_2 \alpha (2m+1)}{1+\alpha} = 1.18$$

$$\frac{K(i+1)}{K(i)} = \left[ \frac{w(i+1)}{w(i)} \right]^{-0.18} \quad (35)$$

Equation (35) shows that travel time  $K$  is inversely proportional to storage  $w$ . In practice, when the cross-section approximates a triangular or parabolic shape, channel roughness decreases with the increase of the water level.

From eqn. (27a), the following formula can be obtained:

$$X(i+1) = 0.5 - \frac{b_0 \beta}{2LS_0} [Q(i+1)]^\beta \quad (27c)$$

$$X(i) = 0.5 - \frac{b_0 \beta}{2LS_0} [Q(i)]^\beta \quad (27d)$$

On subtracting eqn. (27d) from eqn. (27c)

$$X(i+1) - X(i) = \frac{b_0 \beta}{2LS_0} \{ [Q(i)]^\beta - [Q(i+1)]^\beta \} \quad (27e)$$

It is, thus, seen that the relationship between the travel time and storage depends on the hydraulic characteristics of the channel.

Three versions of the Muskingum method with variable parameters are now developed.

#### *Version 1: dependence of travel time on storage*

Equation (32) can be rewritten as

$$K(i+1) = K(i) \left[ \frac{w(i+1)}{w(i)} \right]^{1.0 - [\alpha(2m+1)\beta_2 / (1+\alpha)]} = K(i) \left[ \frac{w(i+1)}{w(i)} \right]^{\gamma_1} \quad (32a)$$

where  $\gamma_1 = 1.0 - [\alpha(2m+1)\beta_2 / (1+\alpha)]$ . Taking the finite difference approximation of eqn. (8), the water balance equation can be obtained as

$$w(i+1) = \frac{I(i+1) + I(i)}{2} \Delta t - \frac{Q(i+1) + Q(i)}{2} \Delta t + w(i) \quad (36)$$

When inflow  $I(i+1)$ ,  $w(i)$  and  $Q(i)$  are given,  $Q(i+1)$  can be calculated as follows:

- (1) Assume a value of  $Q^{(1)}(i+1)$ .
- (2) Calculate  $w(i+1)$  from eqn. (36) using  $Q^{(1)}(i+1)$ .
- (3) Calculate  $X(i+1)$  from eqn. (27e) using  $Q^{(1)}(i+1)$ .
- (4) Substitute the values of  $K(i+1)$  and  $X(i+1)$  into eqns. (2)–(5) to calculate the  $\hat{Q}(i+1)$ .
- (5) Compare  $\hat{Q}(i+1)$  with  $Q^{(1)}(i+1)$ . If the difference between  $\hat{Q}(i+1)$  and  $Q^{(1)}(i+1)$  is less than a pre-assigned error, then  $\hat{Q}(i+1)$  is accepted. If  $\hat{Q}(i+1) > Q^{(1)}(i+1)$ , then

$$Q^{(2)}(i+1) = Q^{(1)}(i+1) + \frac{\hat{Q}(i+1) - Q^{(1)}(i+1)}{2}$$

Otherwise

$$Q^{(2)}(i+1) = Q^{(1)}(i+1) - \frac{Q^{(1)}(i+1) - \hat{Q}(i+1)}{2}$$

(6) Substitute  $Q^{(2)}(i+1)$  for  $Q^{(1)}(i+1)$ , return to step (2) and continue to iterate, until an acceptable value of  $Q(i+1)$  is obtained.

*Version 2: Dependence of travel time on discharge and storage*

Ponce (1979) and Koussis (1976) proposed the Muskingum method with variable parameters. The travel time can be expressed as

$$K = \frac{\Delta x}{C} = \frac{\Delta x}{(\beta Q)/A} = \frac{A\Delta x}{\beta Q} \quad (6a)$$

With  $\Delta x = L$ , eqn. (6a) becomes

$$K = \frac{A\Delta x}{\beta Q} = \frac{AL}{\beta Q} = \frac{w}{\beta Q} \quad (6b)$$

When  $[\alpha(2m+1)]/(1+\alpha) = 1.0$ , eqn. (20) reduces to eqn. (6b). Therefore, eqn. (6b) is a special case of eqn. (20). The following procedure can be used to obtain the routed outflow:

- (1) Assume a value of  $Q^{(1)}(i+1)$ .
- (2) Calculate  $w(i+1)$  from eqn. (36).
- (3) Estimate  $K(i+1)$  from eqn. (30) using  $Q^{(1)}(i+1)$  and  $w(i+1)$ .

The rest of the steps are the same as for the first method described above.

*Version 3: dependence of travel time on discharge and storage*

Equation (30) can be rewritten as

$$K(i+1) = K(i) \left[ \frac{w(i+1)}{w(i)} \right] \left[ \frac{Q(i)}{Q(i+1)} \right]^{\alpha(2m+1)/(1+\alpha)} \quad (30)$$

The procedure for calculating  $Q(i+1)$  is similar to that in the first case. First,  $Q^{(1)}(i+1)$  is assumed. Then  $w(i+1)$  is calculated from eqn. (36),  $K(i+1)$  is estimated from eqn. (30) and so on.

## VALIDATION OF VARIABLE PARAMETER VERSIONS

### *Inflow-outflow data*

The three versions of the Muskingum method with variable parameters

TABLE 1

Parameters of the three versions for three data sets

Version	Parameters	Data set		
		I	II	III
1	$K(1)$	8.64	33.19	26.93
	$X(1)$	0.13	0.285	0.285
	$\gamma_1$	0.4	-0.06	-0.37
	$\alpha_1$	0.001	0.0014	0.0005
	$\beta$	0.5	0.5	0.5
	$w(1)$	1260	450000	450000
2	$K(1)$	16.15	23.74	18.97
	$X(1)$	0.05	0.275	0.275
	$\gamma$	1.0	1.0	1.0
	$\alpha_1$	0.001	0.0014	0.0005
	$\beta$	0.5	0.5	0.5
	$w(1)$	1260	450000	450000
3	$K(1)$	10.88	26.15	22.51
	$X(1)$	0.05	0.275	0.275
	$\gamma$	0.6	1.15	1.47
	$\alpha_1$	0.001	0.0014	0.0005
	$\beta$	0.5	0.5	0.5
	$w(1)$	1260	450000	450000

were applied to three actual sets of inflow-outflow data (Table 1). The first data set was taken from Wu et al. (1985), and was utilized for evaluating the optimal value of  $\alpha$  using a statistical  $t$ -test approach. The second data set was taken from Wang et al. (1987) and the third data set from Yang (1988). Both the second and third data sets were provided by the Yangtze River Planning Office in China. The Yangtze River is known for its rampaging floods which have caused damage of catastrophic proportions throughout history. The river reach under consideration is between Wan Xian, Sichuan Province, at the upstream end and Yichang, Hubei Province, at the downstream end. The three data sets are shown in Tables 2, 3 and 4, respectively.

#### *Determination of parameters*

The three versions of the Muskingum method, discussed above, are based on the nonlinear storage equation, which involves five common parameters:  $w(1)$ ,  $K(1)$ ,  $X(1)$ ,  $\alpha_1$  and  $\beta$ . In addition, the first version also includes an exponent  $\gamma_1 = 1.0 - [x(2m+1)\beta_2]/(1+\alpha)$ ; and the third version includes

TABLE 2

Muskingum method with variable parameters for data of Wu et al. (1985)

Recorded			Routed					
Time (h)	Inflow (cfs)	Outflow (cfs)	$K(t)$	$w(t)$ (cfs h <sup>-1</sup> )	$w'(t)$ (cfs h <sup>-1</sup> )	$Q(t)$ (cfs) TS	$Q(t)$ (cfs) W	$Q(t)$ (cfs) TE
0	56	70	—	1260.0	—	—	—	—
6	66	66	11.15	1221.9	723.1	64.7	66.6	65.6
12	250	102	12.81	1728.0	1335.0	82.6	74.0	48.0
18	550	185	16.82	3418.2	3430.5	154.0	135.0	68.9
24	595	265	20.48	5587.5	6303.4	267.9	251.0	183.1
30	420	335	22.12	6773.0	7963.5	351.9	338.4	301.4
36	295	370	22.10	6759.9	7930.8	367.5	355.6	342.6
42	210	368	21.26	6136.9	6995.0	345.4	335.4	339.0
48	147	310	19.99	5261.7	5690.4	303.6	298.3	313.3
54	100	245	18.50	4334.2	4327.6	252.6	254.7	276.9
60	74	200	16.98	3498.8	3128.4	199.9	211.0	235.8
66	60	165	15.63	2841.1	2212.5	153.4	172.8	197.3
72	51	132	14.52	2363.7	1573.4	116.8	141.4	164.4
78	46	100	13.67	2035.2	1150.0	89.7	116.3	136.9

TS: for the results obtained from this study;  $SM = 2730.4$ ,  $\Delta t = 6$  h.W: for the results obtained from Wu et al. (1985);  $SM = 5525.6$  where  $X = 0.1$ ,  $K = 20.9$  h,  $\Delta t = 6$  h.TE: for the results obtained by graphical procedure of trial and error;  $SM = 31566.0$  where  $X = 0.2$ ,  $K = 26.7$  h,  $\Delta t = 6$  h.

$\gamma = [\alpha(2m+1)]/(1+\alpha)$ . If the hydraulic characteristics of the channel reach are known, then the exponent  $\gamma_1$  or  $\gamma$  can be estimated from  $\alpha$ ,  $\beta_2$  and  $m$ ;  $\alpha_1 = (b_0\beta)/(2LS_0)$  and  $\beta$  can be determined from the stage-discharge curve of steady flow of the channel. The initial storage of reach  $w(1)$  can be determined from the initial inflow, outflow and the length or the corresponding travel time of the reach. Therefore, the parameters to be determined in the three versions are similar to those in the conventional Muskingum method, that is,  $K(1)$  and  $X(1)$ . If the hydraulic characteristics of the channel reach are unknown, then  $\gamma_1$ ,  $\beta$  or  $\gamma$  are to be estimated from observed inflow and outflow hydrographs. Since the parameters to be estimated are only a few, the direct search method was used to obtain their optimum values by minimizing the sum of the squares of differences between observed and computed outflows.

The direct search methods require evaluation of only the objective function and do not use the partial derivatives of the function in finding the minimum. These methods are most suitable for simple problems involving a relatively

TABLE 3

Muskingum method with variable parameters for data of Wang et al. (1987)

Recorded			Routed						
Time	Inflow ( $\text{m}^3 \text{s}^{-1}$ )	Outflow ( $\text{m}^3 \text{s}^{-1}$ )	$X(t)$	$K(t)$ (h)	$w(t)$ ( $\text{m}^3 \text{s}^{-1} \text{h}^{-1}$ ) ( $10^3$ )	$w'(t)$ ( $\text{m}^3 \text{s}^{-1} \text{h}^{-1}$ ) ( $10^3$ )	$Q(t)$ ( $\text{m}^3 \text{s}^{-1}$ ) SV	$Q(t)$ ( $\text{m}^3 \text{s}^{-1}$ ) W	$Q(t)$ ( $\text{m}^3 \text{s}^{-1}$ ) TE
7.27	17900.0	17900.0	0.24	23.74	454.8	424.1	17900.0	17900.0	17900.0
28	18200.0	18000.0	0.239	26.13	609.0	567.9	18000.0	18000.0	17994.8
29	25700.0	18100.0	0.233	29.17	879.37	812.9	18952.0	19287.0	20494.9
30	36500.0	23700.0	0.205	30.11	1008.3	919.4	24878.6	25079.0	27198.5
31	38700.0	32700.0	0.172	27.39	993.7	904.6	33264.8	32521.0	33773.4
8.1	35700.0	36300.0	0.161	26.17	899.7	818.9	36388.4	35641.0	35939.4
2	30500.0	35400.0	0.168	26.29	841.6	764.8	34493.7	34486.0	34144.6
3	28400.0	31800.0	0.182	27.28	962.86	874.8	31000.1	31358.0	31177.1
4	35300.0	30200.0	0.184	29.31	1080.8	979.5	30037.6	30510.0	31602.4
5	39100.0	35100.0	0.168	28.87	1125.3	1018.1	34007.9	33989.0	35140.7
6	39200.0	38300.0	0.157	28.05	1130.76	1022.96	37299.5	36963.0	37675.0
7	38300.0	38400.0	0.154	28.00	1111.44	1005.5	38089.6	37911.0	38354.5
8	36800.0	37000.0	0.156	28.17	1096.7	992.07	37665.4	37580.0	37846.0
9	36000.0	36300.0	0.159	28.59	1337.2	1209.7	3667.8	36644.0	36932.0
10	48300.0	38800.0	0.153	30.10	1770.3	1589.2	38135.7	38117.0	40230.3
11	65400.0	47900.0	0.123	29.39	1993.3	1767.4	47886.9	47205.0	50735.8
12	67700.0	58400.0	0.0896	27.39	1888.4	1672.4	59521.0	58890.0	60732.1
13	56800.0	61000.0	0.0811	26.65	1692.9	1497.5	61968.9	62204.0	61691.6
14	47500.0	56300.0	0.097	27.34	1457.5	1284.5	56045.3	56789.0	55660.2
15	37800.0	47800.0	0.122	28.48	1227.6	1075.4	47986.7	48646.0	47436.3
16	29600.0	38900.0	0.150	29.86	1043.4	907.4	39616.0	39918.0	38753.4
17	23900.0	31500.0	0.179	31.68	964.5	834.4	32001.7	32098.0	31165.9
18	23200.0	26000.0	0.199	33.91	1147.5	992.2	26696.6	26612.0	26351.8
19	33100.0	24500.0	0.204	38.50	1491.4	1281.3	25116.7	25954.0	27488.5
20	45200.0	30300.0	0.181	39.81	1736.98	1472.2	30262.5	32445.0	34859.9
21	49500.0	39500.0	0.150	36.89	1715.7	1448.5	39070.6	40979.0	42755.0
22	42900.0	43800.0	0.134	34.56	1583.9	1337.0	43938.8	44802.0	44932.6
23	36300.0	41200.0	0.141	34.50	1514.8	1276.5	42119.8	42027.0	41561.8
24	35300.0	38600.0	0.154	35.78	1551.2	1306.7	38396.8	37883.0	37919.7
25	38200.0	36100.0	0.159	37.25	1518.7	1279.3	36668.1	36463.0	37180.3
26	31300.0	34900.0	0.165	36.95	1313.4	1104.6	35466.7	34946.0	34713.9
28	27500.0	31800.0	0.176	37.72	1219.0	1023.3	32443.9	31724.0	31354.9
29	25000.0	28700.0	0.189	38.88	1183.0	991.64	29237.9	28419.0	28128.0

SV: the results obtained from the special version yield  $SM = 15\,507\,000.0$ ,  $\Delta t = 24$  h.W: the results obtained by Wu et al. (1985),  $SM = 26\,211\,660.0$ ,  $X = 0.17$ ,  $K = 30.9$  h.TE: the results obtained by graphical method of trial and error yield  $SM = 88\,740\,000.0$ ,  $X = 0.0$ ,  $K = 26.0$  h.

TABLE 4

Muskingum method with variable parameters for data of Yang et al. (1988)

Recorded			Routed			
Time	Inflow	Outflow	TV		O	TE
			$K(t)$	$Q(t)$		
7.2	21300.0	22200.0	22.67	22000.0	22000.0	22200.0
0.14	27900.0	22800.0	27.78	21646.9	22680.0	22962.0
3.2	38800.0	23400.0	24.90	23671.4	26700.0	27693.0
14	47300.0	30100.0	20.63	30680.3	33900.0	35305.0
4.2	52000.0	39900.0	18.03	39825.3	41170.0	42678.0
14	53800.0	46800.0	16.84	47049.2	46760.0	48057.0
5.2	52700.0	50900.0	16.64	50858.6	50080.0	50953.0
14	48900.0	51100.0	17.05	51191.6	50830.0	51179.0
6.2	43400.0	49200.0	18.10	48930.6	49110.0	48906.0
14	37800.0	44800.0	19.36	44751.8	45300.0	44871.0
7.2	32000.0	39900.0	20.86	40127.3	40890.0	39951.0
14	26900.0	34900.0	22.77	35298.6	35790.0	34688.0
8.2	23400.0	30600.0	24.64	30638.4	30920.0	29817.0
14	21400.0	26700.0	26.21	26923.2	26980.0	25970.0
9.2	19600.0	23700.0	27.67	24168.4	23950.0	23159.0
14	18600.0	21800.0	28.02	22000.0	21670.0	21046.0
10.2	17200.0	20100.0	28.69	20675.4	19960.0	19459.0
14	16400.0	18900.0	29.64	19288.2	18490.0	18087.0
11.2	16400.0	17800.0	30.40	18101.2	17460.0	17175.0
14	17000.0	17300.0		17434.0	17020.0	16870.0

TV: the results from this version,  $SM = 3\ 004\ 235.0$ ,  $\Delta t = 12$  h.O: the results obtained from the method of optimizing  $X$  value yield  $SM = 31\ 225\ 100.0$ ,  $X = 0.123$ ,  $K = 20.92$  h,  $\Delta t = 12$  h.TE: the results obtained by graphical method of trial and error yield  $SM = 58\ 656\ 232.0$ ,  $X = 0.10$ ,  $K = 18$  h.

small number of parameters. All the direct search methods are iterative in nature and hence they require an initial point  $Y_i$  to start the iterative procedure, and differ from one another only in the method of generating the new point  $Y_{i+1}$  (from  $Y_i$ ) and in testing the point  $Y_{i+1}$  for optimality. In this study, the simplex method was used to optimize the parameters. The basic idea of this method is to compare the values of the objective function at the  $n+1$  vertices of a general simplex and move this simplex gradually towards the optimum point during the iterative process. The movement of the simplex is achieved by using three operations known as reflection, contraction and

expansion. A complete discussion of the simplex method can be found in Himmelblau (1972).

According to the general principle of determining the parameters mentioned above, the three versions of the Muskingum method were applied to the three data sets. The initial storage  $w(1)$  was estimated from the initial inflow, outflow and the reach length or the average travel time of the reach. The rating curve for the steady flow was used to determine  $b_0$ ,  $\beta$  and  $\alpha_1 = (b_0\beta)/(2LS_0)$ . Then the direct search method was used to optimize  $K(1)$ ,  $X(1)$ ,  $\gamma_1$  or  $\gamma$ . For the second (special) version,  $\gamma = 1.0$ , only  $K(1)$  and  $X(1)$  needed to be optimized. The parameters of the three versions for three data sets are listed in Table 1 which shows that the initial storage  $w(1)$  is the same in the three versions developed. The values of  $X(1)$ , estimated using a direct search method, are the same except for the first version.

### *Flow routing*

Each version with the parameters obtained above, as well as the graphical trial and error method, were applied to all three data sets. For purposes of comparison of the methods, the sum ( $SM$ ) of the squares of the deviations ( $d$ ) between observed and computed outflows,  $SM = \sum d^2$ , was utilized.

#### *Application of version 1*

The results of flow routing by the first version are shown only for the first example data set to save space. Table 2 includes recorded inflow and outflow, as well as routed outflow obtained from the first version and the graphical method. Also included are the results of Wu et al. (1985). The results of calculations show that for  $\Delta t = 6$  h,  $SM = 2730.4$  for this version,  $SM = 5523.6$  for the method of Wu et al. (1985) with  $X = 0.1$  and  $K = 20.9$  h and  $SM = 31\,566.0$  by the graphical method with  $X = 0.2$  and  $K = 26.7$  h. Clearly for this data set the first version of the Muskingum method was the best of the three methods.

#### *Application of version 2 (special case)*

The results of flow routing by the special version are shown only for the second example data set. Table 3 includes inflow and outflow, as well as the routed outflow,  $X(1)$  and  $K(1)$  obtained from the special version and the graphical method. Also included are the results obtained from the method of Wu et al. (1985). The computed results show that for  $\Delta t = 24$  h,  $SM = 15\,507\,000.0$  for this version,  $SM = 26\,211\,660.0$  for the method of Wu et al. (1985) with  $X = 0.170$  and  $K = 30.9$  h and  $SM = 88\,740\,000.0$  by the graphical method with  $X = 0.0$ ,  $K = 26.0$  h. For this data set, the special version of the Muskingum method was the best of the three methods.

TABLE 5

Comparison of the results obtained from the three versions developed with those of the conventional trial-and-error method

Event	Routed outflow ( $\sum d^2$ )			
	First version	Second version (special)	Third version	Conventional trial-and-error method
1	2730.4 8.7%	4714.8 14.9%	3866.0 12.2%	31566.0 100%
2	17101110.0 19.25%	15507000.0 17.5%	13811000.0 15.56%	88740000.0 100%
3	8484371.0 14.46%	9119755.0 15.55%	3004235.0 5.12%	58656232.0 100%

#### *Application of version 3*

The results of calculation for the third version are shown only for third data set of Yang (1988). The routed results are given in Table 4. The flow was also routed using the method of optimizing  $X$  as well as the graphical method.  $SM = 3\,004\,235.0$  for this version,  $SM = 31\,225\,100.0$  for the method by Yang (1988) with  $X = 0.123$ ,  $K = 20.92$  h and  $SM = 58\,656\,232.0$  by the graphical method with  $X = 0.1$ ,  $K = 18$  h,  $\Delta t = 12$  h. Clearly, for this data set, the third version of the Muskingum method was the most accurate of the three methods.

#### *Discussion of the results*

The three versions of the Muskingum method with variable parameters were compared with the graphical method for the three data sets. The method presented by Ponce (1979) and Koussis (1976) is regarded as a special case of the method developed in this study. The results of this version were also compared with the other two versions, and are summarized in Table 5 which shows that the methods developed in this study are more accurate than the conventional trial and error method. For the third event, the squared error obtained from the third version was only 5.12% of that of the conventional trial and error method. Even for the worst of the three versions for three events, the error was 19.25% of that of the conventional trial and error method. Table 5 also shows a comparison of the results from the special version (second) presented by Ponce (1979) and Koussis (1976) with those from the other two versions. For the first data set, the first version gave the best result; for the second and third data sets, the third version produced the

best results. Only for the second data set was the result from the second version better than the first version.

It is well known that the routing accuracy of the conventional Muskingum method depends on the relationship between the storage  $w(i)$  and  $Q'(i)$  [ $Q'(i) = XI(i) + (1-x)Q(i)$ ]. If an optimum method is used to obtain the value  $X$  which makes the relationship between the storage  $w(i)$  and  $Q'(i)$  a straight line, then the routing result is the best that can be achieved by the conventional method; this is possible only under the condition that  $[\alpha(2m+1)\beta_2]/(1+\alpha) = 1.0$ .

In general,  $[\alpha(2m+1)\beta_2]/(1+\alpha)$  is not equal to 1.0, so that it is impossible to optimize the value of  $X$  to make the relation between  $w(i)$  and  $Q'(i)$  a straight line. In some channel reaches, the relation  $w(i)$  and  $Q'(i)$  is a curve in which case the reach travel time  $K$  is not constant.

The parameters  $K$  and  $X$  vary with time in this study. It is possible to make the relationship between the storage calculated from the water balance equation and that calculated from the storage equation  $w'(i+1) = K(i+1)\{X(i+1)I(i+1) + [1-X(i+1)]Q(i+1)\}$  plot as a straight line.

Figure 1 shows the relation between  $w$  and  $w'$  for the first flood event, where the ordinate is

$$w(i+1) = \frac{I(i+1) + I(i)}{2} \Delta t - \frac{Q(i+1) + Q(i)}{2} \Delta t + w(i)$$

and the abscissa is  $w'(i+1) = K(i+1)\{X(i+1)I(i+1) + [1-X(i+1)]Q(i+1)\}$  where

$$K(i+1) = K(i) \left[ \frac{w(i+1)}{w(i)} \right]^{0.40}$$

It can be seen that the data points from the first version are quite close to a straight line. The results from the conventional Muskingum method are also shown in Fig. 1, where the loop is formed by the data points.

Figure 2 shows the relation between  $w$  and  $w'$  for the second flood event of Changjiang River (Yangtze), where the abscissa is

$$w'(i+1) = K(i+1)\{X(i+1)I(i+1) + [1-X(i+1)]Q(i+1)\}$$

where

$$K(i+1) = K(i) \left[ \frac{w(i+1)}{w(i)} \right] \left[ \frac{Q(i)}{Q(i+1)} \right]^{1.15}$$

It can be seen that the data points almost lie on the straight line (if all the points lie exactly on a straight line, then the computed outflows will be just the same as the observed outflows). The relation of  $w$  with  $w'$  calculated from

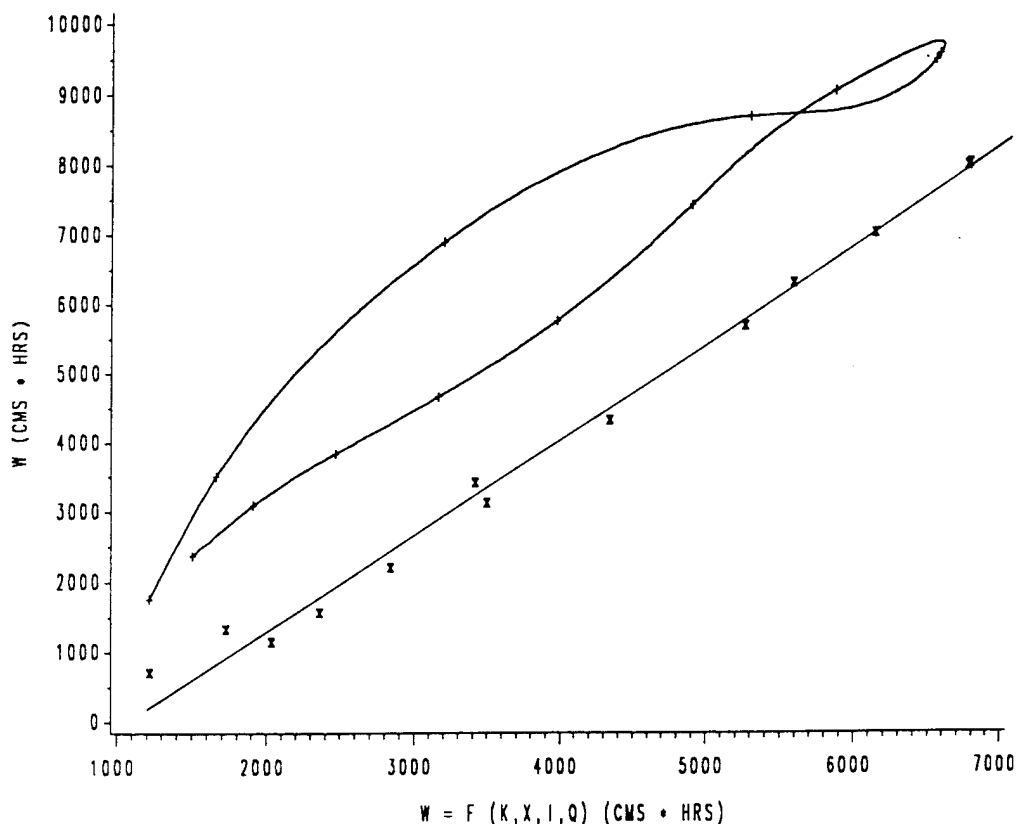


Fig. 1. Relationship between channel storage and  $w = F(K, X, I, Q)$  for event 1.

the conventional Muskingum method is also shown in Fig. 2, where a loop is formed by the points.

Figure 3 shows the third flood event of Changjiang River, where the abscissa is  $w'(i+1) = K(i+1)\{X(i+1)I(i+1) + [1 - X(i+1)]Q(i+1)\}$  where

$$K(i+1) = K(i) \left[ \frac{w(i+1)}{w(i)} \right] \left[ \frac{Q(i)}{Q(i+1)} \right]^{1.47}$$

It can be seen that the data points almost lie on the curve. The results from graphical trial and error methods are also shown in Fig. 3, where the shape of the curves formed by the data points calculated from the two methods are similar, in which case the reach travel time is not constant; therefore, the discharge of outflows estimated from this study are more accurate than the conventional Muskingum method in which the reach travel time is considered constant.

#### SUMMARY AND CONCLUSIONS

In this study, three versions of the Muskingum method with variable parameters were derived by simplifying the St. Venant equations for unsteady

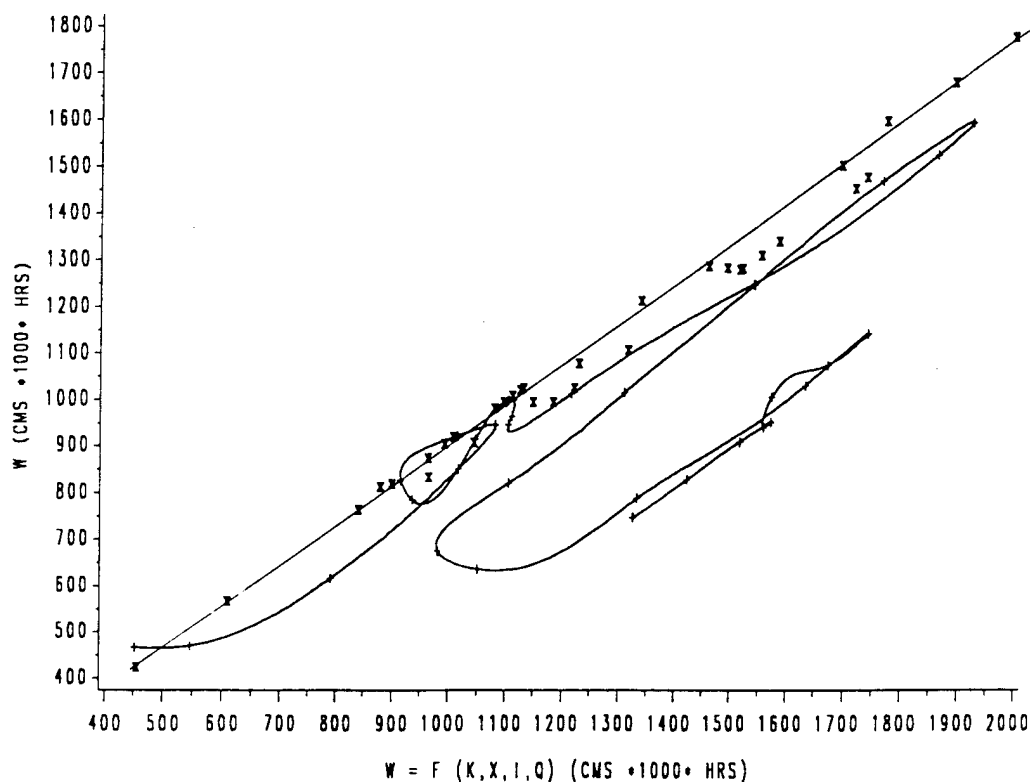


Fig. 2. Relationship between channel storage and  $w = F(K, X, I, Q)$  for event 2.

flow. These versions are simple to apply, and it is relatively easy to determine the parameters using a direct-search method. The following conclusions are drawn from this study.

(1) The relationship between the reach travel time and storage depends on the hydraulic characteristics of the channel reach. If  $[\alpha(2m+1)\beta_2]/(1+\alpha) < 1.0$ , then the relation between the travel time and storage is in direct proportion; if  $[\alpha(2m+1)\beta_2]/(1+\alpha) > 1.0$ , then it is in inverse proportion; if  $[\alpha(2m+1)\beta_2]/(1+\alpha) = 1.0$ , a special case of this relation does not exist. These relations between storage and travel time are identified by routing observed floods.

(2) The Muskingum method with variable parameters can overcome the drawback of the conventional graphical trial and error loop method or of optimum methods, which are inadequate to represent the storage hysteresis.

(3) The three versions of the Muskingum method are several times more accurate than the conventional trial and error method.

(4) The reach travel time which depends on the storage, channel characteristics and discharge is obtained from the simplification of the St. Venant equations, when the exponent of discharge  $[\alpha(2m+1)\beta_2]/(1+\alpha) = 1.0$ , eqn. (20) reduces to eqn. (6) presented by Ponce (1979) and Koussis (1976), which

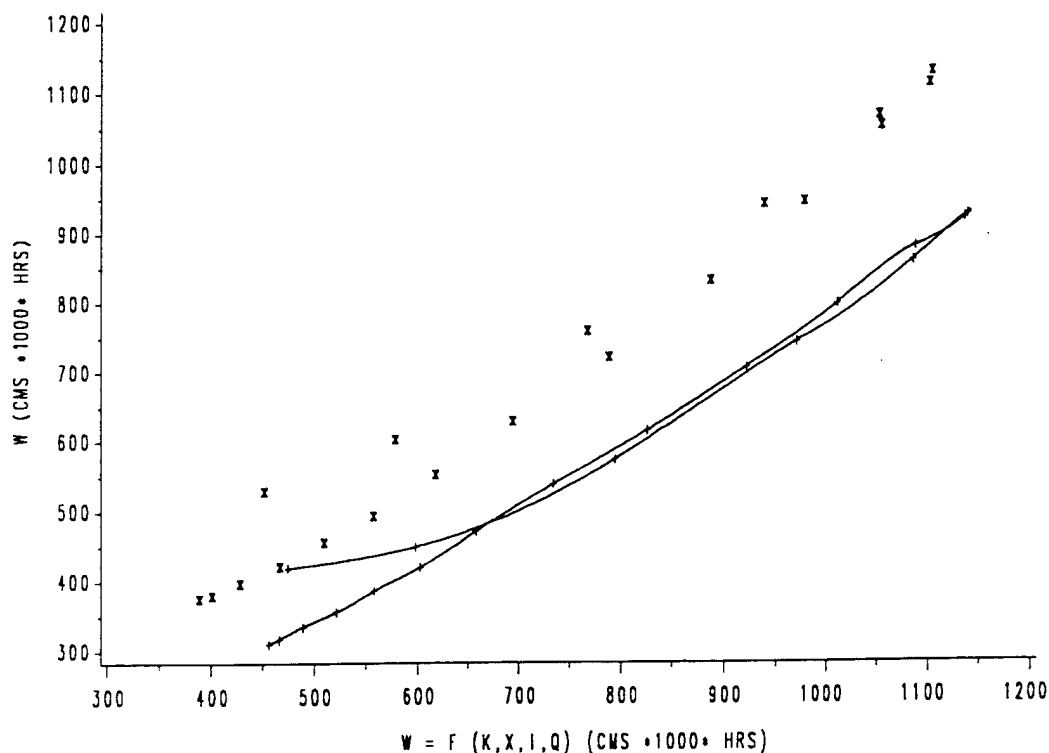


Fig. 3. Relationship between channel storage and  $w = F(K, X, I, Q)$  for event 3.

is regarded as a special case of the method developed. The results show that the special version is several times more accurate than the conventional trial and error method, but less accurate than the other two versions.

#### ACKNOWLEDGMENTS

The first author expresses his appreciation for financial support from the National Scientific Fund Committee of China. The authors received partial support from the project, A Continuum Method for Streamflow Synthesis, supported by Army Research Office through Southern University.

#### REFERENCES

- Apollov, B.A., Kalinin, G.P. and Komarov, V.D., 1969. Hydrologische prognosen (German translation from the Russian original), German Air Force.
- Cunge, J.A., 1969. On the subject of a flood propagation computation method, Muskingum method. *J. Hydraul. Res.*, 7(2): 205-230.
- Dooge, J.C.I., 1973. Linear theory of hydrologic systems. Technical Bulletin No. 1468. USDA Agricultural Research Service.
- Henderson, F.M., 1966. Open channel flow. Macmillan, New York.
- Himmelblau, D.M., 1972. Applied nonlinear programming. McGraw-Hill, New York.

- Hydrologic Engineering Center, 1982. Hydrologic analysis of ungaged watersheds using HEC-1. Training Document No. 15, U.S. Army Corps of Engineers, Davis, California.
- Kalinin, J.P. and Milyukov, P.I., 1957. On the computation of unsteady flow in open channels. *Meteorologiya Jidro logiya zhurnal*, Leningrad, 10: 10-18.
- Koussis, A., 1976. An approximate dynamic flood routing method. Proceedings of the International Symposium on Unsteady Flow in Open Channels, Paper L1, Newcastle-upon-Tyne, UK, pp. L1-1-L1-12.
- Koussis, A., 1978. Theoretical estimation of flood routing parameters. *ASCE J. Hydraul. Div.*, 104(HY1): 109-115 (Proc. Paper 13456).
- Koussis, A., 1980. Comparison of Muskingum method difference schemes. *ASCE J. Hydraul. Div.*, 106(HY5): 925-929.
- Koussis, A., 1983. Unified theory for flood and pollution routing. *J Hydraul. Eng.*, 109(12): 1652-1664.
- McCarthy, G.T., 1938. The unit hydrograph and flood routing. Conf. North Atlantic Division, US Army Corps. of Engineers.
- Miller, W.A. and Cunge, J.A., 1975. Simplified Equations of Unsteady Flow. In: K. Mahmood and V. Yevjevich (Editors), *Unsteady Flow in Open Channels*. Water Resources Publications, Fort Collins, CO, pp. 183-257.
- Ponce, V.M., 1979. Simplified Muskingum routing equation. *ASCE J. Hydraul. Div.*, 105(HY1): 85-91.
- Ponce, V.M. and Yevjevich, V., 1978. The Muskingum-Cunge method with variable parameters. *ASCE J. Hydraul. Div.*, 104(HY12): 1663-1667.
- Ponce, V.M. and Theurer, F.D., 1982. Accuracy criteria in diffusion routing. *ASCE J. Hydraul. Div.*, 108(HY6): 747-757.
- Singh, V.P., 1988. *Hydrologic Systems*, Vol. 1. Rainfall-Runoff Modeling. Prentice Hall, Englewood Cliffs, NJ.
- Wang, G.T., Yu, Y.-S. and Wu, K., 1987. Improved flood routing by ARMA modeling and Kalman filter technique. *J. Hydrol.*, 93: 175-190.
- Weinmann, P.E. and Laurenson, E.M., 1979. Approximate flood routing methods: a review. *ASCE J. Hydraul. Div.*, 105(HY12): 1521-1536.
- Wu, Jy.S., King, E.L. and Wang, M., 1985. Optimal identification of Muskingum routing coefficients. *Water Resour. Bull.*, 21(3): 417-421.
- Yang, R.F., 1988. Research on method of estimating optimum parameters for Muskingum method. *Hydrology No. 4* (in Chinese), pp. 35-40.

[4]

## A rainfall–runoff model for small watersheds

Guang-Te Wang<sup>a</sup>, V.P. Singh<sup>b</sup> and F.X. Yu<sup>b</sup>

<sup>a</sup>*Institute of Geography, Chinese Academy of Sciences, 100101 Beijing, People's Republic of China*

<sup>b</sup>*Department of Civil Engineering, Louisiana State University, Baton Rouge, LA 70803-6405, USA*

(Received 19 November 1991; revision accepted 6 February 1992)

### ABSTRACT

Wang, G.-T., Singh, V.P. and Yu, F.X., 1992. A rainfall–runoff model for small watersheds. *J. Hydrol.*, 138: 97–117.

A rainfall–runoff model was developed by combining the excess-rainfall process and the runoff-concentration process. The excess rainfall was modeled by using the two-parameter Green–Ampt infiltration approach. A six-parameter linear–discrete model was used to model the runoff hydrograph. The infiltration parameters were estimated by using the simplex method, and the runoff parameters by least squares. The model was calibrated on ten watersheds and verified on seven. The model-simulated runoff hydrographs were in close agreement with observed runoff hydrographs.

### INTRODUCTION

For the purposes of modeling, the rainfall–runoff process is divided into the excess-rainfall process and the runoff-concentration process. The former focuses on estimating the infiltration process, and the latter on calculating the outlet hydrograph from excess rainfall using a mathematical model.

In 1911, Green and Ampt developed an infiltration equation, with the horizontal wetting front separating the wetted and dry parts of the soil during soil-water movement. Many infiltration formulae have since been proposed (see Singh (1989) for a recent review). The Green–Ampt (GA) equation, however, has lately been receiving a great deal of attention. Mein and Larson (1973) and Swartzendruber (1974) developed modified versions of the GA equation for determining the ponding time and modeled infiltration during a steady rain. Chu (1978) extended their analysis to unsteady rainfall events. He used two time parameters (the ponding time and the pseudotime) to modify the GA equation, to describe infiltration during an unsteady rain.

After excess rainfall is calculated, the runoff hydrograph can then be

---

Correspondence to: G.-T. Wang, Department of Civil Engineering, Louisiana State University, Baton Rouge, LA 70803-6405, USA.

estimated using a suitable runoff model. In 1957, Nash reported a two-parameter linear model with  $N$  reservoirs in series. The Nash model has been extensively used in applied hydrology. Most runoff models are continuous-time models (Singh, 1988), although discrete-time models have also been developed. O'Connor (1982) used the transfer function approach to derive discretely coincident forms of several linear, time-invariant models. Wang and Yu (1986) suggested a more general linear discrete model from which some of the existing models can be derived as special cases. These models attempt to establish a relationship between excess-rainfall, calculated using an infiltration formula, and the resulting direct runoff hydrograph.

Mays and Taur (1982) used a nonlinear programming formulation to determine simultaneously the coordinates and the period of excess rainfall. Wang and Yu (1990), and Wang et al. (1992) modeled the rainfall-runoff process by considering losses. In these models, the number of interval losses computed was equal to the number of periods of rainfall intervals used. In practical applications, however, it is difficult to use these models for predicting the runoff hydrograph, because the number of rainfall excess intervals of one event may not be exactly equal to that for another. Therefore, the computed interval losses cannot be used for predicting another event.

In this study, an effort was made to combine the excess-rainfall process and the runoff-concentration process into a unified process. The computation of excess rainfall during an unsteady rain has been given by Chu (1978). With the use of measured rainfall hyetographs and runoff hydrographs, optimal values of infiltration and runoff model parameters were simultaneously estimated.

#### RAINFALL-RUNOFF PROCESS DURING UNSTEADY RAIN

##### *Determination of excess rainfall*

For many rainfall events, there is an initial period during which all of the rainfall infiltrates into the soil. During this period, the capacity of the soil to absorb water decreases until it becomes less than the rainfall intensity. At this point, the ground surface becomes ponded with water. As rainfall continues, the surface pondage exceeds the surface retention capacity and the runoff begins. Under ponded conditions, the infiltration process is independent of the time distribution of rainfall. For an unsteady rainfall event, there may be several periods during which the rainfall intensity exceeds the current infiltration rate and ponding may appear and disappear.

The GA equation describes the infiltration process under a ponded surface, and can be written (Mein and Larson, 1973) as

$$f_p = \frac{dF}{dt} = K \left( 1 + \frac{SM}{F} \right) \quad (1)$$

where  $f_p$  is the infiltration capacity ( $\text{mm min}^{-1}$ ),  $K$  is the average hydraulic conductivity of the wetted zone ( $\text{mm min}^{-1}$ ),  $S$  (mm) and  $M$  are the difference of the average capillary potential and the difference of the average soil moisture before and after wetting, respectively, expressed as volume fraction of soil (volume/volume), and  $F$  is the cumulative infiltration (mm).

If we let  $t_p$  be the time at which surface ponding starts from a stage without surface ponding,  $F_0$  be the cumulative infiltration at  $t = t_p$ , and  $F_p$  be the cumulative infiltration under ponding, integration of (1) from  $t = t_p$  to  $t$  and from  $F = F_0$  to  $F_p$ , and rearrangement, yield.

$$\frac{F_p}{SM} - \ln \left( 1 + \frac{f_p}{SM} \right) - \frac{F_0}{SM} + \ln \left( 1 + \frac{F_0}{SM} \right) = \frac{K(t - t_p)}{SM} \quad (2)$$

In practice, the duration of a rainfall event is divided into many short periods in such a way that within each period, the rainfall intensity is essentially constant. For such a case,

$$i(t) = \frac{P(t_n) - P(t_{n-1})}{t_n - t_{n-1}} = I = \text{constant}, \quad n = 0, 1, 2, \dots \quad (3)$$

where  $i(t)$  is the rainfall intensity,  $t_n - t_{n-1}$  is the  $n$ th time interval (short),  $P(t_n)$  is the cumulative rainfall in millimeters at the end of the  $n$ th time interval, and  $P(t_{n-1})$  is the cumulative rainfall in millimeters at the beginning of the  $n$ th time interval.

The variable cumulative rainfall  $P(t)$  within a short period can be written as

$$P(t) = P(t_{n-1}) + \int_{t_{n-1}}^t i(t) dt = P(t_{n-1}) + (t - t_{n-1})I \quad (4)$$

Combining (2), (3) and (4), and letting  $t = t_p$ , we obtain the ponding time for this special case:

$$f(t) = i(t) < f_p \quad (5)$$

$$\frac{dR}{dt} = 0 \quad (6)$$

Assuming that the evaporation during a rain period is negligible, the infiltration process during an unsteady rain can now be separated into two stages. In the first stage, there is no surface ponding for the period from  $t_{n-1}$  to  $t_n$ . In this period, the infiltration rate and cumulative rainfall excess  $R(t)$  satisfy

$$R(t) = R(t_{n-1}), \quad t_{n-1} \leq t \leq t_n \quad (7)$$

The cumulative infiltration can be obtained by the mass-balance principle as

$$F(t) = P(t) - R(t_{n-1}) \quad (8)$$

In the second stage, there is surface ponding for the period from  $t_{n-1}$  to  $t_n$ . In this period, the infiltration rate is given by (1), and the cumulative rainfall excess  $R(t)$  can be expressed using the mass-balance principles:

$$R(t) = P(t) - F_p - D, \quad t_{n-1} \leq t \leq T_n \quad (9)$$

where  $D$  is the surface retention capacity. Let us define a time constant  $t_s$  called pseudotime

$$t_s = \frac{F_0}{K} - \frac{SM}{K} \ln \left( 1 + \frac{F_0}{SM} \right) \quad (10)$$

$$\frac{F_p}{SM} - \ln \left( 1 + \frac{F_p}{SM} \right) = K \frac{t - t_p + t_s}{SM} \quad (11)$$

Surface ponding occurs when rainfall intensity equals the infiltration capacity, which is defined as the rate of infiltration that reaches its maximum capacity for a given type of soil and moisture condition, so that

$$i(t_p) = f_p \quad (12)$$

with use of (12), (1) becomes

$$F_p = \frac{KSM}{i(t_p) - K} \quad (13)$$

Application of (8) at the time of ponding to (13) yields

$$P(t_p) - R(t') = \frac{KSM}{i(t_p) - K}, \quad i > K \quad (14)$$

Equation (14) is an implicit expression for determining the ponding time  $t_p$ .

After  $t_p$  is determined, the pseudotime  $t_s$  can then be calculated by (1), where

$$F_0 = P(t_p) - R(t'), \quad t_{n-1} < t' < t_n \quad (15)$$

For a constant rainfall intensity, we can write

$$i(t) = \frac{P(t_n) - P(t_{n-1})}{t_n - t_{n-1}} = I = \text{constant} \quad (16)$$

The ponding time can be obtained simply by combining (4) and (14) and letting  $t' = t_{n-1}$  and  $t = t_p$ :

$$t_p = \frac{\frac{KSM}{I - K} - P(t_{n-1}) + R(t_{n-1})}{I} + t_{n-1} \quad (17)$$

*Discrete linear model*

The discrete excess rainfall-runoff model is applied to calculate the hydrograph of a watershed from the excess rainfall estimated as above. The model can be written as

$$Q(t) = a_1 Q(t-1) + a_2 Q(t-2) + \dots + a_p Q(t-p) + b_0 I(t) + b_1 I(t-1) + \dots + b_q I(t-q) \quad (18)$$

where  $Q(t)$  and  $I(t)$  are the direct runoff and excess rainfall at time  $t$ , respectively, and  $a$ s and  $b$ s are the time-invariant parameters. A complete discussion of the discrete linear model has been given by Wang and Yu (1986) and Wang et al. (1992).

## DETERMINATION OF MODEL PARAMETERS

The rainfall-runoff process model includes two groups of parameters. In one group are soil infiltration process parameters  $K$ ,  $S$  and  $M$ . Parameters  $S$  and  $M$  always appear together; thus, the product  $SM$  can be treated as one parameter which represents the antecedent soil moisture condition. This reduces to two the number of parameters for the soil infiltration process. The number of parameters for excess rainfall-runoff process depends on the order of the model. In general, six parameters of excess rainfall-runoff process model suffice to calculate the hydrograph. Therefore, for the rainfall-runoff process model, eight parameters are to be estimated from measured rainfall hyetographs and runoff hydrographs.

In this paper, a direct search method was used to estimate the infiltration parameters ( $K$  and  $SM$ ). The excess rainfall hyetograph was then calculated, and the excess rainfall-runoff model parameters were determined by minimizing the sum of squares of differences between the observed and calculated discharges. The parameter estimation method can be described in the following steps:

(1) A rainfall hyetograph is divided into several periods during which the rainfall intensity is constant and the value of retention capacity  $D$  is selected.

(2) Starting from the first period, the rainfall intensity  $I(t)$  is compared with  $K$ . If  $I(t)$  is less than  $K$ , then excess rainfall  $R(t) = 0$  and the cumulative infiltration  $F(t) = P(t)$ . If  $I(t)$  is greater than  $K$ , then the surface condition indicator can be estimated as

$$C_u = P(t) - R(t-1) - \frac{KSM}{I(t) - K} \quad (19)$$

If  $C_u$  is less than zero, excess rainfall  $R(t) = 0$ , and  $F(t) = P(t)$ . If  $C_u$  is greater

than zero, then the ponding time can be calculated from (17), and the cumulative rainfall prior to ponding time can be computed as

$$t_p = \frac{K \frac{SK}{I - K} - P(T_{n-1}) + R(t_{n-1})}{I} + T_{n-1} \quad (20)$$

$$P(t_p) = P(t - 1) + [t_p - (t - 1)\Delta t]I(t) \quad (21)$$

and we shift the time as

$$t_s = \frac{P(t_p) - R(t - 1)}{K} - \ln \left[ 1 + \frac{P(t_p) - R(t - 1)}{SM} \right] \frac{SM}{K} \quad (22)$$

The time on the shifted time-scale is

$$T = t_n - t_p + t_s \quad (23)$$

and  $F_p$  can be calculated as

$$\frac{F_p}{SM} - \ln \left( 1 + \frac{F_p}{SM} \right) = \frac{KT}{SM} \quad (24)$$

This formula is implicit in  $F_p$ , so the Newton-Raphson iteration can be used to estimate  $F_p$ . The cumulative excess rainfall is calculated as

$$R(t) = P(t) - F(t) - D \quad (25)$$

The excess rainfall is calculated for the next period, and so on.

(3) After the excess rainfall is estimated, the least-squares method can be used to determine the parameters of the excess rainfall-runoff model as

$$\beta = [a_1 a_2 a_3 b_0 b_1 b_2]^T = [A^T A]^{-1} A^T E \quad (26)$$

where

$$A = \begin{bmatrix} 0 & 0 & 0 & I(1) & 0 & 0 \\ Q(1) & 0 & 0 & I(2) & I(1) & 0 \\ Q(2) & Q(1) & 0 & I(3) & I(2) & I(1) \\ Q(3) & Q(2) & Q(1) & I(4) & I(3) & I(2) \\ \vdots & \vdots & \vdots & \vdots & \vdots & \vdots \\ \vdots & \vdots & \vdots & I(k) & I(k-1) & I(k-2) \\ \vdots & \vdots & \vdots & 0 & 0 & 0 \\ Q(m-1) & Q(m-2) & Q(m-3) & \vdots & \vdots & \vdots \end{bmatrix} \quad (27)$$

$$E = [Q(1)Q(2)Q(3) \dots Q(m)]^T \quad (28)$$

(4) We then calculate

$$F = \sum_{i=1}^m (Q_i - \hat{Q}_i)^2 \quad (29)$$

where  $\hat{Q}_i$  is the computed discharge at the  $i$ th time.

(5) According to the value of  $F$ , the values of  $K$  and  $SM$  are determined for the next iteration based on the principle of the simplex method. We then return to step (2). The details of computation steps are shown in the flow chart (Fig. 1).

Although there are eight parameters in the rainfall-runoff model, only two parameters, representing the infiltration process, are determined by iteration, and for this purpose it is convenient to use the simplex method. A detailed discussion of this method has been given by Himmelblau (1972).

#### ESTIMATION OF PARAMETERS OF EXCESS RAINFALL-RUNOFF PROCESS FROM MULTIPLE EVENTS

If data are available on several excess rainfall-runoff events, the average values of the model parameters can be estimated by using the least-squares method throughout. We assume that the first excess-rainfall hyetograph is

$$I_{11} I_{21} I_{31} \dots I_{n1} \quad (30)$$

and the corresponding runoff hydrograph is

$$Q_{11} Q_{21} Q_{31} \dots Q_{n1} \dots Q_{m1} \quad (31)$$

The second excess-rainfall hyetograph is

$$I_{12} I_{22} I_{32} I_{42} \dots I_{n2} \quad (32)$$

and corresponding runoff hydrograph is

$$Q_{12} Q_{22} Q_{32} Q_{42} \dots Q_{m2} \quad (33)$$

According to the least-squares method, the average model parameters are as follows:

$$\bar{\beta} = [\bar{a}_1 \bar{a}_2 \bar{a}_3 \bar{b}_0 \bar{b}_1 \bar{b}_2]^T = [B^T B]^{-1} B^T Y \quad (34)$$

where

$$B^T B = [A_1^T A_2^T] \begin{bmatrix} A_1 \\ A_2 \end{bmatrix} = A_1^T A_1 + A_2^T A_2 \quad (35)$$

$$B^T Y = [A_1^T A_2^T] \begin{bmatrix} Y_1 \\ Y_2 \end{bmatrix} = A_1^T Y_1 + A_2^T Y_2 \quad (36)$$

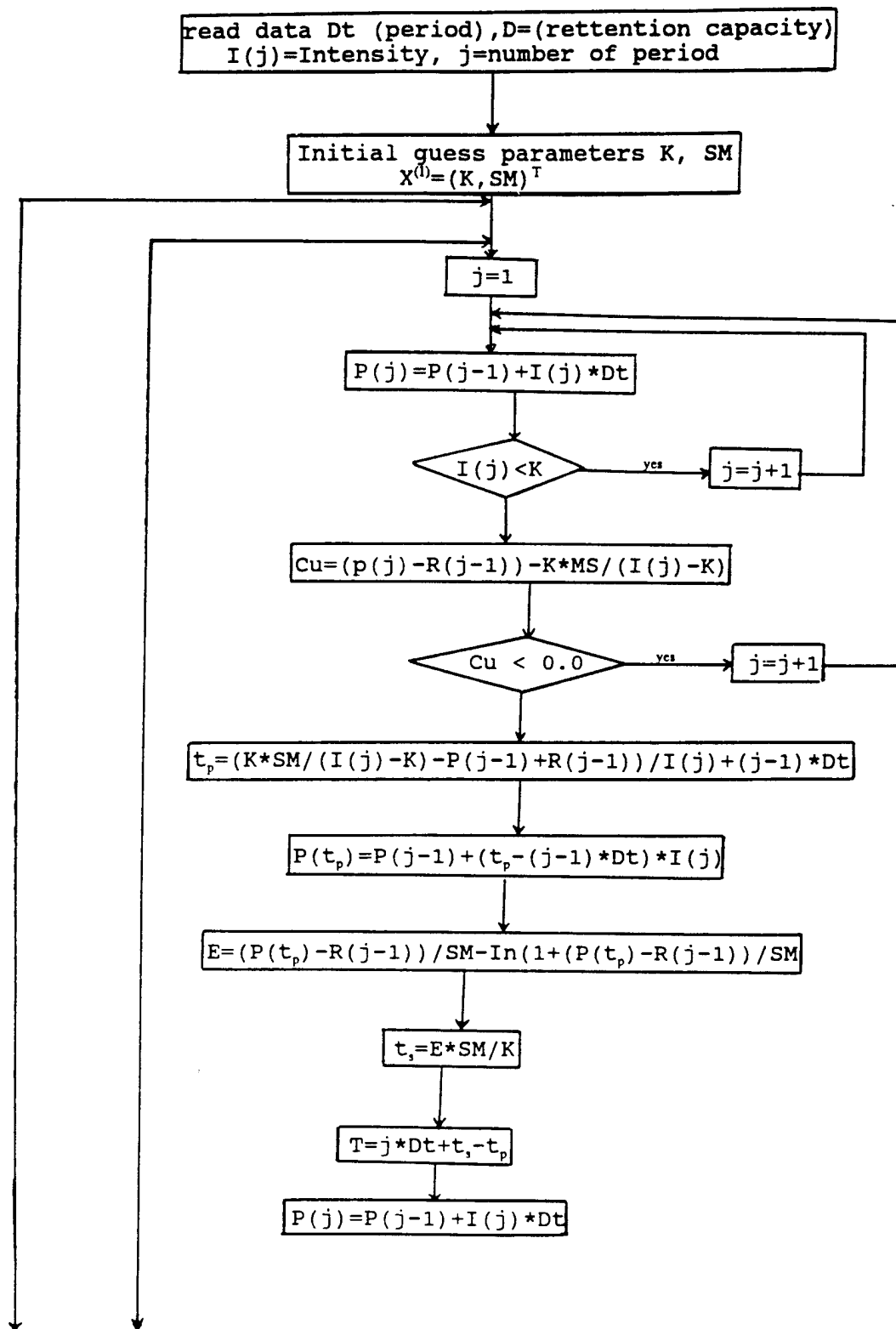
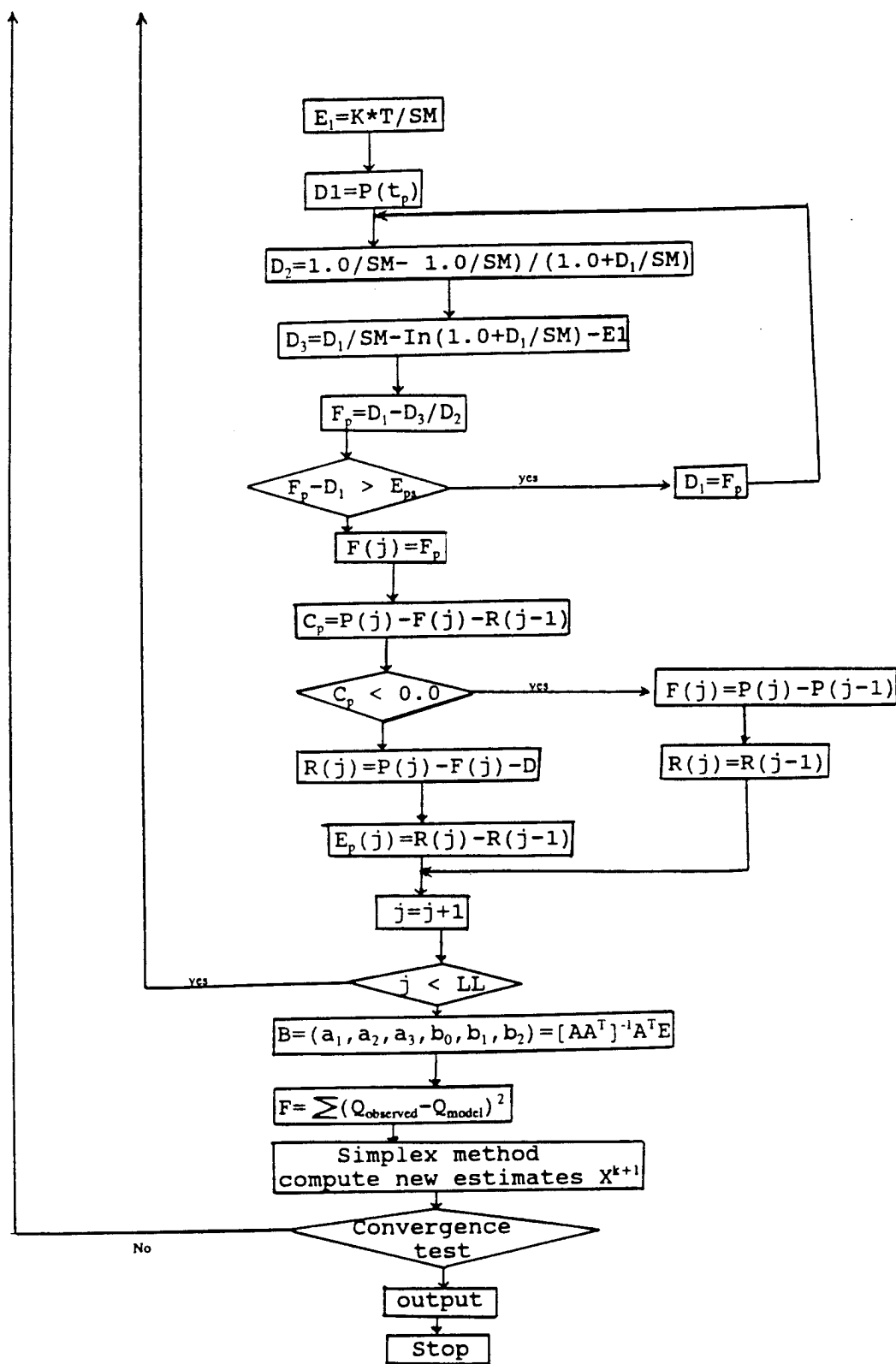


Fig. 1. Flow chart.



$$A_1 = \begin{bmatrix} 0 & 0 & 0 & I_{11} & 0 & 0 \\ Q_{11} & 0 & 0 & I_{21} & I_{11} & 0 \\ Q_{21} & Q_{11} & 0 & I_{31} & I_{21} & I_{11} \\ Q_{31} & Q_{21} & Q_{11} & I_{41} & I_{31} & I_{21} \\ \vdots & \vdots & \vdots & \vdots & \vdots & \vdots \\ \vdots & \vdots & \vdots & I_{n1} & I_{n-1,1} & I_{n-2,1} \\ \vdots & \vdots & \vdots & \vdots & \vdots & \vdots \\ Q_{m-1,1} & Q_{m-2,1} & Q_{m-3,1} & 0 & 0 & 0 \end{bmatrix} \quad (37)$$

$$A_2 = \begin{bmatrix} 0 & 0 & 0 & I_{12} & 0 & 0 \\ Q_{12} & 0 & 0 & I_{22} & I_{12} & 0 \\ Q_{22} & Q_{12} & 0 & I_{32} & I_{22} & I_{12} \\ Q_{32} & Q_{22} & Q_{12} & I_{42} & I_{32} & I_{22} \\ \vdots & \vdots & \vdots & \vdots & \vdots & \vdots \\ Q_{n-1,2} & Q_{n-2,2} & Q_{n-3,2} & I_{n2} & I_{n-1,2} & I_{n-2,2} \\ \vdots & \vdots & \vdots & \vdots & \vdots & \vdots \\ Q_{m-1,2} & Q_{m-2,2} & Q_{m-3,2} & 0 & 0 & 0 \end{bmatrix} \quad (38)$$

$$Y_1 = [Q_{11} \ Q_{21} \ Q_{31} \ \cdots \ Q_{m1}]^T \quad (39)$$

$$Y_2 = [Q_{12} \ Q_{22} \ Q_{32} \ \cdots \ Q_{m2}]^T \quad (40)$$

#### APPLICATION

The proposed model was applied to simulate the runoff hydrograph on ten watersheds, seven of which are located in the loess plateau and Sichan Province in China, and three in Texas, USA, respectively. The rainfall-runoff events were divided into two groups. One group was utilized to calibrate the model and estimate its parameters, and the other was used for model verification.

##### *Model calibration*

The model chosen for simulating the excess rainfall-runoff process has auto-regressive order three and moving average order three. Ten rainfall-runoff events over ten watersheds were used to estimate the infiltration parameters. In the estimation of parameters by the simplex method, the water

TABLE I

Model parameters for calibration events

Name of basin	Area of basin (km <sup>2</sup> )	Events	Parameters of infiltration		Parameters of excess-runoff model					
			K	SM						
Dujia	96.1	15-8-1966	0.06	14.35	$a_1 = 2.003,$ $b_0 = 0.0219,$	$a_2 = -1.62,$ $b_1 = -0.0386,$	$a_3 = 0.5405$ $b_2 = 0.0974$			
Xizhun	49.0	28-8-1966	0.06	4.17	$a_1 = 0.1399,$ $b_0 = -0.004,$	$a_2 = -0.126,$ $b_1 = 0.3188,$	$a_3 = 0.3346$ $b_2 = 0.332$			
Xizhun	49.0	17-7-1966	0.06	265.5	$a_1 = 1.164,$ $b_0 = 0.0527,$	$a_2 = -0.217,$ $b_1 = 0.0238,$	$a_3 = -0.0787$ $b_2 = 0.00742$			
Shejia	4.26	15-8-1966	0.06	94.5	$a_1 = 0.1205,$ $b_0 = 0.0882,$	$a_2 = 0.1235,$ $b_1 = 0.507,$	$a_3 = -0.02278$ $b_2 = 0.1808$			
Shanchuan	21.0	28-8-1966	0.06	31.0	$a_1 = 0.9666,$ $b_0 = -0.0025,$	$a_2 = -0.2364,$ $b_1 = -0.0056,$	$a_3 = 0.03112$ $b_2 = 0.233$			
Wuansun	3.9	29-8-1970	0.09	134.5	$a_1 = 1.123,$ $b_0 = 0.034,$	$a_2 = -0.705,$ $b_1 = 0.00854,$	$a_3 = 0.398$ $b_2 = 0.1161$			
Fuxiq	1.39	21-7-1971	0.12	514.0	$a_1 = 0.482,$ $b_0 = 0.091,$	$a_2 = 0.1086,$ $b_1 = 0.0393,$	$a_3 = 0.1458$ $b_2 = 0.0868$			
Little Walnut Creek	14.42	19-7-1971	0.10	52.5	$a_1 = 1.727,$ $b_0 = 0.326,$	$a_2 = 0.584,$ $b_1 = -0.481,$	$a_3 = -0.762$ $b_2 = -0.428$			
Shoal Creek	18.21	16-4-1979	0.04	16.7	$a_1 = 2.28,$ $b_0 = 0.0755,$	$a_2 = -1.927,$ $b_1 = -0.107,$	$a_3 = 0.6055$ $b_2 = 0.0521$			
Grace Creek	13.08	9-5-1968	0.06	52.0	$a_1 = 1.143,$ $b_0 = 0.0188,$	$a_2 = -0.402,$ $b_1 = -0.0269,$	$a_3 = 0.0895$ $b_2 = 0.1278$			

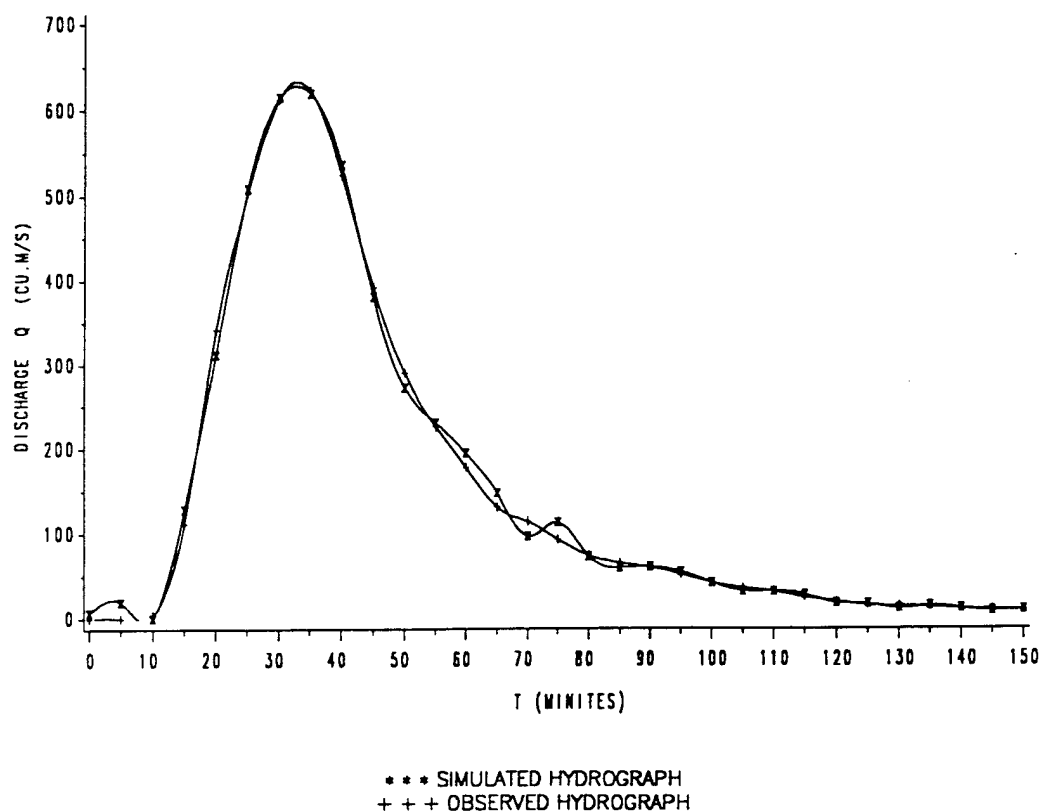


Fig. 2. Comparison of observed runoff hydrograph with that calculated from a new approach for the calibration of the Dujia event (15-8-1966).

balance condition had to be satisfied. Accordingly, the volume of the runoff calculated from the hydrograph was equal to that of the excess rainfall calculated from the hyetograph. The values of the parameters obtained for the watersheds are shown in Table 1. A comparison of observed and calculated hydrographs for three representative sample calibration events, ranging from the worst calibration to the best calibration, is shown in Figs. 2-4. For further evaluation of the calibration performance of the model, the goodness of fit of a computed hydrograph to an observed hydrograph was determined by means of the following four criteria.

(a) Relative squared error (RSE)

$$\text{RSE} = \frac{\sum_{i=1}^m [Q_c(t) - Q(t)]^2}{\sum_{i=1}^m Q^2(t)}$$

where  $Q_c(t)$  is the computed discharge at time  $t$ ,  $Q(t)$  is the observed discharge at time  $t$  and  $m$  is the number of discharge ordinates (RSE represents the

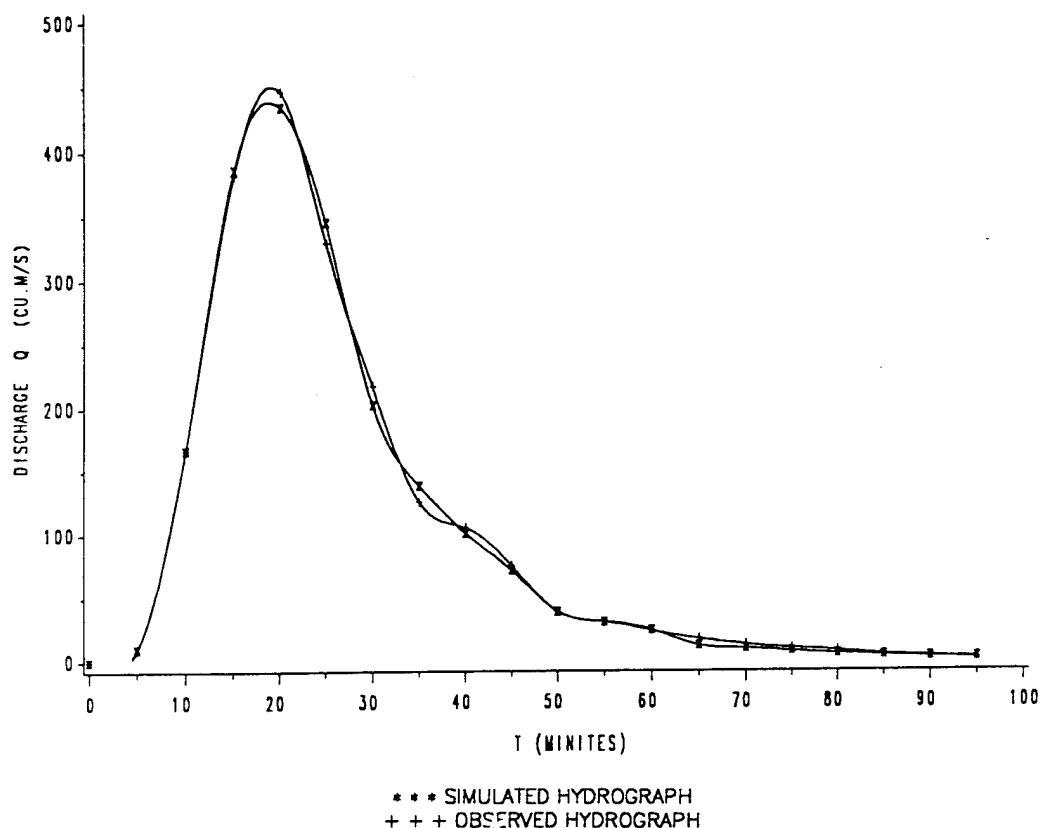


Fig. 3. Comparison of observed runoff hydrograph with that calculated from a new approach for the calibration of the Xizhun event (28-8-1966).

overall shape of the hydrograph, and if  $RSE = 0$ , the computed hydrograph will coincide with the observed hydrograph);

(b) Relative error in estimated peak ( $E_p$ )

$$E_p = \frac{|Q_p^c - Q_p|}{Q_p}$$

(c) Time of peak discharge;

(d) Time base of the hydrograph.

Table 2 gives values of these four criteria for all calibration events. The table shows that the RSE generally was less than 0.01; for only one event it exceeded 0.02. The maximum value of RSE was 0.1166, and the minimum was only 0.00157. The difference between observed and computed peak discharge was very small. The average value of  $E_p$  was 0.0239; the maximum value of  $E_p$  was 0.0645 and the minimum was only 0.003. The time of peak discharge calculated from the model and that from the observed data were the same for all but two calibration events. The computed time base was the same as the

TABLE 2

Comparison of computed and observed hydrograph for all calibration events

Basin	Area of basin (km <sup>2</sup> )	Event	Peak discharge (m <sup>3</sup> s <sup>-1</sup> )		$E_p$	Peak time		RSE	Time base (h)	
			Observed	Computed		Observed	Computed		Observed	Computed
Dujia	96.1	15-8-1966	621.0	618.1	0.005	19.30	19.30	0.00209	3 $\frac{1}{2}$	3 $\frac{1}{2}$
Xizhun	49.0	28-8-1966	446.6	434.8	0.026	19.00	19.00	0.00157	1 $\frac{3}{4}$	1 $\frac{3}{4}$
Xizhun	49.0	17-7-1966	280.0	277.8	0.008	18.35	18.35	0.00168	2 $\frac{1}{2}$	2 $\frac{1}{2}$
Shejia	4.26	15-8-1968	44.1	43.7	0.009	19.25	19.25	0.0076	1	1
Shanchuan	21.0	28-8-1968	109.7	112.8	0.003	19.20	19.20	0.00338	2 $\frac{1}{2}$	2 $\frac{1}{2}$
Wuansun	3.9	29-8-1970	46.6	45.1	0.032	0.45	0.50	0.0125	3 $\frac{1}{4}$	3 $\frac{1}{4}$
Fuxiq	1.39	29-7-1966	27.0	28.1	0.0407	0.45	0.45	0.0188	3 $\frac{1}{2}$	3 $\frac{1}{2}$
Little Walnut Creek	14.42	19-7-1979	49.6	50.1	0.01	21.15	21.15	0.00373	9	9
Shoal Creek	18.21	16-4-1977	8.21	8.74	0.0645	11.30	11.30	0.00784	9	9
Grace Creek	13.08	9-5-1980	19.40	20.2	0.041	16.40	17.00	0.1166	5	5

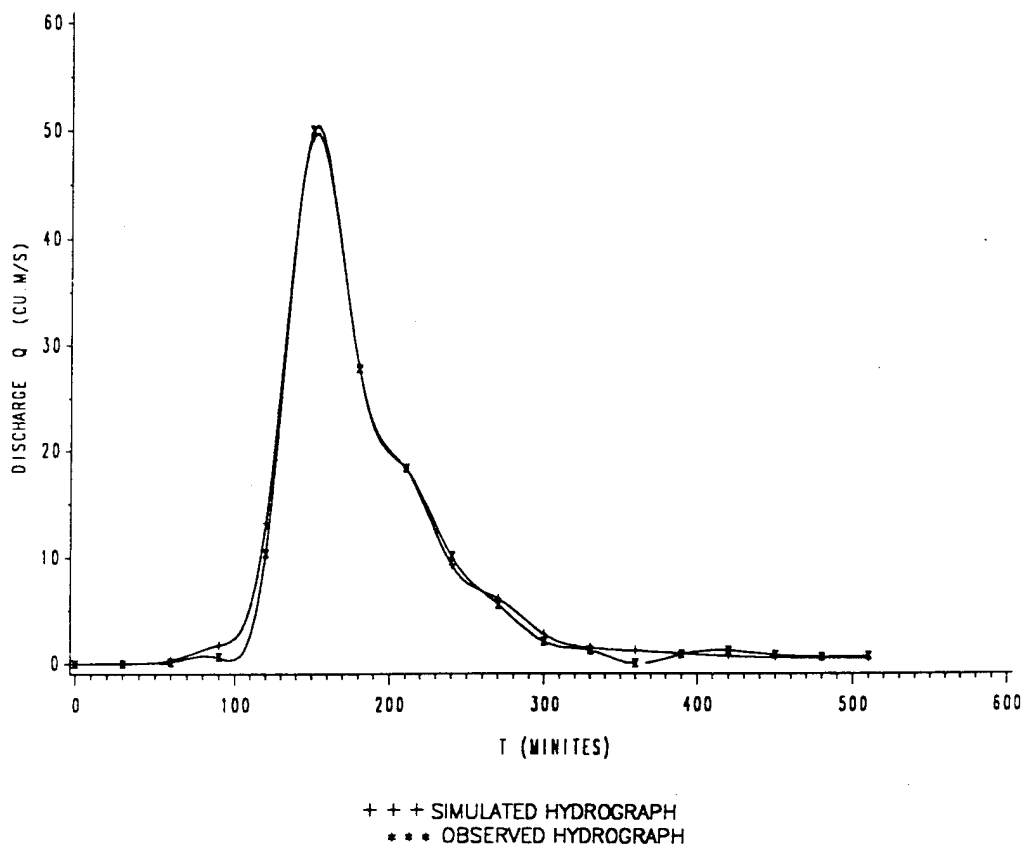


Fig. 4. Comparison of observed runoff hydrograph with that calculated from a new approach for the calibration of the Little event (19-7-1979).

TABLE 3

Calibration for parameters of the excess rainfall-runoff model by using multiple least-squares method

Name of basin	Area of basin (km <sup>2</sup> )	Parameters of excess-runoff model						
		$a_1$	$a_2$	$a_3$	$b_0$	$b_1$	$b_2$	$\Sigma$
Dujia	96.1	1.292	-0.416	-0.00771	0.0353	-0.0518	0.1164	0.968
Xizhun	49.0	0.501	0.1017	-0.0978	0.1024	0.145	0.140	0.982
Shejia	4.26	0.615	-0.178	0.0525	0.183	0.365	-0.0537	0.994
Shanchuan	21.0	0.755	-0.253	0.161	0.0245	0.226	0.0176	1.005
Wuansun	3.9	1.074	-0.546	0.266	0.108	-0.207	0.266	0.962
Fuxiq	1.39	1.318	-0.495	0.0552	0.0373	-0.00831	0.0569	0.964
Shoal	18.2	0.222	-0.00623	0.0999	0.394	0.250	0.0942	0.962

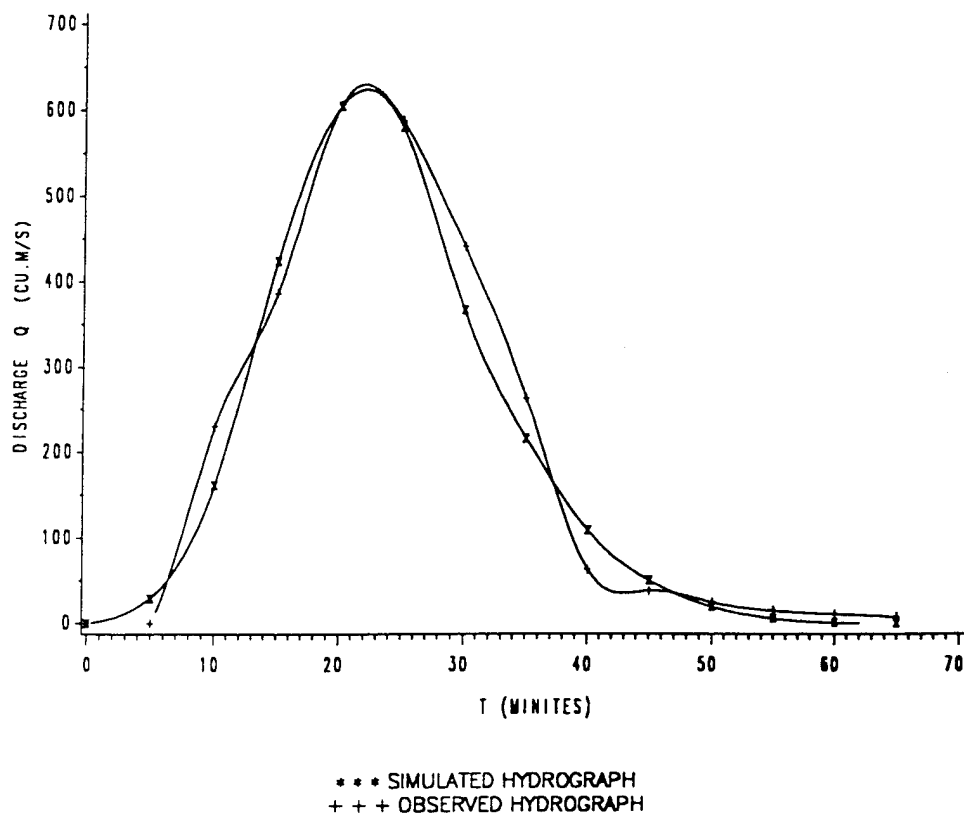


Fig. 5. Comparison of observed runoff hydrograph with that calculated from a new approach for the verification of the Xizhun event (15-8-1966).

observed value for each calibration event. Therefore, the overall features of hydrograph calculated from the model were very similar to those observed.

When the excess rainfall events were calculated, two or more than two corresponding runoff events in the same basin were utilized to estimate the average parameters of the excess rainfall-runoff model by using the multiple least-squares method as discussed above. The values of the parameters so obtained are shown in Table 3.

#### *Model verification*

With the values of the infiltration parameters obtained by calibration for each watershed, the excess rainfall hyetograph was computed for each event. The runoff hydrograph was then computed for each excess-rainfall hyetograph, using the runoff model parameters obtained for multiple events during calibration. To test the model, seven rainfall-runoff events were used. The RSE was computed for the computed hydrograph of each event. The

TABLE 4

Comparison of computed and observed hydrographs for verification events

Basin	Area of basin (km <sup>2</sup> )	Event	Peak discharge (m <sup>3</sup> s <sup>-1</sup> )		$E_p$	Peak time		RSE	Time base (h)	
			Observed	Computed		Observed	Computed		Observed	Computed
Xizhun	49.0	15-8-1966	606.0	604.6	0.0023	19.05	19.05	0.0147	1 $\frac{1}{2}$	1 $\frac{1}{2}$
Shanchuan	21.0	15-8-1966	354.8	334.6	0.057	19.20	19.15	0.0158	1 $\frac{7}{12}$	1 $\frac{7}{12}$
Shejia	4.26	17-7-1966	33.1	31.6	0.045	18.45	18.50	0.0176	2 $\frac{3}{4}$	2 $\frac{3}{4}$
Wuansun	3.9	4-7-1967	51.30	45.8	0.107	0.35	0.35	0.1095	2 $\frac{7}{12}$	2 $\frac{7}{12}$
Fuxiq	1.39	29-7-1966	29.5	19.9	0.325	0.50	0.45	0.1355	2 $\frac{11}{12}$	2 $\frac{11}{12}$
Shoal Creek	18.2	19-7-1977	59.7	39.6	0.336	21.20	21.20	0.1095	8 $\frac{1}{2}$	8 $\frac{1}{2}$

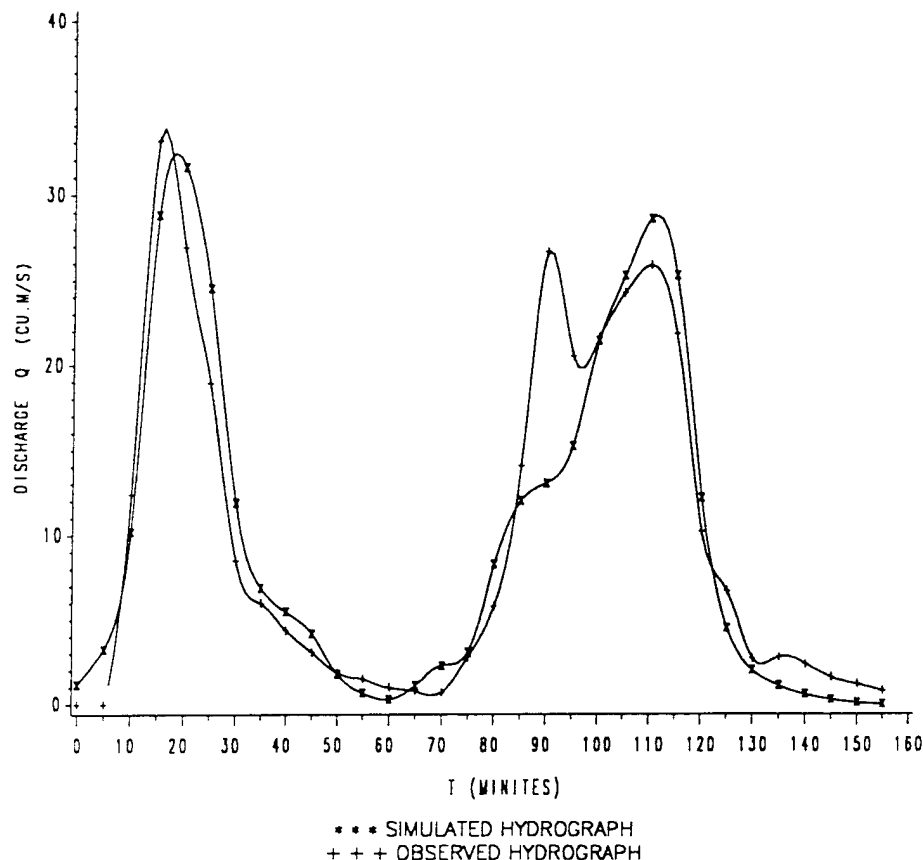


Fig. 6. Comparison of observed runoff hydrograph with that calculated from a new approach for the verification of the Shejia event (14-7-1966).

results of computations are shown in Table 4, and for three representative sample events in Figs. 5-7. The values of RSE generally were less than 0.11, with the average being 0.0671. The maximum value of RSE was 0.1355, and the minimum was only 0.0147. The average relative error of the estimated peaks ( $E_p$ ) was 0.145. The maximum value of  $E_p$  was 0.336, and the minimum was 0.0023, and the peak occurred at almost the correct time for all the verification events. The time base of hydrograph calculated from the model was the same as the observed value for each verification event.

The accuracy of the model depends on the spatial distribution of rainfall and other factors. If the rainfall was distributed uniformly in space, the model parameters estimated using the least-squares method will approximate the true values. For one event, the rainfall center may be located in the lower reaches, and for the other event it may be located in the upper reaches. If the

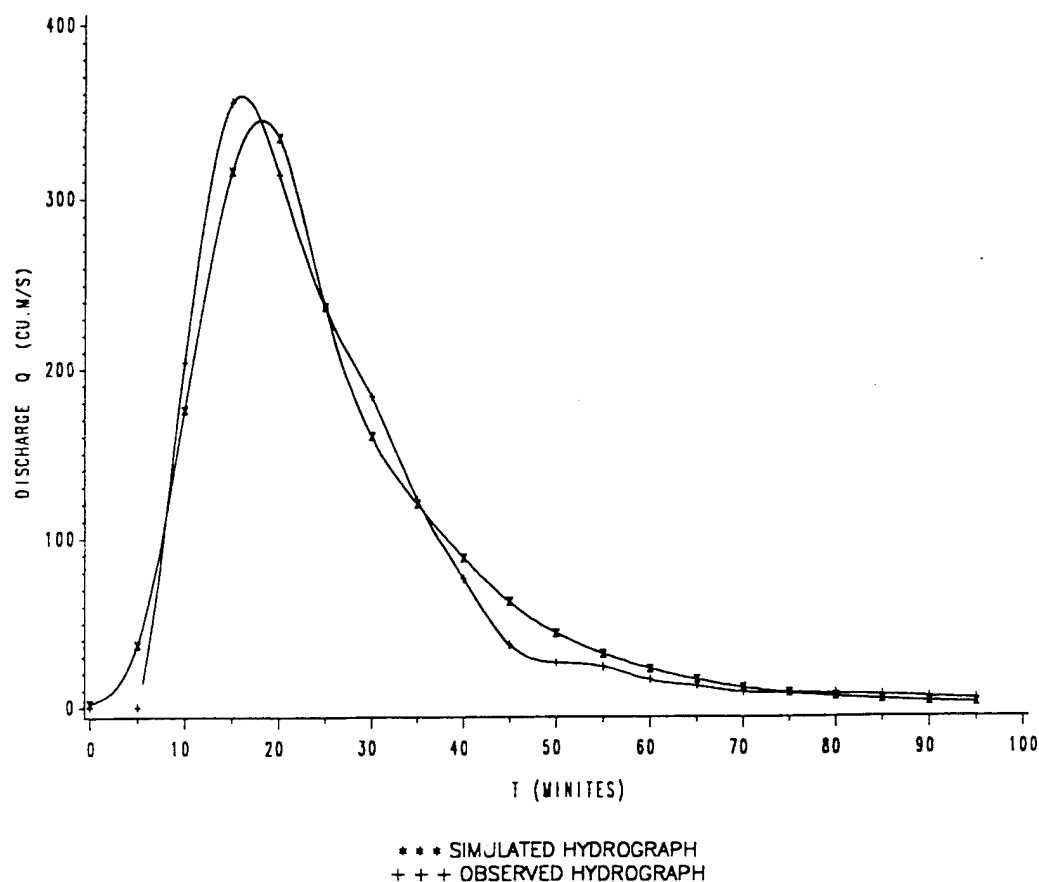


Fig. 7. Comparison of observed runoff hydrograph with that calculated from a new approach for the verification of the Shanchua event (15-8-1966).

parameters estimated from the one event are used to predict the runoff hydrograph of the other event, the prediction values would have some errors. Therefore, multiple excess rainfall-runoff events were applied to estimate the average values of the model parameters which were then used to predict the runoff hydrograph of other events. In this case, the results would be better than the parameters based on a single event. Let us consider, for example, the Xizhun watershed. The runoff hydrograph of 15 August 1966, was calculated by using two groups of parameters. In one group, the parameters were estimated from a single event shown in Table 1 and in the other group are the average parameters Table 2.  $RSE = 0.1482$  and  $E_p = 0.31$  for a single event, and  $RSE = 0.0147$  and  $E_p = 0.0023$  for the average parameters. Therefore, the results showed that the parameters based on multiple events were better than those based on single events.

## SUMMARY AND CONCLUSIONS

The model developed in this study combines the excess-rainfall process and the runoff-concentration process. Parameters of these processes were simultaneously estimated by minimizing the sum of squared differences between observed and computed discharges, subject to the constraint of maintaining the water balance. The model has the following advantages:

(1) With the assumed initial values of  $K$  and  $SM$ , the excess rainfall hyetograph can be estimated for any event and the least-squares method can then be used to determine the parameters of the excess rainfall-runoff process from the observed hydrograph. The sum of squared differences between observed and computed hydrographs can be utilized to determine the values of  $K$  and  $SM$  for the next iteration. Thus, parameter estimation is simple and easy.

(2)  $K$  depends on the soil properties and can be taken as constant for a fixed watershed.  $SM$  depends on the capillary potential and the antecedent soil moisture; however,  $SM$  can be estimated, based on laboratory or field observations.

(3) There exists an enormous volume of data on rainfall-runoff events for watersheds in various countries. These data can be analyzed to estimate  $K$  and  $SM$ , and to establish a relationship between  $SM$  and antecedent soil moisture. The prediction of excess rainfall can be carried out when  $K$  and  $SM$  are given.

(4) Figures 2-4 and 5-7 show that observed and estimated runoff hydrographs are in good agreement for calibration as well as verification events. The model can be adapted for real-time flow forecasting.

## ACKNOWLEDGMENT

The study was supported in part by the National Scientific Fund of the People's Republic of China.

## REFERENCES

- Chu, T.C., 1978. Infiltration during an unsteady rain. *Water Resour. Res.*, 14(3): 461-466.
- Green, D.W. and Ampt, G.A., 1911. Studies on soil physics: I. Flow of air and water through soils. *J. Agr. Sci.*, 4(1): 1-24.
- Himmelblau, D.M., 1972. *Applied Nonlinear Programming*. McGraw-Hill, New York, pp. 148-157.
- Mays, L.W. and Taur, C.K., 1982. Unit hydrographs via nonlinear programming. *Water Resour. Res.*, 18(4): 744-752.
- Mein, R.G. and Larson, C.L., 1973. Modeling infiltration during a steady rain. *Water Resour. Res.*, 9(2): 384-394.

- Nash, J.E., 1957. The form of the instantaneous unit hydrograph. IAHS Publ., 45(3): 114-121.
- O'Connor, K.M., 1982. Derivation of discretely coincident forms of continuous linear time-invariant models using the transfer function approach. J. Hydrol., 59: 1-48.
- Singh, V.P., 1988. Hydrologic Systems: Vol. 1. Rainfall-Runoff Modeling. Prentice-Hall, Englewood Cliffs, NJ.
- Singh, V.P., 1989. Hydrologic Systems: Vol. 2. Watershed Modeling. Prentice-Hall, Englewood Cliffs, NJ.
- Swartzendruber, D., 1974. Infiltration constant flow rainfall into soil as analyzed by the approach of Green and Ampt. Soil Sci., 117: 272-281.
- Wang, G.T. and Yu, Y.S., 1986. Estimation of parameters of the discrete linear, input-output model. J. Hydrol., 85: 15-30.
- Wang, G.T. and Yu, Y.S., 1990. Modeling rainfall-runoff process including losses. Water Resour. Bull., 26(1): 61-66.
- Wang, G.T., Singh, V.P., Guo, C.L. and Huang, K.X., 1992. Discrete linear model for runoff and sediment discharges for loess plateau of China. J. Hydrol., 127: 153-171.

[4]

## Discrete linear models for runoff and sediment discharge from the Loess Plateau of China

Wang Guang-Te<sup>\*a</sup>, V.P. Singh<sup>b</sup>, Guo Changling<sup>a</sup> and Huang KeXin<sup>a</sup>

<sup>a</sup>*Institute of Geography, Chinese Academy of Science, Building 917, Dutun Road, Beijing 100101, China*

<sup>b</sup>*Department of Civil Engineering, Louisiana State University, Baton Rouge, LA 70803, USA*

(Received 3 February 1990; revised and accepted 3 January 1991)

### ABSTRACT

Wang, G.-T., Singh, V.P., Guo, C. and Huang, K.X., 1991. Discrete linear models for runoff and sediment discharge from the Loess Plateau of China. *J. Hydrol.*, 127: 153–171.

Discrete linear models were developed for estimating runoff and sediment discharge hydrographs from the Loess Plateau of China. A regression equation was also established relating runoff rate and sediment discharge. Tested on five small basins, the results were in good agreement with observations. For the discrete linear transfer runoff model, the values of the integral square error were generally less than 1% for all calibration events, and around 10% with an average value of 9.36% for all verification events. For the discrete linear transfer sediment model, the calibration coefficient of determination  $R^2$  for all five basins was more than 97%, and the verification  $R^2$  was more than 91% with an average of 94.3%.

### INTRODUCTION

The upper and middle reaches of the Yellow River in China flow through a wide plateau with an area of about 580 000 km<sup>2</sup>; it is covered with loess and red loess. The Loess Plateau is located in a transition zone with monsoons in the southeast and an arid climate in the northwest. It borders the Qinghai-Tibet Plateau on the east and is bounded by Mongolia-Xin Plateau on the north. In the winter, the region is controlled by high pressure systems in Mongolia, when the Arctic cold air mass moves in, causing strong breezes and falling temperatures. In the summer, subtropical Pacific air masses with much more moisture reach the region and cause rainfall. Owing to differing distance from the ocean, the east to west variation of precipitation is large. The distribution of precipitation in time is also extremely nonuniform. For example, the precipitation in July, August and September is about 70% of the annual total. The precipitation for one event is generally about 10% of the

---

<sup>\*</sup> Visiting Scholar, Department of Civil Engineering, Louisiana State University, Baton Rouge, LA 70803, U.S.A.

annual total but as much as 43% has been recorded. The maximum precipitation of 53.1 mm recorded for 5 min in China is from this region. The potential evaporation is about 2500 mm year<sup>-1</sup>. The ground water is more than 100 m below ground level. Therefore, the soil stratum seldom develops saturated conditions.

Owing to the particular physiographic characteristics of the Loess Plateau, the distinguishing features of runoff from rainfall are as follows.

(1) Rivers, with drainage areas of less than 500 km<sup>2</sup>, are nearly dry valleys. In the summer, when the rainstorms occur, the resulting runoff hydrographs are characterized by short durations and high flood peaks. Generally, there is little baseflow to be separated from the hydrographs. Therefore, discrete linear transfer function models can be suitable for simulating the hydrographs from this region.

(2) The sediment yield for the basins is caused by storm rainfall and runoff. Therefore, the relationship between sediment and runoff discharge is very strong. The regression equation and discrete linear transfer models are proposed for simulating the relation of sediment discharge to the runoff hydrograph.

A large amount of sediment is eroded from the Loess Plateau and enters the Yellow River. Evaluation of this yield is therefore important in the design of soil conservation and pollution control practices, as well as in the design and management of dams, canals and other hydraulic structures. A number of studies have been carried out to investigate soil and water conservation aspects of the Loess Plateau (Gong and Jiang, 1977). Yin and Chen (1989) analyzed over 4000 observations on 58 small watersheds with basin area from 0.193 to 329 km<sup>2</sup>. The data, covering the period 1954–1982, included 21 variables. They related erosion intensity to a composite index of basin surface characteristics (Yin and Chen, 1989).

This paper develops a linear discrete model to simulate runoff and sediment discharge from the Loess Plateau, taking into account its physiographic characteristics.

#### DISCRETE LINEAR TRANSFER FUNCTION MODELS FOR SMALL BASINS IN THE LOESS PLATEAU

The discrete, linear rainfall–runoff model given by Wang and Yu (1986) can be expressed as

$$Q(t) = a_1 Q(t-i) + \dots + a_p Q(t-p) + b_0 I(t) + b_1 I(t-1) + \dots + b_q I(t-q) \quad (1)$$

where  $Q(t)$  is direct runoff discharge at time  $t$ ,  $Q(t-1)$  is direct runoff discharge at time  $(t-1)$ ,  $i = 1, 2, \dots, p$ ,  $I(t)$  is excess rainfall at time  $t$ .

$I(t - j)$ ,  $j = 1, 2, \dots, q$ , is excess rainfall at time  $(t - j)$ , and  $a_j$  and  $b_j$  are coefficients.

In the model used in this study, the excess rainfall (effective rainfall) is expressed as the difference between rainfall  $P(t)$  and losses  $L(t)$  over the same time period, that is

$$I(t) = P(t) - L(t) \quad \text{for } t = 1, 2, \dots, s \quad (2)$$

Inserting eqn. (2) in eqn. (1) yields

$$\left. \begin{aligned} Q(1) &= b_0[P(1) - L(1)] \\ Q(2) &= a_1 Q(1) + b_0[P(2) - L(2)] + b_1[P(1) - L(1)] \\ &\vdots \\ Q(s) &= a_1 Q(s-1) + \dots + a_p Q(s-p) + b_0[P(s) - L(s)] \\ &\quad + \dots + b_q[P(s-q) - L(s-q)] \\ &\vdots \\ Q(m) &= a_1 Q(m-1) + \dots + a_p Q(m-p) \end{aligned} \right\} \quad (3)$$

For discrete linear models represented by eqn. (1), the parameters can easily be determined from effective rainfall and discharge data by ordinary least-squares, correlation analysis, linear programming or other methods. However, for the discrete linear models given by eqn. (3), both the model parameters  $a_1, a_2, \dots, a_p, b_0, \dots, b_q$  and the time-variant losses  $L(t)$ , which are not known beforehand, must be estimated simultaneously. In this study, the parameter estimation problem is formulated as a nonlinear minimization problem as follows.

Let the residuals between  $Q'(t)$  and estimated  $Q(t)$  discharge rates be represented by  $e_t$  as

$$e_t = Q'(t) - Q(t) \quad \text{for } t = 1, 2, \dots, m \quad (4)$$

substitution of eqn. (3) into eqn. (4) yields the following equation for residuals:

$$\left. \begin{aligned} e_1 &= b_0[P(1) - L(1)] - Q(1) \\ e_2 &= a_1 Q(1) + b_0[P(2) - L(2)] + b_1[P(1) - L(1)] - Q(2) \\ &\vdots \\ e_m &= a_1 Q(m-1) + a_2 Q(m-2) + \dots + a_p Q(m-p) - Q(m) \end{aligned} \right\} \quad (5)$$

For convenience, let the unknown  $a$ ,  $b$  and  $L(s)$  values in eqn. (5) be the components of a column vector  $X$

$$X = [a_1, a_2, \dots, a_p, b_0, b_1, \dots, b_q, L(1), L(2), \dots, L(s)]^T \quad (6)$$

where  $T$  denotes the transpose. The residuals  $e_1, e_2, \dots, e_m$  in eqn. (5) are then a function of  $X$ . The optimal estimate of  $X$  can be obtained by solving the unconstrained nonlinear minimization problem with the following objective function:

$$F(X) = \sum_{j=1}^m e_j^2(X) = E^T(X)E(X) \quad (7)$$

where  $E(X) = [e_1(X), e_2(X), \dots, e_m(X)]^T$ . Taking the first derivative of eqn. (7) with respect to  $X$  yields

$$\frac{dF}{dX} = \frac{d}{dX} [E^T(X)E(X)] = 2 \frac{dE^T(X)}{dX} E(X) = 2A^T E \quad (8)$$

where

$$A(X) = \begin{bmatrix} \frac{\partial e_1(X)}{\partial a_1} & \frac{\partial e_1(X)}{\partial a_2} & \dots & \frac{\partial e_1(X)}{\partial L(s)} \\ \frac{\partial e_2(X)}{\partial a_1} & \frac{\partial e_2(X)}{\partial a_2} & \dots & \frac{\partial e_2(X)}{\partial L(s)} \\ \vdots & \vdots & \ddots & \vdots \\ \frac{\partial e_m(X)}{\partial a_1} & \frac{\partial e_m(X)}{\partial a_2} & \dots & \frac{\partial e_m(X)}{\partial L(s)} \end{bmatrix}$$

Taking the second derivative of eqn. (7) with respect to  $X$  yields

$$\frac{d^2 F}{dX^2} = \frac{d^2 [E^T(X)E(X)]}{dX^2} = \frac{2A^T dE}{dX} = \frac{2dA^T}{dX} E(X) = 2A^T A + \frac{2d^2 E}{d^2 X} \cdot E(X)$$

Neglecting the second-order term gives

$$\frac{d^2 F}{dX^2} = 2A^T A \quad (9)$$

Substituting eqns. (8) and (9) into the Newton-Raphson iterative formula yields

$$X^{(K+1)} = X^{(K)} - \frac{\frac{dF(X)}{dX}}{\frac{d^2 F(X)}{dX^2}} = X^{(K)} - (A^T A)^{-1} A^T E \quad (10)$$

When eqn. (10) is solved iteratively, two problems may arise. First, the matrix  $(A^T A)$  is sometimes ill-conditioned and it is difficult to find the inverse. Second, if the direction of search and the gradient of the vector  $X$  are approximately orthogonal, the iterative speed is very slow. In order to overcome these problems, Marquardt (1963) suggested a revised iterative method which changes eqn. (10) to the following form:

$$X^{(K+1)} = X^{(K)} - [A^T A + WI]^{-1} A^T E \quad (11)$$

where  $I$  is a unit matrix and  $W$  is constant. When  $W = 0$ , eqn. (11) reduces to eqn. (10). With  $W$  sufficiently large,  $WI$  can overwhelm  $A^T A$  and the minimization approaches a steepest descent search. Therefore, the Marquardt method can be seen to be a combination of the Gauss-Newton iterative method and steepest descent. This method forces the Hessian matrix to be positive definite at each stage of minimization and ensures that the estimate of its inverse is also positive definite. The algorithm using the Marquardt method is described by Bard (1970).

#### RUNOFF AND SEDIMENT DISCHARGE FROM SMALL BASINS OF THE LOESS PLATEAU

The sediment yield from the Loess Plateau basins is caused by storm rainfall and runoff. The greater the rainfall intensity, the more the runoff; and the sediment transporting capacity increases with runoff discharge. The influence of runoff discharge on sediment discharge is more evident than that of rainfall and its intensity. Two methods were used to study the relationship between runoff discharge and sediment discharge.

##### *Regression method*

Gong and Jiang (1977) plotted on log-log paper the relation between observations in time of runoff discharge and the corresponding sediment discharge for four basins of the Loess Plateau. They concluded that for discharges more than  $10 \text{ m}^3 \text{ s}^{-1}$ , the relation between runoff discharge and sediment discharge was very close to a straight line, but was erratic for discharges less than  $10 \text{ m}^3 \text{ s}^{-1}$ . The runoff discharge and sediment discharge data from six small basins were analyzed in this study. For each basin, the regression equation was derived from the runoff sediment discharge data of more than two events. The results are given in Table 1.

Table 1 shows that the exponent of each regression equation approximates 1.0, with the average exponent index for the six basins (of area from 0.18 to

TABLE I

Regression equation between runoff and sediment discharge rate for the six small basins

	Twanshan	Shejia	Shanchuan	Xizhuang	Dujiago	Caoping
Area of basin (km <sup>2</sup> )	0.18	4.26	21.0	49.0	96.1	187.0
Regression equation	$G = 0.336Q^{1.0209}$	$G = 0.339Q^{0.9985}$	$G = 0.38Q^{0.984}$	$G = 0.557Q^{0.9466}$	$G = 0.428Q^{0.9924}$	$G = 0.4Q$
Correlation coefficients	0.983	0.9831	0.9907	0.984	0.991	0.99

 $G$  = sediment discharge (m<sup>3</sup> s<sup>-1</sup>),  $Q$  = runoff discharge (m<sup>3</sup> s<sup>-1</sup>).

187.0 km<sup>2</sup>) being 0.089. The regression coefficient ranges from 0.335 to 0.557. The exponents and coefficients do not depend on the basin area because sediment discharge depends mainly on storm rainfall and runoff. The flow velocities in dry valleys are high, with the maximum velocity being 5.0–6.0 m s<sup>-1</sup>. The travel time for the basin is relatively short and runoff with sediment reaches the outlet quickly. Field investigations showed that there was little sediment deposited in the dry valley during the flood period.

For use on a particular basin, the runoff discharge, from which sediment discharge rates would be calculated using the regression equation, can be estimated by applying the discrete linear model to the rainfall data.

### *Discrete linear model for sediment discharge*

Caroni et al. (1984) applied two simple stochastic models to sediment yield data from an experimental basin in the U.S.A. Wang and Yu (1986) proposed a more general linear discrete transfer function model of the type introduced by Box and Jenkins (1976) expressed as

$$Q(t) = a_1 Q(t-1) + \dots + a_p Q(t-p) + b_0 I(t) + \dots + b_q I(t-q) \quad (1a)$$

This type of model is proposed for estimating sediment discharge from small basins of the Loess Plateau in China. This model is superior to regression equations which cannot account for the time-series nature of rainfall, runoff and sediment discharge processes. When eqn. (1) is applied to sediment discharge rates of small basins,  $Q(t)$  is replaced by  $G(t)$ , and  $I(t)$  by  $Q(t)$ .

$$G(t) = C_1 G(t-1) + \dots + C_p G(t-p) + W_0 Q(t) + \dots + W_q Q(t-q) \quad (12)$$

where  $C_1, C_2, \dots, C_p$  and  $W_0, W_1, \dots, W_q$  are parameters. The model parameters can be estimated from observed runoff and sediment discharge data using ordinary least-squares. Let  $e_g(t)$  be the difference between observed sediment discharge and sediment discharge computed from eqn. (12) using the observed runoff discharge as input

$$e_g(t) = G(t) - [C_1 G(t-1) + \dots + C_p G(t-p) + \dots + W_0 Q(t) + \dots + W_q Q(t-q)] \quad (13)$$

The objective function for estimating the parameters  $C$  and  $W$  values can be expressed as

$$F = \sum_{t=1}^m e_g^2(t) = \sum_{t=1}^m \left[ G(t) - \sum_{i=1}^P C_i G(t-i) - \sum_{j=0}^q W_j Q(t-j) \right]^2 \quad (14)$$

The necessary conditions for eqn. (14) to have an optimal solution for  $C$  and  $W$  values are

$$\frac{\partial F}{\partial C_i} = \frac{\partial \sum_{t=1}^m \left[ G(t) - \sum_{i=1}^P C_i G(t-i) - \sum_{j=0}^q W_j Q(t-j) \right]^2}{\partial C_i} = 0$$

for  $i = 1, 2, 3, \dots, P$

$$\begin{aligned} \sum_{t=1}^m G(t)G(t-k) &= \sum_{t=1}^m \sum_{i=1}^P C_i G(t-i)G(t-k) \\ &\quad + \sum_{t=1}^m \sum_{j=0}^q W_j Q(t-j)G(t-k) \end{aligned} \quad (15)$$

letting

$$r_{GG}(k-i) = \sum_{t=1}^m G(t-i)G(t-k)$$

$$r_{QG}(k-j) = \sum_{t=1}^m Q(t-j)G(t-k)$$

Equation (15) reduces to

$$\begin{aligned} r_{GG}(k) &= C_1 r_{GG}(k-1) + \dots + C_P r_{GG}(0) + W_0 r_{QG}(k) \\ &\quad + \dots + W_q r_{QG}(k-q) \end{aligned} \quad (16)$$

In the same manner, let

$$\frac{\partial F}{\partial W_j} = 0 \quad \text{for } j = 0, 1, 2, \dots, q$$

which yields

$$\begin{aligned} r_{QG}(-l) &= C_1 r_{QG}(-l+1) + \dots + C_P r_{QG}(P-l) + W_0 r_{QQ}(l) \\ &\quad + \dots + W_q r_{QQ}(0) \end{aligned} \quad (17)$$

The model parameter can be estimated from a subset of eqns. (16) and (17) which relate the model parameters to the correlation functions calculated from observed runoff and sediment discharge rate series. The number of eqns. (16) and (17) is equal to the number of model parameters.

Setting  $k = 1, 2, \dots, P$  and  $l = 0, 1, 2, \dots, q$  in eqns. (15) and (16), respectively, yields the following equations:

$$\left. \begin{aligned}
 r_{GG}(1) &= C_1 r_{GG}(0) + \dots + C_P r_{GG}(P-1) + W_0 r_{QG}(1) \\
 &\quad + \dots + W_q r_{QG}(1-q) \\
 r_{GG}(2) &= C_1 r_{GG}(1) + \dots + C_P r_{GG}(P-2) + W_0 r_{QG}(2) \\
 &\quad + \dots + W_q r_{QG}(2-q) \\
 &\vdots \\
 r_{GG}(P) &= C_1 r_{GG}(P-1) + \dots + C_P r_{GG}(0) + W_0 r_{QG}(P) \\
 &\quad + \dots + W_q r_{QG}(P-q) \\
 \text{and} \\
 r_{GQ}(0) &= C_1 r_{GQ}(1) + \dots + C_P r_{GQ}(P) + W_0 r_{QQ}(0) \\
 &\quad + \dots + W_q r_{QQ}(q) \\
 r_{GQ}(-1) &= C_1 r_{GQ}(0) + \dots + C_P r_{GQ}(P-1) + W_0 r_{QQ}(1) \\
 &\quad + \dots + W_q r_{QQ}(q-1) \\
 &\vdots \\
 r_{GQ}(-q) &= C_1 r_{GQ}(1-q) + \dots + C_P r_{GQ}(P-q) + W_0 r_{QQ}(q) \\
 &\quad + \dots + W_q r_{QQ}(0)
 \end{aligned} \right\} \quad (18)$$

There are  $(p + q + 1)$  parameters in the same number of linear algebraic equations. The solution of eqn. (18) in matrix form is

$$\mathbf{B} = \mathbf{A}^{-1} \mathbf{D} \quad (19)$$

where  $\mathbf{B} = [C_1, C_2, \dots, C_P, W_0, W_1, \dots, W_q]^T$

$$\mathbf{A} = \begin{bmatrix}
 r_{GG}(0) & \dots & r_{GG}(P-1) & r_{QG}(1) & \dots & r_{QG}(1-q) \\
 r_{GG}(1) & \dots & r_{GG}(P-2) & r_{QG}(2) & \dots & r_{QG}(2-q) \\
 \vdots & \vdots & \vdots & \vdots & \vdots & \vdots \\
 r_{GG}(P) & \dots & r_{GG}(0) & r_{QG}(P) & \dots & r_{QG}(P-q) \\
 r_{GQ}(1) & \dots & r_{GQ}(P) & r_{QQ}(0) & \dots & r_{QQ}(q) \\
 r_{GQ}(0) & \dots & r_{GQ}(P-1) & r_{QQ}(1) & \dots & r_{QQ}(q-1) \\
 \vdots & \vdots & \vdots & \vdots & \vdots & \vdots \\
 r_{GQ}(1-q) & \dots & r_{GQ}(P-q) & r_{QQ}(q) & \dots & r_{QQ}(0)
 \end{bmatrix}$$

$$\mathbf{D} = [r_{GG}(1)r_{GG}(2) \dots r_{GG}(P)r_{GQ}(0) \dots r_{GQ}(-q)]^T$$

## APPLICATION OF MODELS

The two discrete linear models were applied to rainfall-runoff and sediment discharge data. One model was used to estimate the runoff hydrograph from observed rainfall, and the other was used to calculate sediment discharge from computed runoff.

*Rainfall-runoff-sediment data*

The data used in this study were collected from the hydrologic yearbook for an experimental basin designated as Chobagou basin, in Zizhou county, ShaanXi, on the Loess Plateau of China. The basin area is 187.0 km<sup>2</sup>. There are six subbasins with areas ranging from 0.017 to 96.1 km<sup>2</sup>. The location of these subbasins is shown in Fig. 1. Rainfall at 28 gauges within the basin, and runoff and sediment concentration at their outlets are recorded in data files at unequal time intervals. A 5 min interval was chosen for all the subbasins except Twanshan and Twanshan (No. 9) (1 min interval) in order to get a sufficiently detailed resolution of data. The location of gauging stations for rainfall and runoff discharge is also shown in Fig. 1. The mean areal rainfall was estimated as the arithmetic mean of the station records in the neighborhood of the centroid of the subbasin.

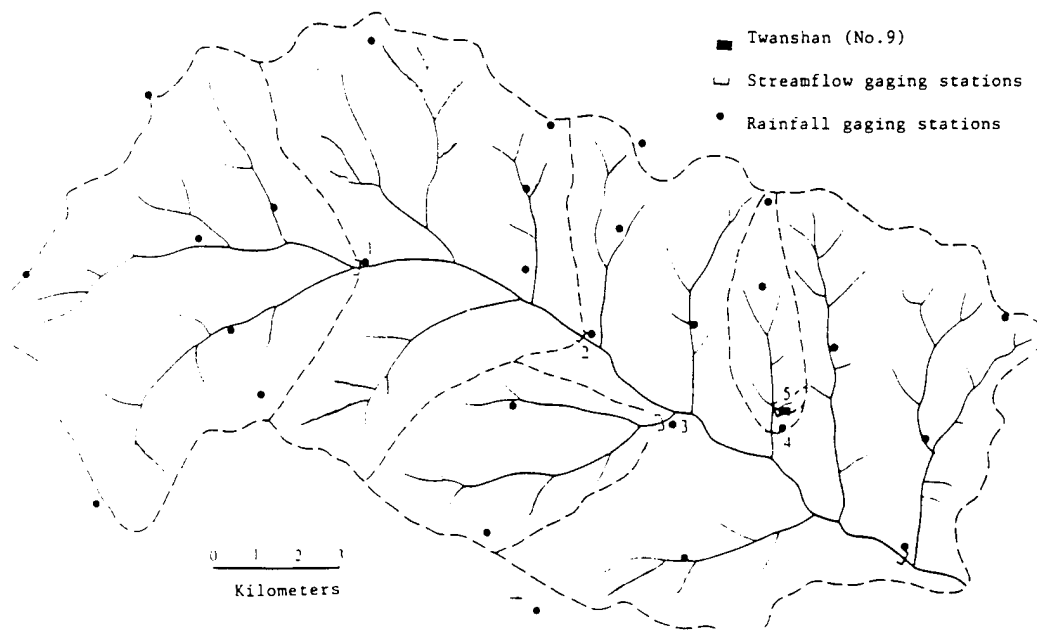


Fig. 1. Location of rainfall and streamflow gauging stations. 1. Xihuang; 2. Dujiago; 3. Shanchuan; 4. Shejia; 5. Twanshan.

Thirteen rainfall-runoff-sediment events were selected to assess the adequacy of the discrete linear models for simulating runoff and sediment hydrographs. The data were divided into two sets: a calibration set, and a prediction set. The data in the calibration set consisted of eight events which were used for parameter estimation. The data in the prediction set consisted of five events which were used for model verification.

#### *Calibration of runoff hydrograph model*

The model chosen has autoregressive order three and moving average order three. Eight rainfall-runoff events over five basins were used to estimate the model parameters and losses. There were thus five model parameters and losses  $L(1)$ ,  $L(2)$ ,  $\dots$ ,  $L(s)$ , to be determined in the model. The number of interval losses depends on that of rainfall intervals. For minimizing the residual sum of squares of differences between observed and estimated discharges, Marquardt's (1963) iterative algorithm for computing nonlinear least-squares solutions was used. The algorithm needs some starting values for the parameters and criteria for convergence. The goodness of fit of the computed hydrograph to the observed hydrograph was estimated by means of the following three criteria:

- (1) Integral square error (ISE)

$$\text{ISE} = \frac{\sqrt{\sum_{i=1}^m [Q'(t) - Q(t)]^2}}{\sum_{i=1}^m Q(t)} \times 100\%$$

- (2) Relative error in estimated peak (EP)

$$\text{EP} = \frac{|Q'_p - Q_p|}{Q_p} \times 100\%$$

- (3) Time of peak discharge.

Table 2 gives the three criteria for all calibration runs.

Table 2 shows good agreement between observed and simulated hydrographs for all calibration events. The values of ISE generally are less than 1.0%; for only two events did ISE exceed 5.0%. The maximum value of ISE is 6.3%, and the minimum is only 0.03%. The differences between observed and computed peak discharges are very small and the times of peak discharge were also well reproduced for all calibration events. The model parameters for the five small basins are given in Table 3.

#### *Verification of runoff hydrograph model*

The values of the parameters from calibration events for each basin were applied to calculate runoff hydrographs using the excess rainfall, which was

TABLE 2

Comparison of computed and observed hydrographs for calibration events of the Loess Plateau region

Basin	Area (km <sup>2</sup> )	Event	Peak discharge (m <sup>3</sup> s <sup>-1</sup> )		EP (%)	Peak time		ISE (%)
						Observed	Computed	
			Observed	Computed				
Dujiago	96.1	668028	419	423	0.9	19:25	19:25	5.63
Xizhuang	49	660815	606	607.3	0.3	19:05	19:05	0.65
		660717	280	280	0.0	18:35	18:35	1.90
		660627	16.0	15.9	0.4	15:05	15:05	6.30
Shanchuan	21	660717	40.8	40.8	0.0	18:45	18:45	0.63
		660828	109.7	109.8	0.09	19:20	19:20	0.80
Shejia	4.26	660815	44.1	44.1	0.0	19:25	19:25	0.03
Twanshan	0.18	660717	2.08	2.07	0.3	18:39	18:39	0.48

estimated from the rainfall and loss processes obtained from calibration events. In order to assess the accuracy of the discrete linear model, five rainfall-runoff events were used. The results are given in Table 4.

Table 4 shows the results of applying the discrete linear hydrograph model for all verification events. The values of ISE generally are around 10% with the average being 9.36%. The maximum value of ISE is 12.9%, and the minimum is only 4.4%. The average relative error in estimated peak (EP) is 18.92%. The maximum value of EP is 33.4%, and the minimum is only 3.3%, and the peak occurred at almost the correct time for all the verification events.

TABLE 3

Calibration results for runoff hydrograph model

Basin	Area (km <sup>2</sup> )	Parameters					
		$a_1$	$a_2$	$a_3$	$b_0$	$b_1$	$b_2$
Dujiago	96.1	1.121	-0.252	-0.028	0.223	-0.510	0.447
Xizhuang	49.0	0.3674	0.0962	0.1622	0.0294	0.1608	0.1589
Shanchuan	21.0	1.0387	-0.4346	0.1574	0.0062	-0.0341	0.2636
Shejia	4.26	0.6127	-0.3316	0.0637	0.0004	0.4822	0.1696
Twanshan	0.18	1.341	-0.642	0.076	0.282	-0.091	0.023

TABLE 4

Verification results for runoff hydrograph model

Basin	Area (km <sup>2</sup> )	Event	Peak discharge (m <sup>3</sup> s <sup>-1</sup> )		EP (%)	Peak time		ISE (%)
			Observed	Computed		Observed	Computed	
Dujiago	96.1	660815	621.2	641.7	3.3	19:30	19:30	7.0
Xizhuang	49.0	660828	446.6	297.4	33.4	19:00	19:00	10.7
Shanchuan	21.0	660815	354.8	274.7	22.6	19:20	19:15	12.9
Shejia	4.26	660717	33.1	38.7	16.9	18:45	18:40	11.8
Twanshan	0.18	660815	6.97	5.69	18.4	19:17	19:16	4.4

*Calibration of sediment discharge models*

The equations for the regression of sediment discharge on runoff discharge are given in Table 1, which can be used for estimating sediment discharge from computed runoff discharge.

For application of the discrete linear model, sediment discharge data from five small basins were utilized for estimation of parameters. The model chosen has autoregression and moving averages each of order two. That is

$$G(t) = C_1G(t-1) + C_2G(t-2) + W_0Q(t) + W_1Q(t-1) \quad (20)$$

The parameters of eqn. (20) were estimated from one event for each basin by least-squares. The residual square error (RSE) was used to compute the proportion of variance explained by the coefficient of determination

$$R^2 = 1 - (\text{RSE}/S_y)^2$$

where  $S_y$  is the output standard error of estimate. Five events were selected for the calibration for five tested basins. The model parameters and calibration coefficient of determination  $R^2$  for the five basins are given in Table 5, as are the results of calibration. The good agreement expressed by high values of the coefficient of determination  $R^2$  is compatible with a low range of residuals.

*Prediction of sediment discharge*

The values of the parameters from the calibration events for each basin were applied to calculate sediment discharge using the estimated runoff discharge. For the regression equation, the coefficient and exponent were determined from the data of more than two events. In order to assess the

TABLE 5

The calibration results for sediment discharge rates

Basin	Area (km <sup>2</sup> )	Event	Parameter				$R^2$
			$C_1$	$C_2$	$W_0$	$W_1$	
Dujiago	96.1	660828	0.433	-0.0703	0.275	0.01224	0.9971
Xizhuang	49.0	660717	-0.175	0.1596	0.2893	0.0632	0.9715
Shanchuan	21.0	660828	-0.676	0.0717	0.2156	0.4250	0.9975
Shejia	4.26	660815	0.4908	-0.079	0.3287	-0.1421	0.9925
Twanshan	0.18	660717	0.5705	-0.1333	0.3805	-0.1518	0.981

accuracy of the two models, five rainfall-runoff-sediment discharge events were used. The results are given in Table 6.

Table 6 shows that for verification events, both models gave good results. For the discrete linear function model, the value of  $R^2$  is more than 91.0% with an average value of 94.26%. The maximum is 96.4%, and the minimum is 91.0%. For regression equations, the agreement expressed by high values of the coefficient of determination is comparable with that of discrete linear transfer model.

TABLE 6

Verification results for sediment discharge rates

Basin	Area (km <sup>2</sup> )	Event	Peak sediment discharge (m <sup>3</sup> s <sup>-1</sup> )			EP		$R^2$	
			Observed	Computed		DLFM	RE	DLFM	RE
				DLFM	RE				
Dujiago	96.1	660815	280.0	262.7	261.5	6.2	6.6	96.4	95.4
Xizhuang	49.0	660828	145.0	96.5	122.2	33.4	15.7	96.4	98.2
Shanchuan	21.0	660815	136.8	108.3	97.7	20.8	28.6	91.1	93.4
Shejia	4.26	660717	12.6	13.1	13.0	4.0	3.2	91.0	91.0
Twanshan	0.18	660815	3.1	2.35	1.97	24.2	36.5	96.4	93.6

## DISCUSSION OF RESULTS

Discrete linear transfer function models for runoff discharge were used to estimate the parameters  $a_1, a_2, \dots, a_p, b_0, b_1, \dots, b_q$  and  $L(1), L(2), \dots, L(s)$ , and these parameters were used to calibrate the model. The calibration results are in excellent agreement with observations. Strictly speaking, these

parameters cannot directly be used for another rainfall-runoff event for the following reasons.

(1) The number of rainfall periods in the events used for calibration is not equal to those of the events used for verification.

(2) The infiltration intensity is related to the rainfall intensity on the Loess Plateau based on the analysis of the data from observed storm runoff in small basins and artificial rainfall tests in the field (Liu and Wang, 1980). The loss of rainfall is mainly related to rainfall intensity ( $a$ ) and soil flow properties. The average loss rate  $\mu$  can be plotted against the average intensity ( $a$ ) as

$$\mu = R \cdot a^r$$

where  $R$  is the coefficient of loss related to the kind of soil or soil flow properties, and  $r$  is the index of loss.

(3) The condition of rainfall-runoff events for calibration is not the same as that of rainfall-runoff events for verification.

(4) The soil moisture of rainfall-runoff events for calibration is not the same as that of rainfall-runoff events for verification.

Therefore, this method in practice cannot directly be used for prediction of runoff discharge. However, the method can be applied to analyze the loss process from the hydrograph for calibration events, which can then be used to estimate the loss process for verification events based on the rainfall intensity and soil moisture, and excess rainfall can be calculated from the rainfall and loss process. In this way, the model parameters from the calibration event can be utilized to calculate the runoff hydrograph using the excess rainfall for the verification event.

The rainfall-runoff-sediment relationship is time-dependent. Consequently, the model parameters for a particular event will differ from the average parameter values. In order to overcome this drawback, simultaneous estimation of model parameters for more than two isolated events was performed to achieve better parameter values.

With a sufficient number of calibration events, the dependency of the models as well as parameter values on hydrological, meteorological, vegetational or other characteristics of the basin can be investigated.

#### SUMMARY AND CONCLUSIONS

A discrete linear model was employed for simulating runoff and sediment hydrograph for five small basins in the Loess Plateau of China. The model parameters were estimated using a nonlinear least-squares method in conjunction with Marquardt's (1963) iterative algorithm from the calibration events. The results showed good agreement between observed and estimated

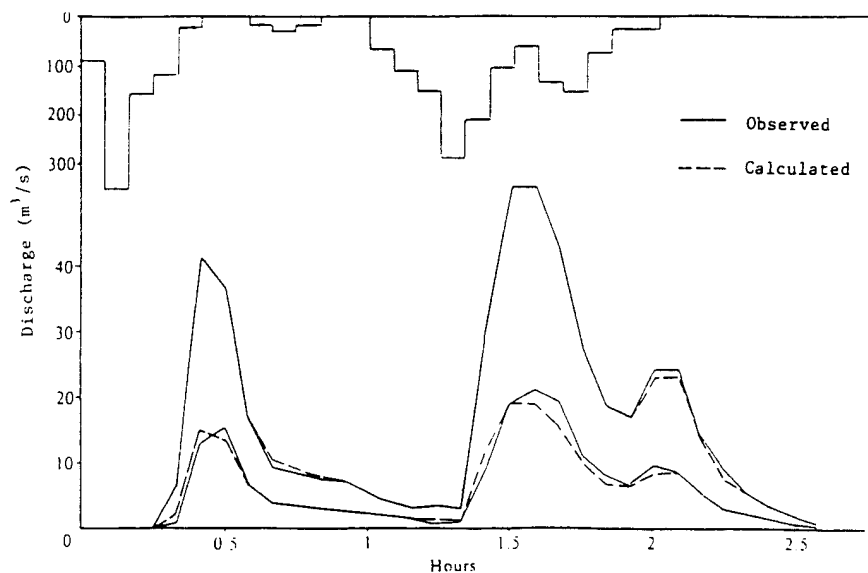


Fig. 2. Comparison of observed runoff and sediment discharge hydrographs with those calculated from discrete linear models for a calibration event on 17 July, 1966, in Shanchuan basin.

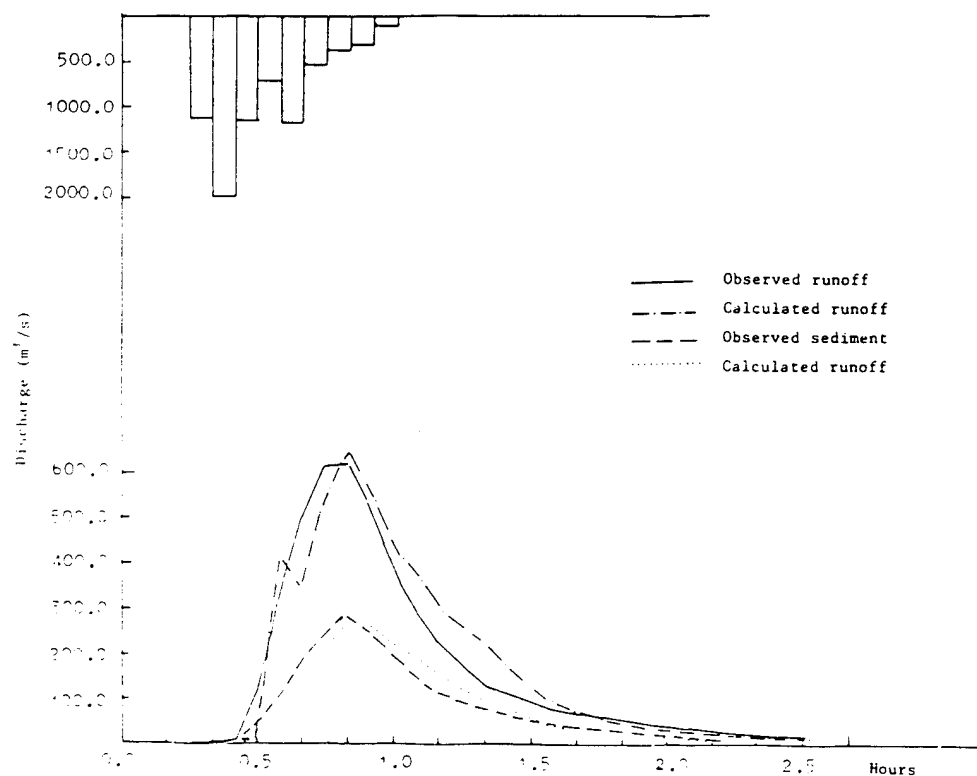


Fig. 3. Comparison of observed runoff and sediment discharge hydrographs with those calculated from discrete linear models for the verification event of 15 August, 1966 in Dujiago basin.

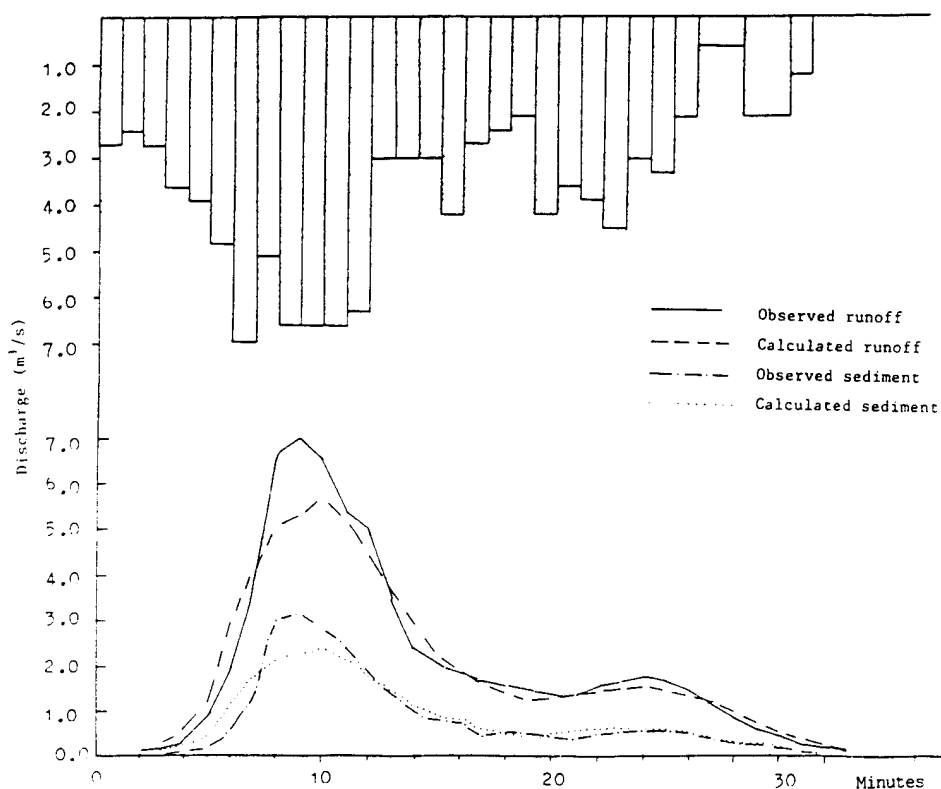


Fig. 4. Comparison of observed runoff and sediment discharge hydrographs with those calculated from discrete linear models for the verification event of 15 August, 1966 in Twanshan basin.

hydrographs for the five tested basins. The values of ISE generally were less than 1.0%. The coefficient and exponent of the regression equation were determined using the data from more than two events, and the parameters of the discrete linear model for sediment were estimated using ordinary least-squares in the calibration events. The calibration coefficient of determination  $R^2$  for five small basins was more than 97%. Figure 2 shows the relationship between observed and estimated runoff and sediment discharge for a sample event. The agreement between computed and observed values lends credence to the models.

The results from the verification events were not as good as those from the calibration events, but the prediction accuracy of the discrete linear models both for runoff and sediment discharge was satisfactory.

For the discrete linear transfer model of the runoff hydrograph, the values of ISE were around 10% with the average value being 9.36%. For the sediment models, both discrete linear model and regression equation gave good results: the value of  $R^2$  for both were more than 91.0%. The regression equation, with the average value of  $R^2$  being 94.32%, was a little better than the discrete linear model, where the average value of  $R^2$  was 94.26%. However,

for relative error of peak sediment discharge, the discrete linear model gave better results; the average value of EP was 17.72% compared with 18.12% for the regression equation.

Figures 3 and 4 show the relationship between observed and estimated runoff and sediment for sample events selected from verification. The good agreement between observed and predicted runoff and sediment discharge so obtained support the adaptability of these models to real-time forecasting schemes in the Loess Plateau in China.

#### ACKNOWLEDGMENTS

Wang Guang-Te expresses his appreciation of the financial support from the fund of the National Scientific Committee, China. V.P. Singh received partial support from the project 'A Continuum Model for Streamflow Synthesis' funded by the Army Research Office through Southern University.

#### REFERENCES

- Bard, Y., 1970. Comparison of gradient methods for the solution of nonlinear parameter estimation problems. *SIAM J. Num. Anal.*, 7(1): 157-186.
- Box, G.E.P. and Jenkins, E.M., 1976. *Time Series Analysis, Forecasting and Control*. Holden-Day, San Francisco.
- Caroni, E., Singh, V.P. and Ubertini, L., 1984. Rainfall-runoff-sediment yield relation by stochastic modelling. *Hydrol. Sci. J.*, 29(2): 203-218.
- Gong, S.Y. and Jiang, D.Q., 1977. The water soil losses and management for small basin in Loess Plateau region. Coordination Group for Yellow River Sediment Research, unpublished.
- Liu, C.M. and Wang, G.T., 1980. The estimation of small-watershed peak flows in China. *Water Resour. Res.*, 16(5): 881-886.
- Marquardt, D.M., 1963. An algorithm for least squares estimation of nonlinear parameters. *SIAM J. Num. Anal.*, 11(2): 431-441.
- Wang, G.T. and Yu, Y.S., 1986. Estimation of parameters of the discrete, linear, input-output model. *J. Hydrol.*, 85: 15-30.
- Yin, G. and Chen, Q., 1989. Characteristics index and statistical model of sediment yield in small drainage basins of Loess Plateau in China. *Acta Geog. Sin.*, 44(1): 32-46.

#### APPENDIX: NOTATION

$a_1, a_2, \dots, a_p,$	parameters for model (1)
$b_0, b_1, \dots, b_q$	
$C_1, C_2, \dots, C_p,$	parameters for model (12)
$W_0, W_1, \dots, W_q$	
$e_1, e_2, \dots, e_m$	the difference between the observed and estimated runoff discharges

$e_g(t)$	the difference between the observed and estimated sediment discharge rates
$G(t)$	observed sediment discharge rate
$G'(t)$	estimated sediment discharge rate
$I(t)$	excess rainfall intensity ( $\text{m}^3\text{s}^{-1}$ )
$L(s)$	the losses of rainfall
$m$	the number of runoff discharge periods
$P, q$	the order of models (1), (3) and (12)
$P(t)$	rainfall intensity ( $\text{m}^3\text{s}^{-1}$ )
$Q_p$	observed peak discharge
$Q'_p$	modeled peak discharge
$Q(t)$	observed runoff discharge ( $\text{m}^3\text{s}^{-1}$ )
$Q'(t)$	estimated runoff discharge ( $\text{m}^3\text{s}^{-1}$ )
$S$	the number of non-zero rainfall periods
$S_y$	estimated standard error of the sediment discharge rates

# DERIVATION OF INFILTRATION EQUATION USING SYSTEMS APPROACH

By V. P. Singh,<sup>1</sup> Member, ASCE, and F. X. Yu<sup>2</sup>

**ABSTRACT:** A general infiltration model is derived using a systems approach. The models of Horton, Kostiaikov, Overton, Green and Ampt, and Philip are some of the example models that are shown as special cases of the general model. An equivalence between the Green-Ampt model and the Philip two-term model is shown. The general model also provides a solution for the Holtan model expressing infiltration as a function of time. This solution of the Holtan model has not been reported in the literature. A first-order analysis is performed to quantify the uncertainty involved with the generalized model. The general infiltration model contains five parameters. Two of the parameters are physically based and can therefore be estimated from the knowledge of soil properties, antecedent soil moisture conditions, and infiltration measurements; the remaining three can be determined using the least squares method. The model is verified using ten observed infiltration data sets. Agreement between observed and computed infiltration is quite good.

## INTRODUCTION

A multitude of infiltration models used in applied hydrology and soil science exists. Some of these models are theoretically based (Dooge 1973; Philip 1957, 1969; Green and Ampt 1911), while others are empirical (Kostiakov 1932; Horton 1938; Holtan 1961; Overton 1964). Some of the empirical models are quite popular and frequently used in various water resources applications. The reason for their popularity is that they are simple and yield satisfactory results in some cases. Since the empirical models are more or less based on experimental observations, they represent the overall infiltration process.

The infiltration process can be represented by a systems approach, which uses an absorber or a network of absorbers. Infiltration constitutes input to the absorber. An absorber can be defined by a relation between its moisture content and the rate of infiltration to it. In this study, a general definition of the absorber is suggested, and a general infiltration model is derived by coupling this general relation with the spatially lumped form of continuity equation to be satisfied by the absorber. The various well-known infiltration models, such as the models of Horton (1938), Kostiaikov (1932), Overton (1964), Holtan (1961), Green and Ampt (1911), and Philip (1957) can be shown as special cases of this general model. Therefore, the systems approach presents a unified framework for all of these models and shows that these models result from different definitions of the absorber. As a consequence, connections between some of these models as well as their parameters can be established. This may help estimate model parameters. In particular, an equivalence between the Green-Ampt model and the Philip two-

<sup>1</sup>Prof. and Coordinator, Water Resour. Program, Dept. of Civ. Engrg., Louisiana State Univ., Baton Rouge, LA 70803-6405.

<sup>2</sup>Grad. Res. Asst., Dept. of Civ. Engrg., Louisiana State Univ., Baton Rouge, LA.

Note. Discussion open until May 1, 1991. To extend the closing date one month, a written request must be filed with the ASCE Manager of Journals. The manuscript for this paper was submitted for review and possible publication on September 12, 1989. This paper is part of the *Journal of Irrigation and Drainage Engineering*, Vol. 116, No. 6, November/December, 1990. ©ASCE, ISSN 0733-9437/90/0006-0837/\$1.00 + \$.15 per page. Paper No. 25352.

term model can be derived. This approach also leads to an explicit solution of the Holtan model, which does not appear to have been reported in the literature.

The objective of this study is to use the systems approach to derive a generalized infiltration model, show the various infiltration equations reported in the literature as special cases of the generalized model, show connections among some of these infiltration models, and derive an explicit solution of the Holtan model. The study also presents a first-order analysis of uncertainty and develops a simple procedure for estimating model parameters. Field data are finally used to verify the proposed infiltration model.

## GOVERNING EQUATIONS

We consider a column of soil matrix with unit area of vertical infiltration as shown in Fig. 1. The initial storage space available in the soil column is denoted as  $S_0$ . If the soil is initially dry, then  $S_0$  equals effective porosity multiplied by the total volume of the column. At time  $t = 0$ , a thin layer of water starts to cover the upper surface of the column. At any time  $t$  the infiltration rate is denoted as  $f(t)$ , seepage rate as  $f_s(t)$ , and the potential water storage space as  $S(t)$ . The spatially lumped continuity equation for the soil column can be written in integral form as

$$S(t) = S_0 - \int_0^t f(t)dt + \int_0^t f_s(t)dt \dots\dots\dots (1)$$

The differential form of continuity equation can be obtained by differentiating Eq. 1 with respect to  $t$  as

$$\frac{dS(t)}{dt} = f_s(t) - f(t) \dots\dots\dots (2)$$

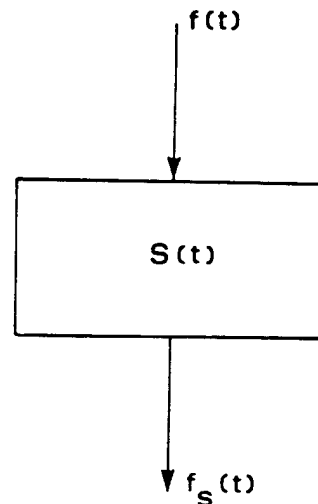


FIG. 1. Systems Representation of Soil Column by Absorber with Varying Vertical Infiltration and Seepage Rate

The amount of water stored in the soil column from  $t = 0$  to any time  $t$  is

$$W(t) = S_0 - S(t) = \int_0^t [f(t) - f_s(t)] dt \dots\dots\dots (3)$$

If  $f_s(t) = 0$  in Eq. 2 (Dooge 1973), then

$$\frac{dW}{dt} = f(t) \dots\dots\dots (4)$$

Eq. 2 contains three unknowns:  $S$ ,  $f$ , and  $f_s$ . To solve this equation, two relationships among the variables,  $S(t)$ ,  $f(t)$ , and  $f_s(t)$ , are required. By analogy to rainfall-runoff modeling (Kulandaiswamy 1964), a possible general relationship among these variables may be expressed as

$$S(t) = \sum_{n=0}^M a_n(f, f_s, t) \frac{d^n f}{dt^n} + b_n(f, f_s, t) \frac{d^n f_s}{dt^n}, \quad M \geq 0 \dots\dots\dots (5)$$

where  $a_n$  and  $b_n$  = coefficients, which may be functions of time  $t$ , infiltration rate  $f(t)$ , and seepage rate  $f_s(t)$ ; and  $M$  = some integer.

It is not clear what the form of the third relationship should be. Of course, one can arbitrarily choose some relationship, linear or nonlinear, to represent the relation among the three variables and then determine their coefficients by experimental data. However, the resulting model (Eqs. 2, 5, and a third relationship) may be too general and too complicated to be of any practical value. Thus, it may be preferable to examine the existing infiltration models and then find an underlying relationship among the potential storage, infiltration, and seepage variables.

#### ANALYSIS OF SOME INFILTRATION MODELS

Overton (1964) has shown that several infiltration models are based on a relationship between infiltration rate (or excess infiltration rate) and the volume of either actual or potential infiltration (or excess infiltration). For example, a form of the Green and Ampt model (1911) can be derived by assuming that

$$f(t) = \frac{a}{F(t)} + f_c \quad \text{or} \quad \frac{dF(t)}{dt} = \frac{a}{F(t)} + f_c \dots\dots\dots (6)$$

where  $F$  = volume of infiltration =  $\int_0^t f(t) dt$ ;  $f_c$  = the ultimate infiltration rate; and  $a$  = constant of proportionality. Integration of Eq. 6 yields a Green and Ampt type model:

$$t = \frac{1}{f_c} \left[ F - \frac{a}{f_c} \ln \left( 1 + \frac{f_c F}{a} \right) \right] \dots\dots\dots (7)$$

Similarly, the Kostiaikov, Philip two-term, Horton, and Overton models can be derived. Table 1 summarizes these models and the postulates on which they are based. In the approach followed by Overton (1964), no consideration is given to the continuity Eqs. 1 and 2.

**TABLE 1. Summary of Some Infiltration Models Derived by Postulating Relationship Between Rate of Infiltration and Volume of Infiltration**

Assumed relation (1)	Ultimate (constant) rate of infiltration, $f_i$ (2)	Resulting equation (3)	Analogous to (4)
$f(t) = a/[F(t)]$	0	$F = \sqrt{2at}$ or $f = \sqrt{2/a} t^{-1/2}$ $a = \text{constant of proportionality}$	Kostiakov model
$f(t) - f_i$ $= a/[F(t)]$	$f_i$	$t = (1/f_i)(F - (a/f_i) \ln \{1 + [F/(a/f_i)]\})$ $a = \text{constant or proportionality}$	Green-Ampt model
$f(t) - f_i$ $= a/[F(t) - f_i t]$	$f_i$	$F = f_i t + \sqrt{2at}$ or $f = f_i + \sqrt{a/2} t^{-1/2}$	Philip two- term model
$f(t) - f_i$ $= f_0 - f_i$ $= a[F(t) - f_i t]$	$f_i$	$f = f_i + (f_0 - f_i) \exp(-at)$ $F = f_i t + [(f_0 - f_i)/a][1 - \exp(-at)]$ $a = \text{parameter, } f_0 = \text{initial infiltration rate}$	Horton model
$f(t) - f_i$ $= a[f_i t - F(t)]^2$	$f_i$	$f = f_i \sec^2[(t_i - t) \sqrt{af_i}]$ $t_i = (1/\sqrt{af_i}) \tan^{-1}[F_i(a/f_i)^{1/2}]$ $F_i = \text{ultimate volume of infiltration}$	Overton model

These models plus some others can be derived using the systems approach of Eqs. 2 and 5. According to this approach, the potential storage  $S(t)$  and the seepage rate  $f_s(t)$  are postulated for each model. The relationships expressing these postulates are then substituted into Eq. 2 to obtain the corresponding infiltration model.

A summary of eight popular infiltration models is given in Table 2. These models are presented in two ways: (1) The usually reported form in literature (column 6); and (2) the form derived by systems approach (column 5). The potential storage function  $S(t)$  and seepage rate function  $f_s(t)$  for each model are also given in Table 2:  $a$ ,  $b$ ,  $A$ ,  $S_p$ ,  $W_0$ , and  $n$  are constants;  $f_i$  and  $K$  denote steady-state infiltration rate;  $h$  is the depth of ponded water on the soil surface (a constant);  $\theta_i$  is volumetric water content in transmission zone; and  $S_e$  is an effective matrix suction head at the wetting front.

It may be pertinent to comment briefly on the Zhao model, which is commonly used in China. Zhao (1981) hypothesized the infiltration system to be comprised of an absorber and a regulator. The absorber was assumed to be inversely proportional to the amount of water stored in a finite soil column, and the regulator to be directly proportional to the same amount of water. This hypothesis leads to the Zhao model as shown in Table 2.

From column 2 of Table 2, it is seen that, except for Zhao's model (1981),  $f_i(t)$  is either equal to zero (the Kostiakov model) or equal to the steady-state infiltration rate. If we compare these models with a typical infiltration curve shown in Fig. 2, then  $f_i(t)$  actually represents the steady-state flow rate, which is either equal to a constant or zero. From this point of view, Zhao's model may not be appropriate because the steady-state infiltration rate may not, in general, be proportional to the amount of water stored in the soil column. Therefore, a generalized relationship sought between  $f(t)$  and  $S(t)$  should not conform to this model. As seen from Fig. 2, the quantity  $\{f(t) - f_i(t)\}$  actually represents the nonsteady infiltration rate, and this function, according to column 3 of Table 2, is either directly proportional to the

TABLE 2. Summary of Some Infiltration Models

Model (1)	$f(t)$ assumed (2)	$f(t)$ assumed (3)	$S(t)$ derived form (4)	$f(t)$ derived form (5)	$f(t)$ reported form (6)
Horton (1933)	$L$	$[S(t)]/a$	$S_0 e^{-at}$ $a > 0$	$L - S_0/a e^{-at}$	$L - (L_0 - L) e^{-at}$
Dickson (1961)	$L$	$a[S(t)]^2 \quad a > 0$	$1/(1/S_0 + at)$	$L - [a/(1/S_0 + at)]^2$	$L$ , see <sup>2</sup> function $(bS_0 a)/(\sqrt{L/a})$ $\sqrt{at}$ , $t]$
Horton (1961)	$L$	$a[S(t)]^m$ $a > 0, m > 0$ $m \neq 2$	$[S_0^m - at]^{-1/(m+1)}$ $m > 0$	$L - a[S_0^m - at]^{-m/(m+1)}$	no general solution
Philip (1957)	$L$	$a/[S_0 - S(t)]$	$S_0 - \sqrt{2at}$	$L - (a/2a)^{1/2}$	$L - (1/2)S_0 a^{1/2}$
Kostiakov (1942)	0	$a/[S_0 - S(t)]^n$ $a > 0$	$S_0 [a(n+1)at]^{1/(n+1)}$	$a[1(n+1)at]^{-n/(n+1)}$	$KAt^{1/2}$
Kostiakov (modified) (1941)	$L$	$a/[S_0 - S(t)]^n$ $a > 0$	$S_0 [a(n+1)at]^{1/(n+1)}$	$L - a[1(n+1)at]^{-n/(n+1)}$	$L - KAt^{1/2}$
Green-Ampt (1911)	$K$	$[K_0(h + S_0)/S_0 - S(t)]$ $b/[S_0 - S(t)]$	$S_0 - \sqrt{2K_0(h + S_0)}$ $S_0 [b(n+1)at]^{1/2}$ $a > 0, b > 0$	$K - [K_0(h + S_0)/(2n)]^{1/2}$ $(b/a)^{1/2} [1 - e^{-(2n/ab)t}]^{1/2}$	$e^{-(b/a)^{1/2} t} [1 - (W_0/ab)] e^{-(2n/ab)t}$
Zhao (1981)	$[S_0 - S(t)]/a$	$[K_0(h + S_0)/S_0 - S(t)]$ $b/[S_0 - S(t)]$	$S_0 - \sqrt{2K_0(h + S_0)}$ $S_0 [b(n+1)at]^{1/2}$ $a > 0, b > 0$	$K - [K_0(h + S_0)/(2n)]^{1/2}$ $(b/a)^{1/2} [1 - e^{-(2n/ab)t}]^{1/2}$	$e^{-(b/a)^{1/2} t} [1 - (W_0/ab)] e^{-(2n/ab)t}$

<sup>2</sup>No explicit form obtained

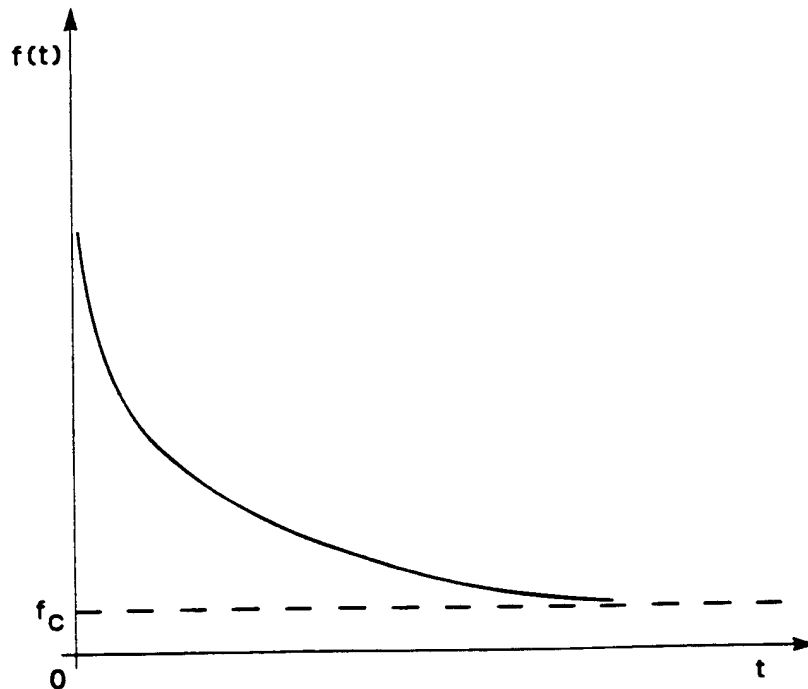


FIG. 2. Typical Infiltration Curve

potential storage  $S(t)$  (Horton 1938; Overton 1964; Holtan 1961) or inversely proportional to the amount of water stored in the soil column,  $W(t) = [S_0 - S(t)]$  (Philip 1957; Kostiakov 1932; Green-Ampt 1911).

#### GENERALIZED INFILTRATION MODEL

Based on this analysis, we might propose a generalized infiltration model of the following form of which all seven of these popular models are special cases:

$$f(t) - f_s(t) = \frac{a[S(t)]^m}{[S_0 - S(t)]^n} \quad (8)$$

where  $a$ ,  $m$ , and  $n$  = positive real constants. According to Eq. 8,  $f(t) \rightarrow \infty$  at  $t = 0$ , and  $f(t) \rightarrow f_s(t)$  at  $t = \infty$ . The general form of  $f_s(t)$  may be proposed as

$$f_s(t) = f_c \quad (9)$$

where  $f_c$  = a constant. Eqs. 2, 8, and 9 constitute the generalized infiltration model.

Substituting Eq. 8 into Eq. 2 yields

$$\frac{dS(t)}{dt} = \frac{-a[S(t)]^m}{[S_0 - S(t)]^n} \quad (10)$$

Eq. 8 can be expressed with the use of Eq. 9 as

$$f(t) = f_c + \frac{a[S(t)]^m}{[S_0 - S(t)]^n} \dots\dots\dots (11)$$

Integrating Eq. 10

$$\int_{S_0}^{S(t)} \frac{[S_0 - S(t)]^n}{[S(t)]^m} dS(t) = -at \dots\dots\dots (12)$$

If  $n$  is an integer, then Eq. 12 becomes

$$\int_{S_0}^{S(t)} \sum_{j=0}^n (-1)^j \binom{n}{j} S_0^{n-j} [S(t)]^{j-m} dS(t) = -at \dots\dots\dots (13a)$$

or

$$\sum_{j=0}^n (-1)^j \binom{n}{j} S_0^{n-j} \int_{S_0}^{S(t)} S^{j-m} dS = -at \dots\dots\dots (13b)$$

For  $m \neq 0$ ,  $n \neq 0$ , and  $n \neq m$  ( $n$  and  $m$  are integers), Eqs. 13a and b can be integrated as

$$\begin{aligned} & \sum_{j=m+1}^n (-1)^j \binom{n}{j} S_0^{n-j} \frac{\{[S(t)]^{j-m+1} - S_0^{j-m+1}\}}{j-m+1} \\ & + (-1)^{m-1} \binom{n}{m-1} S_0^{n-m+1} \ln \left[ \frac{S(t)}{S_0} \right] = -at \dots\dots\dots (14) \end{aligned}$$

If  $m$  is not an integer, the solution of Eqs. 13a and b is

$$\sum_{j=1}^n (-1)^j \binom{n}{j} S_0^{n-j} \frac{\{[S(t)]^{j-m+1} - S_0^{j-m+1}\}}{j-m+1} = -at \dots\dots\dots (15)$$

The generalized infiltration model is given in parametric form by Eqs. 14 and 11 or by Eqs. 15 and 11 for  $n$  being an integer. For the cases  $0 \leq n \leq 2$  and  $0 \leq m \leq 2$ , solutions of Eqs. 11 and 12 leading to some special cases of the generalized model are shown in Table 3. If  $m = 0$  and  $n > 0$ , then the generalized infiltration model reduces to the Kostiakov model; and when  $n = 0$  and  $m > 0$ , the generalized model becomes the Holtan model, as shown in Table 2. If  $n$  is not an integer and  $m \neq 0$ , then Eq. 12 may not have a general analytical solution. If the five parameters,  $a$ ,  $m$ ,  $n$ ,  $S_0$ , and  $f_c$  are known, then the infiltration rate can be calculated numerically by using Eqs. 11 and 12 and  $S$  as a parameter ( $0 \leq S \leq S_0$ ). A simple least-squares procedure is presented in Appendix I to determine the five parameters using observed data.

Eq. 12 can also be solved in terms of the beta functions. Define  $r = S(t)/S_0$  and  $S_0 dr = dS(t)$ . Therefore, Eq. 12 can be expressed as

$$S_0^{n-m+1} \int_1^r (1-r)^n r^{-m} dr = -at \dots\dots\dots (16a)$$

or

$$S_0^{n-m+1} \left[ \int_0^1 (1-r)^n r^{-m} dr - \int_0^r r^{-m} (1-r)^n dr \right] = at \dots\dots\dots (16b)$$

TABLE 3. Some Solutions as Special Cases of Generalized Model

$m$ (1)	$n$ (2)	$S(t)^a$ (3)	$f(t)$ (4)
0	0	$S_0 - at$	$f_c + a$
0	1	$S_0 - \sqrt{2at}$	$f_c + (a/2)^{1/2} t^{-1/2}$
0	2	$S_0 - (3at)^{1/3}$	$f_c + (a/9)^{1/3} t^{-2/3}$
0	$n > 0$ $n \neq 2$	$S_0 - [(n+1)at]^{1/(n+1)}$	$f_c + \{[(n+1)/a^{1/n}]t\}^{-n/(n+1)}$
1	0	$S_0 e^{-at}$	$f_c + S_0 a e^{-at}$
1	1	$\ln(S/S_0) - (S/S_0) = 1 - (at/S_0)$	$f_c + \{[aS(t)]/[S_0 - S(t)]\}$
1	2	$\ln(S/S_0) - 2(S/S_0) - (1/2)(S/S_0)^2$ $= -[(3/2) + (at/S_0^2)]$	$f_c + \{aS(t)/[S_0 - S(t)]^2\}$
2	0	$[(1/S_0) + at]^{-1}$	$f_c + [\sqrt{a}/(1/S_0 + at)]^2$
2	1	$\ln(S/S_0) + (S_0/S) = 1 + at$	$f_c + \{[(1 + at)S(t)^2]/[S_0 - S(t)]\}$
2	2	$(S/S_0) - (S_0/S) - 2 \ln(S/S_0)$ $= -(at/S_0)$	$f_c + \{[atS^2(t)]/[(S_0 - S)^2]\}$
$m > 1$	0	$[S_0^{1-m} - (1-m)at]^{1/(1-m)}$	$f_c + a[S_0^{1-m} - (1-m)at]^{m/(1-m)}$

<sup>a</sup>If an equal sign appears in an expression, that equation is independent of this heading.

or

$$S_0^{n-m+1} \left[ \int_0^1 (1-r)^{n_*-1} r^{m_*-1} dr - \int_0^r r^{m_*-1} (1-r)^{n_*-1} dr \right] = at \dots \dots \dots (16c)$$

where  $m_* = -m + 1$ ; and  $n_* = n + 1$ . This can be expressed as

$$S_0^{n-m+1} [B(m_*, n_*) - B_r(m_*, n_*)] = at \dots \dots \dots (16d)$$

where  $B(\cdot, \cdot)$  = the complete beta function, which can also be expressed in terms of the gamma function as

$$B(m_*, n_*) = \frac{\Gamma(m_*)\Gamma(n_*)}{\Gamma(m_* + n_*)} \dots \dots \dots (17)$$

and  $B_r(\cdot, \cdot)$  = the incomplete beta function, which can be expressed as

$$B_r(a; b) = \int_0^r x^{a-1} (1-x)^{b-1} dx; \quad a > 0, \quad b > 0, \quad r \in (0, 1) \dots \dots \dots (18a)$$

$$B_r(a; b) = \frac{r^a (1-r)^b}{a} \left[ 1 - \sum_{j=0}^{\infty} \frac{B(a-1; j+1)}{B(a-b; j+1)} r^{j+1} \right] \dots \dots \dots (18b)$$

Considerable simplification occurs if  $m = n$  in Eqs. 11 and 12. Using Eq. 11,  $S(t)$  can be expressed as an explicit function of  $f(t)$  as

$$S(t) = \frac{S_0 \left[ \frac{f(t) - f_c}{a} \right]^{1/n}}{1 - \left[ \frac{f(t) - f_c}{a} \right]^{1/n}} \dots \dots \dots (19)$$

TABLE 4. Special Cases of the Generalized Model

Parameters in Eq. 8			Resulting model (4)
$m$ (1)	$n$ (2)	$f_c$ (3)	
0	1	$f_c$	Philip two-term or Green-Ampt model
0	$> -1$	0	Kostiakov model
0	$> -1$	$f_c$	Modified Kostiakov model
1	0	$f_c$	Horton model
2	0	$f_c$	Overton model
$> 0$	0	$f_c$	Holtan model
$\neq 2$			

### Special Cases

Seven of the eight cited models are special cases of the generalized model. Some of these special cases can be inferred from Table 2. For clarity, these and other special cases are shown in Table 4. The Zhao model (1981) is not one of the special cases for the reasons cited earlier.

For  $m = 0$ ,  $n > 0$ , Eq. 12 becomes

$$S(t) = S_0 - [(n + 1)at]^{1/(n+1)} \quad (20)$$

Using Eqs. 8 and 9, Eq. 20 leads to

$$f(t) = f_c - \left[ \frac{(n+1)}{a^{1/n}} t \right]^{-n/(n+1)} \quad (21)$$

Eq. 21 is the modified Kostiakov model. If  $f_c = 0$ , Eq. 21 reduces to the Kostiakov model.

Similarly, for  $m = 0$ ,  $n = 1$ , the generalized model reduces to the Philip two-term model (Philip 1957) or the Green-Ampt model (Green and Ampt 1911), and also to the Kirkham-Feng model (1949) for horizontal flow. It will be shown in the ensuing discussion that the Green-Ampt model is equivalent to the Philip two-term model. If  $n = 0$ ,  $m = 1$ , the generalized model becomes the Horton model (1938), and for  $n = 0$ ,  $m = 2$ , the resulting model is the Overton model (1964).

For  $m > 1$ ,  $n = 0$ , and  $m \neq 2$ , Eq. 12 has the solution

$$S(t) = [S_0^{1-m} + (m-1)at]^{1/(1-m)} \quad (22)$$

Therefore, Eq. 8 becomes

$$f(t) = f_c - aS^m(t) \quad (23)$$

Substituting Eq. 22 in Eq. 23 yields

$$f(t) = f_c - a[S_0^{1-m} + (1-m)at]^{m/(1-m)} \quad (24)$$

Eq. 24, the general solution for the Holtan model (1961), does not appear to have been reported before.

Some of the infiltration models listed in column 5 of Table 2 may not look exactly like their usually reported form shown in column 6 of the same table. These forms of infiltration models are actually equivalent. For example, the Horton model (1938) in the current form is

$$f(t) = f_c + \frac{S_0}{a} e^{-t/a} \quad (25)$$

If we let  $f(0) = f_0$ , Eq. 25 yields

$$\frac{S_0}{a} = f_0 - f_c \quad (26)$$

Substitution of Eq. 26 into Eq. 25 produces exactly the same form of the Horton model.

$$f(t) = f_c + (f_0 - f_c)e^{-t/a} \quad (27)$$

Some of the models in Table 2 do not have general analytical solutions (Holtan model) or do not have explicit analytical solutions for  $f(t)$  (Green-Ampt model) as reported in literature. However, simpler and explicit solutions of  $f(t)$  can be obtained using the systems approach for all of the eight models.

#### Equivalence Between Green-Ampt and Philip Two-Term Models

The Green-Ampt and the Philip two-term models have the same form of solution in column 5 of Table 2. Since  $h$ ,  $\theta_r$ , and  $S_c$  are all constants in the Green-Ampt model, if  $K = f_c$  and  $a = K\theta_r(h + S_c)$ , the Green-Ampt and the Philip two-term models are equivalent. From Table 2, these two models have the same expression for  $S(t)$ :

$$S(t) = S_0 - \sqrt{2at} \quad (28)$$

Substituting Eq. 28 into Eq. 2, and solving with  $f_c = f_i = K$ , we have

$$f(t) = f_c + \alpha t^{-1/2}, \quad \alpha = \sqrt{\frac{a}{2}} \quad (29)$$

which is the Philip two-term infiltration model.

On the other hand, Eq. 28 can be expressed in the form of the Green-Ampt model. We rewrite Eq. 28 as

$$[S_0 - S(t)]^2 = 2at \quad (30)$$

Eq. 30 can also be expressed as

$$\int_0^{S_0 - S(t)} W dW = \int_0^t a d\tau \quad (31)$$

or

$$[S_0 - S(t)]d[S_0 - S(t)] = a dt \quad (32)$$

Rearranging Eq. 32 yields

$$\frac{d[S_0 - S(t)]}{dt} = \frac{a}{S_0 - S(t)} \quad (33)$$

Substituting Eq. 33 into Eq. 2, replacing  $f_c$  by  $K$  and solving, we obtain

$$f(t) = K + \frac{a}{S_0 - S(t)} \quad (34)$$

Notice that  $S_0 - S(t) = W(t) = L\theta_i$ , where  $L$  is the depth of the transmission zone, and  $\theta_i$  is volumetric moisture content. Eq. 34 can then be written with  $a = K\theta_i(h + S_c)$  as

$$f(t) = K \left[ 1 + \frac{\theta_i(h + S_c)}{W} \right] = K \left( \frac{L + h + S_c}{L} \right) \dots \dots \dots (35)$$

which is the Green-Ampt model.

From this proof, we see that the hydraulic conductivity  $K$  defined by Green and Ampt (1911) has the same value as the steady-state infiltration rate in the Philip two-term model (Philip 1957). The coefficient  $a$  in the Philip two-term model is proportional to the sum of the hydraulic head  $h$  and the capillary suction head  $S_c$ . Again, the solutions by systems approach are of simpler form than those derived using some of the other methods.

### SPECIAL CASE OF GENERAL MODEL

It may be useful to examine a special case of the general model. For the case  $n = 1$ ,  $m = 1$ , the generalized model (Eq. 11) becomes

$$f(t) = f_c + \frac{aS(t)}{S_0 - S(t)} \dots \dots \dots (36)$$

and  $S(t)$  is determined by integration of Eq. 12:

$$t = \frac{S_0}{a} \left[ \frac{S}{S_0} + \ln \left( \frac{S_0}{S} \right) - 1 \right] \dots \dots \dots (37)$$

Eqs. 36 and 37 can be considered as a parametric model of  $f(t)$  with  $S$  as the characteristic parameter. This model is actually a combination of the Horton model and the Green-Ampt model (or the Philip two-term model). When  $S(t)$  is removed from the numerator of the second term on the right-hand side of Eq. 36, this equation becomes the Philip two-term model; and when the term  $S_0 - S(t)$  is removed from the denominator, Eq. 36 becomes the Horton model.

The parametric model of Eqs. 36 and 37 can also be expressed in implicit form with  $t$  as a function of  $f(t)$ . From Eq. 36

$$S(t) = \frac{S_0[f(t) - f_c]}{a + f(t) - f_c} \dots \dots \dots (38)$$

Substitution of Eq. 38 in Eq. 37 leads to

$$t = \frac{S_0}{a} \left\{ \frac{f(t) - f_c}{a + f(t) - f_c} - \ln \left[ \frac{f(t) - f_c}{a + f(t) - f_c} \right] - 1 \right\} \dots \dots \dots (39)$$

This model consists of only three parameters:  $f_c$ ,  $S_0$ , and  $a$ . It is not only a simple infiltration model, but also includes consideration of the soil-water content and movement.

Following the concept embodied in this infiltration model, it may be possible to combine existing simple models to derive from the general model new infiltration models with three or less parameters. The parameters  $f_c$  and  $S_0$  of the new models can usually be obtained from parameters evaluated for

**TABLE 5. Relationship among Parameters in Derived and Reported Forms of Infiltration Models**

Model (1)	Parameters in reported form (2)	Parameters in current form (3)	Relationship (4)
Horton	$f_0$	$S_0$	$S_0 = a(f_0 - f_c)$
Horton	$f_c$	$f_c$	$f_c = f_c$
Horton	$a$	$a$	$a = a$
Overton	$f_c$	$f_c$	$f_c = f_c$
Overton	$a$	$a$	$a = a$
Overton	$S_0$	$S_0$	$S_0 = S_0$
Philip	$A$	$f_c$	$f_c = A$
Philip	$S_p$	$a$	$a = (S_p^2)/2$
Kostiakov	$K$	$n$	$n = A/(1 - A)$
Kostiakov	$A$	$a$	$a = AK^{1-n}$
Modified Kostiakov	$f_c$	$f_c$	$f_c = f_c$
Modified Kostiakov	$K$	$n$	$n = A/(1 - A)$
Modified Kostiakov	$A$	$a$	$a = AK^{1-n}$
Zhao	$a$	$a$	$a = a$
Zhao	$b$	$b$	$b = b$
Zhao	$W_0$	—	—

other models as shown in Table 5 or estimated directly from observed data. The proportionality factor  $a$  may be directly determined from observed data using the method of least squares or moments.

#### FIRST-ORDER ANALYSIS OF UNCERTAINTY

Eq. 8 is the fundamental equation of the generalized infiltration model proposed here. There may, however, be uncertainties involved with this equation that must be recognized. Besides the uncertainty of the equation itself, there can be two other sources of error in  $f$  due to spatial and temporal variability. First, the measurement of  $S$  may be inaccurate. Second, the parameters,  $f_c$ ,  $S_0$ ,  $a$ ,  $m$ , and  $n$  may be subject to errors. The first-order analysis of uncertainty can be employed to quantify the expected variability arising from uncertainty in  $S$  and/or  $a$ ,  $f_c$ ,  $S_0$ ,  $m$ , and  $n$ . To illustrate the procedure, let us represent Eq. 8 as

$$f = g(S, a, f_c, S_0, m, n) \dots \dots \dots (40)$$

where  $g$  = some function. It is implied in Eq. 40 that  $f$  and  $S$  depend on  $t$ . If the true values of  $S$ ,  $a$ ,  $f_c$ ,  $S_0$ ,  $m$ , and  $n$  differ from their corresponding nominal (average) values,  $\bar{S}$ ,  $\bar{a}$ ,  $\bar{f}_c$ ,  $\bar{S}_0$ ,  $\bar{m}$ , and  $\bar{n}$ , where

$$\bar{f} = g(\bar{S}, \bar{a}, \bar{f}_c, \bar{S}_0, \bar{m}, \bar{n}) \dots \dots \dots (41)$$

then the effect of this discrepancy on  $f$  can be evaluated by expanding the function  $g(\cdot)$  around the point defined by  $S = \bar{S}$ ,  $a = \bar{a}$ ,  $f_c = \bar{f}_c$ ,  $S_0 = \bar{S}_0$ ,  $m = \bar{m}$ ,  $n = \bar{n}$ .

For purposes of simplicity, let  $x_1 = S$ ,  $x_2 = a$ ,  $x_3 = f_c$ ,  $x_4 = S_0$ ,  $x_5 = m$ , and  $x_6 = n$ . Then the Taylor series expansion of Eq. 40 yields

$$f = g(\bar{S}, \bar{a}, \bar{f}_i, \bar{S}_0, \bar{m}, \bar{n}) + \sum_{i=1}^6 \left[ \left( \frac{\partial g}{\partial x_i} \right)_{-} (x_i - \bar{x}_i) \right. \\ \left. + \frac{1}{2} \sum_{i=1}^6 \sum_{j=1}^6 \left[ \left( \frac{\partial^2 g}{\partial x_i \partial x_j} \right)_{-} (x_i - \bar{x}_i)(x_j - \bar{x}_j) \right] + \text{higher-order terms} \dots \dots \dots \right] \quad (42)$$

where  $[(\partial g / \partial x_i)_{-}]$  = the first-order partial derivative of the function  $g$  with respect to  $x_i$  evaluated at the point of expansion  $(\bar{x}_1, \bar{x}_2, \bar{x}_3, \bar{x}_4, \bar{x}_5, \bar{x}_6)$ ; and  $(\partial^2 g / \partial x_i \partial x_j)_{-}$  = the second-order partial derivative of  $g$  with respect to  $x_i$  and  $x_j$  evaluated at the point of expansion.

If the second- and higher-order terms are neglected, the resulting first-order expression for the error in  $f$  is

$$f - \bar{f} = E = \sum_{i=1}^6 \left( \frac{\partial g}{\partial x_i} \right)_{-} (x_i - \bar{x}_i) \dots \dots \dots \quad (43)$$

The variance of this error is

$$S_f^2 = E[(f - \bar{f})^2] \dots \dots \dots \quad (44a)$$

or

$$S_f^2 = E \left\{ \sum_{i=1}^6 \left[ \left( \frac{\partial g}{\partial x_i} \right)_{-} (x_i - \bar{x}_i) \right]^2 \right\} \dots \dots \dots \quad (44b)$$

where  $E$  = the expectation operator. For simplicity, it is assumed that the variables  $x_i$  are independent.

$$S_f^2 = \sum_{i=1}^6 \left( \frac{\partial g}{\partial x_i} \right)_{-}^2 S_{x_i}^2 \dots \dots \dots \quad (45a)$$

or

$$S_f^2 = \left( \frac{\partial g}{\partial S} \right)_{-}^2 S_S^2 + \left( \frac{\partial g}{\partial a} \right)_{-}^2 S_a^2 + \left( \frac{\partial g}{\partial f_i} \right)_{-}^2 S_{f_i}^2 + \left( \frac{\partial g}{\partial S_0} \right)_{-}^2 S_{S_0}^2 \\ + \left( \frac{\partial g}{\partial m} \right)_{-}^2 S_m^2 + \left( \frac{\partial g}{\partial n} \right)_{-}^2 S_n^2 \dots \dots \dots \quad (45b)$$

where  $S_{x_i}^2$  = the variance of  $x_i$ . From Eq. 8, the partial derivatives  $(\partial g / \partial x_i = \partial f / \partial x_i)$  are

$$\frac{\partial f}{\partial S} = \frac{aS^{m-1}}{(S_0 - S)^n} + \frac{aS^m}{(S_0 - S)^{n+1}} \dots \dots \dots \quad (46a)$$

$$\frac{\partial f}{\partial a} = \frac{S^m}{(S_0 - S)^n} \dots \dots \dots \quad (46b)$$

$$\frac{\partial f}{\partial f_i} = 1 \dots \dots \dots \quad (46c)$$

$$\frac{\partial f}{\partial S_0} = -\frac{aS^m}{(S_0 - S)^{n+1}} \dots \dots \dots \quad (46d)$$

$$\frac{\partial f}{\partial m} = (f - f_c) \log S \dots\dots\dots (46e)$$

$$\frac{\partial f}{\partial n} = -(f - f_c) \log (S_0 - S) \dots\dots\dots (46f)$$

where log denotes the natural logarithm.

By substituting the values of these partial derivatives in Eqs. 45a and b, the error in  $f$  can be computed. If the error in  $f$  is computed due to error in only one variable, say  $S$ , then

$$S_f^2 = \text{var} (f) = \left( \frac{\partial g}{\partial S} \right)_S^2 S_S^2 = \left\{ \frac{aS^{m-1}}{(S_0 - S)^n} \left[ 1 + \frac{nS}{m(S_0 - S)} \right] \right\}^2 S_S^2 \dots\dots\dots (47)$$

The value of  $S_f^2$  = the standard error of estimate of  $f$ . If error in  $f$  is calculated due to error in  $a$  only, then

$$\text{var} (f) = S_f^2 = \left( \frac{\partial g}{\partial a} \right)_a^2 S_a^2 = \left[ \frac{S^m}{(S_0 - S)^n} \right]^2 S_a^2 \dots\dots\dots (48)$$

If only  $f_c$  is to be considered, then

$$S_f^2 = \left( \frac{\partial g}{\partial f_c} \right)_{f_c}^2 S_{f_c}^2 = S_{f_c}^2 \dots\dots\dots (49)$$

If the variable under consideration is  $S_0$ , then

$$S_f^2 = \left( \frac{\partial g}{\partial S_0} \right)_{S_0}^2 S_{S_0}^2 = \left[ \frac{aS^m}{(S_0 - S)^{n+1}} \right]^2 S_{S_0}^2 \dots\dots\dots (50)$$

If the variable under consideration is  $m$ , then

$$S_f^2 = \left( \frac{\partial g}{\partial m} \right)_m^2 S_m^2 = [(f - f_c) \log S]^2 S_m^2 \dots\dots\dots (51)$$

If the variable under consideration is  $n$ , then

$$S_n^2 = \left( \frac{\partial g}{\partial n} \right)_n^2 S_n^2 = [-(f - f_c) \log (S_0 - S)]^2 S_n^2 \dots\dots\dots (52)$$

The total variance of infiltration rate can also be expressed as a function of the coefficients of variation of  $S$ ,  $a$ ,  $f_c$ ,  $S_0$ ,  $m$ , and  $n$  as

$$\begin{aligned} \text{var} (f) = S_f^2 = & \left\{ \frac{aS^{m-1}}{(S_0 - S)^n} \left[ 1 + \frac{nS}{m(S_0 - S)} \right] \right\}^2 S_S^2 + \left[ \frac{S^m}{(S_0 - S)^n} \right]^2 S_a^2 \\ & + S_{f_c}^2 + \left[ \frac{-aS^m}{(S_0 - S)^{n+1}} \right]^2 S_{S_0}^2 + [(f - f_c) \log S]^2 S_m^2 \\ & + [-(f - f_c) \log (S_0 - S)]^2 S_n^2 \dots\dots\dots (53) \end{aligned}$$

The variance of infiltration rate can also be expressed as a function of the coefficients of variation  $CV$  of  $S$ ,  $a$ ,  $f_c$ ,  $S_0$ ,  $m$ , and  $n$  as

$$\text{var} (f) = \bar{f}^2 CV^2(f) = \left[ \frac{aS^m}{(S_0 - S)^n} \right]^2 \left\{ \left[ m \left[ 1 + \frac{nS}{m(S_0 - S)} \right] \right]^2 CV_S^2 + CV_a^2 \right.$$

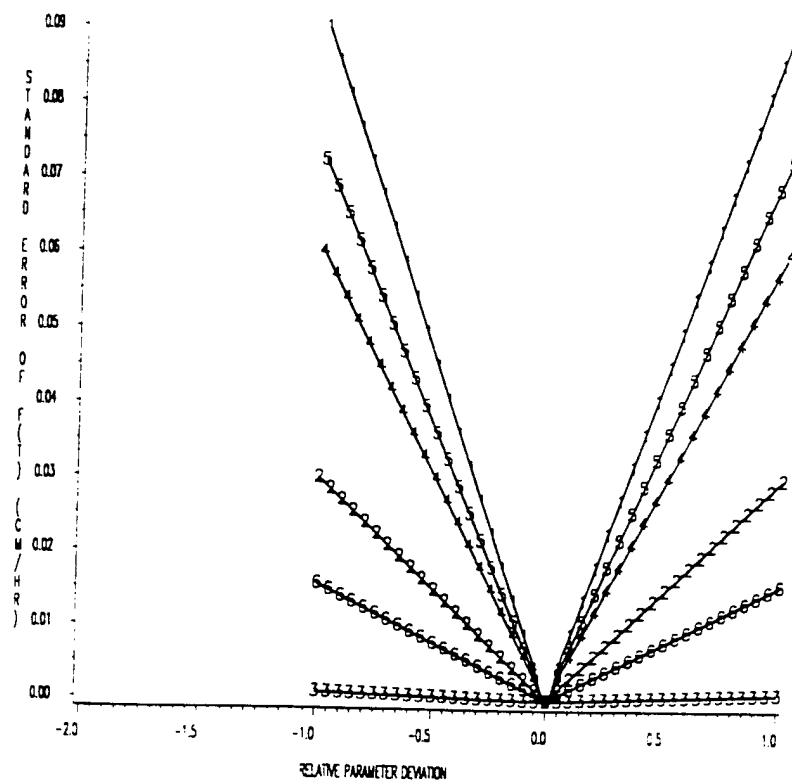


FIG. 3. Standard Error of Estimate of  $f(t)$  as Function of Relative Deviations in Parameter:  $A = 0.1$ ,  $N = 1$ ,  $M = 2$ ,  $S = 0.3$ ,  $S_0 = 0.6$ ,  $f_c = 0.001$ ; 1 = Deviation in Variable  $S$  Only; 2 = Deviation in Parameter  $A$  Only; 3 = Variation in Parameter  $FC$  Only; 4 = Deviation in Parameter  $S_0$  Only; 5 = Deviation in Parameter  $M$  Only; and 6 = Deviation in Parameter  $N$  Only

$$+ (nS_0)^2 CV_{S_0}^2 - (m \log S)^2 CV_m^2 + [n \log (S_0 - S)]^2 CV_n^2) - f_c^2 CV_{f_c}^2 \dots \dots (54)$$

It is seen from Eq. 53 that the variance of  $f(t)$  not only depends on the variance of each parameter but also on the values of the parameters themselves. An illustrative example is shown in Fig. 3 for  $\bar{a} = 0.1$ ,  $\bar{n} = 1$ ,  $\bar{m} = 2$ ,  $\bar{S} = 0.3$  m,  $\bar{S}_0 = 0.6$  m, and  $\bar{f}_c = 0.001$  m/h. These values represent normal cases. Fig. 3 shows that the standard error of estimate of  $f(t)$  is very sensitive to the relative deviations in parameters  $S$ ,  $m$ ,  $S_0$ ,  $a$ , and  $n$  and is relatively insensitive to the relative deviation in parameter  $f_c$ . This conclusion, however, is based on the mean values used and may change with the changes in the mean values.

#### VERIFICATION OF MODEL

The generalized model has five parameters:  $f_c$  (steady-state infiltration rate),  $S_0$  (initial storage space),  $a$  (a proportionality factor), and  $m$  and  $n$  (two exponents). Table 5 presents the relationships between the parameters of the infiltration models derived by the systems approach listed in column 5 of Table 2 and those reported in literature for all six explicit and analytical

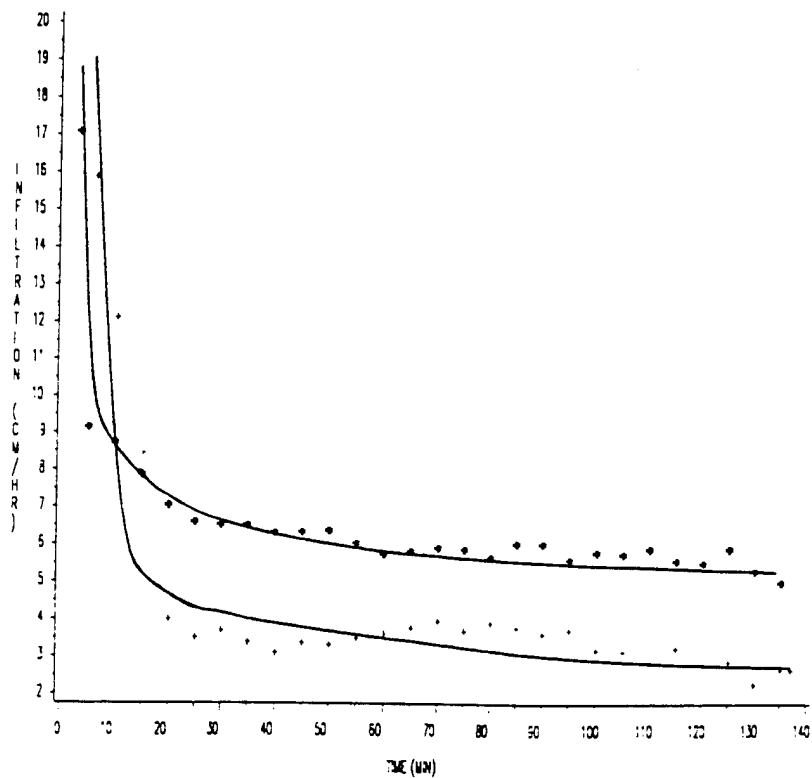


FIG. 4. Calibration of Infiltration Model: Soil Type: Alapaha Loamy Sand ID = 01011D; and Soil Type: Cowarts Loamy Sand ID = 17032D (\* = Observed Data Set 1; + = Observed Data Set 2; and — = Calculated Value)

infiltration models listed in column 6. Once the parameters of the usual form of a listed model are recognized, the corresponding parameters for the model derived by the systems approach can be easily found.

If infiltration observations are available for a soil, then the five model parameters can be estimated for that soil using an iterative procedure. However, this procedure is usually complicated and does not take into account the physical import of the parameters. A simplified procedure was therefore employed in this study. The procedure is based on the premise that  $f_c$  and  $S_0$  can be initially determined from the knowledge of soil properties, antecedent soil moisture conditions, and infiltration measurements. This premise is not unduly restrictive, for both  $f_c$  and  $S_0$  are physical quantities. On one hand,  $f_c$  is the ultimate infiltration rate and can be determined experimentally. In practice,  $f_c$  should satisfy

$$0 \leq f_c < \min [f_0(t_i)] \quad (55)$$

where  $f_0(t_i)$  = the  $i$ th observed infiltration rate; and  $S_0$  = the effective potential storage. Experimentally, it is equal to the soil column times the effective porosity. From Eq. 11, if the soil column is saturated  $S = 0$ , then infiltration rate will equal  $f_c$ . At  $t = 0$ ,  $S = S_0$ , then  $f(0) \rightarrow \infty$ . This is consistent with the Horton model. In practice,  $S_0$  can be selected by considering a practical soil depth and an average soil porosity, since only the top soil zone may significantly affect the dynamic infiltration process (Fok

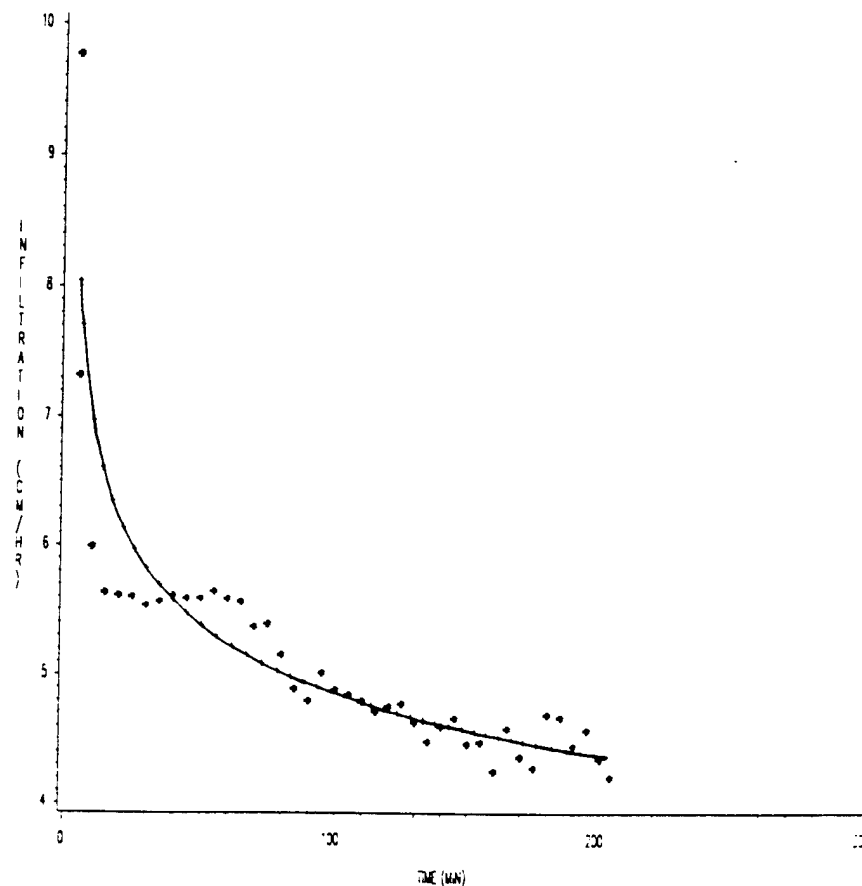


FIG. 5. Calibration of Infiltration Model: Soil Type: Stilson Loamy Sand ID = 10101D [\* = Observed; - = Calculated;  $A = 0.00093$ ;  $B = 1.28$ ;  $N = 0.353$ ;  $S_0 = 27.43$  (cm); and  $FC = 3.048$  (cm/h)]

and Chiang 1984). Normally, this top soil zone is less than 2 m. If average soil porosity is 0.3, then  $S_0$  should satisfy

$$0 \leq S_0 < 0.6 \quad (56)$$

Overton (1964) assumed  $S_0 = 0.2743$  m (soil depth = 36 in.), while Holtan (1961) chose  $S_0 = 0.0457$  m (soil depth = 6 in.). On the other hand, it may be difficult to estimate accurately the actual values of these two parameters in a watershed due to spatial and temporal variabilities. However, once  $f_i$  and  $S_0$  are reasonably chosen following Eqs. 55 and 56, then the other three parameters  $a$ ,  $m$ , and  $n$  can be estimated using the least-squares method. Hence, a good fit to field data can be achieved. An explicit least-squares solution for estimation of these parameters is given in Appendix I.

Ten observed infiltration data sets from Rawls et al. (1976) were used to test the goodness of the generalized infiltration model given in this paper. The generalized model usually gave a better fit than other special models for each data set. The computational procedure is given in Appendix I. For three sample data sets, observed and computed infiltration curves are given in Figs. 4 and 5, respectively, for different types of soil.

Because the five parameters can be determined directly from Appendix I, no iteration or trial-and-error method is involved. However, optimal sets of parameters may not always be unique, and more than one set of optimal parameters may lead to an equally good fit to observed data. From physical considerations, it may, therefore, be preferable to choose  $0.25 \text{ m} \leq S_0 \leq 0.45 \text{ m}$ , and  $f_c$  as slightly smaller than the smallest observed infiltration rate value. Then parameters  $a$ ,  $m$ , and  $n$  are determined by Appendix I. If the computed value of  $a$  is too small ( $a < 10^{-5}$  in cm-h units), one can change  $f_c$  slightly in the range given by Eq. 56. Normally, one or two trials will produce a reasonable set of optimal parameters. In the three data sets shown in Figs. 4 and 5,  $S_0$  was fixed at 27.43 cm where the soil depth considered is 91.44 cm and soil porosity is 30%. In the range given in Appendix I,  $f_c$  was selected so that  $a$  was in the range from  $10^{-2}$  to  $10^{-4}$ . All computations showed that the five parameters were easily determined, and hence produced a good infiltration model.

### CONCLUDING REMARKS

This study utilizes systems approach to derive a generalized infiltration model. Seven popular infiltration models are shown to be special cases of this generalized model. This model has five parameters: steady-state infiltration rate  $f_c$ ; initial storage space available  $S_0$ ; a proportionality factor  $a$ ; and two exponents  $m$  and  $n$ . It may be useful to combine two or three popular infiltration models into one, according to the generalized model, and yield a three-parameter model as illustrated by Eqs. 36 and 37. For 10 observed data sets, the procedure for parameter estimation was quick and efficient. The model reproduced infiltration rates for these data sets reasonably well.

### ACKNOWLEDGMENTS

The work reported in this paper was supported in part by funds provided by the Army Research Office through Southern University under the project on "A Continuum Model for Streamflow Synthesis."

### APPENDIX I. LEAST-SQUARES ESTIMATION OF MODEL PARAMETERS

It is assumed that the model parameters  $f_c$  and  $S_0$  are obtained from soil properties and antecedent conditions. The parameters estimated are  $a$ ,  $m$ , and  $n$ . To that end, the least-squares objective function is constructed in log space as

$$SS = \sum_{i=1}^N \{ \log [f_{\text{obs}}(i) - f_c] - \log [f_{\text{com}}(i) - f_c] \}^2 \dots \dots \dots (57)$$

where  $f_{\text{obs}}(i)$  = observed infiltration rate at the  $i$ th time;  $f_{\text{com}}(i)$  = computed infiltration rate at the  $i$ th time;  $SS$  = the error; and  $N$  = the number of observations or times. It is recognized that the sum of squares of log values is minimized, not the sum of the infiltration rates themselves. As a result, the estimate of  $a$ ,  $n$ , and  $m$  may be somewhat biased. Minimization based on the log values was preferred for two reasons. First, it leads to an ana-

lytical solution. Second, experimental verification of the model showed that the model fit the field data reasonably well. Minimization based on arithmetic values of infiltration rates leads to equations that are not explicit in terms of  $a$ ,  $n$ , and  $m$ , and hence an iterative solution, although not very difficult to accomplish with a computer, is required.

Eq. 57 can be written as

$$SS = \sum_{i=1}^N \left( \log [f_{\text{obs}}(i) - f_c] - \log \left\{ \frac{aS^m(i)}{[S_0 - S(i)]^n} \right\} \right)^2 \dots\dots\dots (58)$$

where  $S(i)$  = the  $i$ th value of  $S(t)$ . For simplicity of notations, the suffix  $i$  is dropped from now on, keeping in mind that  $f_{\text{obs}}$  and  $S$  both are functions of time and vary from one observation to the other. Eq. 58 is written as

$$SS = \sum [\log (f_{\text{obs}} - f_c) - \log a - m \log S + n \log (S_0 - S)]^2 \dots\dots\dots (59)$$

The parameters  $a$ ,  $m$ , and  $n$  are obtained so as to produce the minimum value of  $SS$ . To that end,  $SS$  is partially differentiated with respect to each parameter separately, and each partial derivative is equated to zero. This yields

$$\begin{aligned} \frac{\partial SS}{\partial a} = 0 &= -\frac{1}{a} [\sum \log (f_{\text{obs}} - f_c) - N \log a - m \sum \log S \\ &+ n \sum \log (S_0 - S)] \dots\dots\dots (60) \end{aligned}$$

or

$$N \log a + m \sum \log S - n \sum \log (S_0 - S) = \sum \log (f_{\text{obs}} - f_c) \dots\dots\dots (61a)$$

$$\begin{aligned} \frac{\partial SS}{\partial m} = 0 &= -\sum \log (f_{\text{obs}} - f_c) \log S + \log a \sum \log S + m \sum (\log S)^2 \\ &- n \sum \log (S_0 - S) \log S \dots\dots\dots (61b) \end{aligned}$$

or

$$\begin{aligned} \log a \sum \log S + m \sum (\log S)^2 - n \sum \log (S_0 - S) \log S \\ = \sum \log (f_{\text{obs}} - f_c) \log S \dots\dots\dots (62a) \end{aligned}$$

$$\begin{aligned} \frac{\partial SS}{\partial n} = 0 &= \sum \log (f_{\text{obs}} - f_c) \log (S_0 - S) - \log a \sum \log (S_0 - S) \\ &- m \sum \log (S_0 - S) \log S + n \sum [\log (S_0 - S)]^2 \dots\dots\dots (62b) \end{aligned}$$

or

$$\begin{aligned} \log a \sum \log (S_0 - S) + m \sum \log (S_0 - S) \log S \\ - n \sum [\log (S_0 - S)]^2 = \sum \log (f_{\text{obs}} - f_c) \log (S_0 - S) \dots\dots\dots (63) \end{aligned}$$

Eqs. 61-63 are solved simultaneously by Kramer's rule to obtain the parameters  $a$ ,  $m$ , and  $n$ . In matrix form, these equations can be written as

$$\begin{bmatrix} N & \sum \log S & -\sum \log (S_0 - S) \\ \sum \log S & \sum (\log S)^2 & -\sum \log (S_0 - S) \log S \\ \sum \log (S_0 - S) & \sum [\log (S_0 - S)] \log S & -\sum [\log (S_0 - S)]^2 \end{bmatrix} \begin{bmatrix} \log a \\ m \\ n \end{bmatrix}$$

$$= \begin{bmatrix} \Sigma \log (f_{\text{obs}} - f_c) \\ \Sigma \log (f_{\text{obs}} - f_c) \log S \\ \Sigma \log (f_{\text{obs}} - f_c) \log (S_0 - S) \end{bmatrix} \dots \dots \dots (64)$$

For notational convenience and writing, let  $A = \Sigma \log S$ ,  $B = \Sigma (\log S)^2$ ,  $C = \Sigma \log (S_0 - S)$ ,  $D = \Sigma [\log (S_0 - S)] \log S$ ,  $G = \Sigma [\log (S_0 - S)]^2$ ,  $H = \Sigma \log (f_{\text{obs}} - f_c)$ ,  $I = \Sigma \log (f_{\text{obs}} - f_c) \log S$ ; and  $J = \Sigma \log (f_{\text{obs}} - f_c) \log (S_0 - S)$ . Eq. 64 can be rewritten using these notations as

$$\begin{bmatrix} N & A & -C \\ A & B & -D \\ C & D & -G \end{bmatrix} \begin{bmatrix} \log a \\ m \\ n \end{bmatrix} = \begin{bmatrix} H \\ I \\ J \end{bmatrix} \dots \dots \dots (65)$$

Then

$$\log a = \frac{1}{D_e} \begin{bmatrix} H & A & -C \\ I & B & -D \\ J & D & -G \end{bmatrix} \dots \dots \dots (66)$$

where  $D_e$  = the determinant of the coefficient matrix expressed as

$$D_e = \begin{bmatrix} N & A & -C \\ A & B & -D \\ C & D & -G \end{bmatrix} \dots \dots \dots (67a)$$

$$D_e = N(D^2 - BG) - A(CD - AG) - C(AD - CB) \dots \dots \dots (67b)$$

Hence

$$\log a = \frac{H(D^2 - BG) - A(JD - IG) - C(ID - JB)}{D_e} \dots \dots \dots (68)$$

$$m = \begin{bmatrix} N & H & -C \\ A & I & -D \\ C & J & -G \end{bmatrix} = \frac{N(JD - IG) - H(CD - AG) - C(AJ - CI)}{D_e} \dots \dots (69)$$

$$n = \begin{bmatrix} N & A & H \\ A & B & I \\ C & D & J \end{bmatrix} = \frac{N(BJ - DI) - A(AJ - CI) + H(AD - CB)}{D_e} \dots \dots (70)$$

Eqs. 68–70 explicitly yield optimal estimates of  $a$ ,  $m$ , and  $n$ .

For a given set of infiltration data, i.e.,  $[t_i, f_{\text{obs}}(i)]$ ,  $i = 1, 2, \dots, N$ , one can determine the five parameters as follows.

#### Step 1

Assume initial values  $t = 0$ ,  $S(0) = S_0$ ,  $f(0) \cong f_{\text{obs}}(1)$ .

#### Step 2

Based on the physical meaning of parameters  $S_0$  and  $f_c$  and observed data, choose  $f_c$  in the range

$$0 \leq f_c \leq \min [f_{\text{obs}}(i)], \quad i = 1, 2, \dots, N \dots \dots \dots (71)$$

where  $f_{\text{obs}}(i)$  = the observed infiltration rate. For most types of soils the

infiltration rate may be significantly affected only by the top soil zone (say, soil depth less than 2 m). If soil porosity is 30%, then  $S_0$  may be chosen in the range

$$0 < S_0 < 0.6 \text{ m} \dots\dots\dots (72)$$

### Step 3

From Eq. 2 or Eq. 1, one can calculate  $S(t)$  as

$$\begin{aligned} S_{i+1} &= S_i + \{f_i - 0.5[f_{\text{obs}}(i+1) + f_0(i)]\}(t_{i+1} - t_i) \\ S_1 = S(0) &= S_0, \quad i = 1, 2, \dots, N \dots\dots\dots (73) \end{aligned}$$

### Step 4

Compute parameters  $a$ ,  $m$ , and  $n$  by Eqs. 68, 69, and 70, respectively.

### Step 5

Once all five parameters are determined, the values of infiltration rate can be generated by the model for a given set of values of  $S_i$ ,  $0 \leq S_i \leq S_0$ . Thus

$$f_i = f_c + \frac{aS_i^m}{(S_0 - S_i)^n} \dots\dots\dots (74)$$

and

$$t_{i+1} = t_i + \frac{(S_{i+1} - S_i)}{f_i - 0.5(f_{i+1} + f_i)}, \quad i = 1, 2, \dots, N \dots\dots\dots (75)$$

## APPENDIX II. REFERENCES

- Dooge, J. C. I. (1973). "Linear theory of hydrologic systems." *Tech. Bulletin No. 1468*, U.S. Dept. of Agr., Agric. Res. Service, Washington, D.C.
- Fok, Y. S., and Chiang, S. H. (1984). "2-D infiltration equations for furrow irrigation." *J. Irrig. and Drain. Engrg.*, ASCE, 110(2), 208-217.
- Green, W. H., and Ampt, C. A. (1911). "Studies on soil physics. I. Flow of air and water through soils." *J. Agric. Sci.*, 4, 1-24.
- Holtan, H. N. (1961). "A concept of infiltration estimates in watershed engineering." *ARS 41-51*, U.S. Dept. Agr., Agric. Research Service, Washington, D.C.
- Horton, R. I. (1938). "The interpretation and application of runoff plot experiments with reference to soil erosion problems." *Proc., Soil Science Society of America*, 3, 340-349.
- Kirkham, D., and Feng, C. L. (1949). "Some tests of the diffusion theory, and laws of capillary flow in soils." *Soil Sci.*, 67, 29-40.
- Kostiakov, A. N. (1932). *On the dynamics of the coefficients of water percolations in soils*, Sixth Commission, Int. Soc. Soil Science, Part A, 15-21.
- Kulandaiswamy, V. C. (1964). "A basic study of the rainfall excess-surface runoff relationship in a basin system," thesis presented to the University of Illinois, at Urbana, Ill., in partial fulfillment of the requirements for the degree of Doctor of Philosophy.
- Overton, D. E. (1964). "Mathematical refinement of an infiltration equation for watershed engineering." *ARS 41-99*, U.S. Dept. of Agr., Agric. Res. Service, Washington, D.C.
- Philip, J. R. (1957). "Theory of infiltration, Chapters 1 and Chapter 4." *Soil Sci.*, 83(5), 345-357.
- Philip, J. R. (1969). "Theory of infiltration." *Advances in hydroscience*, vol. 5, K. T. Chow, ed., Academic Press, New York, N.Y., 215-296.

- Rawls, W., Yates, P., and Asmussen, L. (1976). "Calibration of selected infiltration equations for the Georgia coastal plain." *ARS-S-113*, Agr. Res. Service. U.S. Dept. of Agric., New Orleans, La.
- Zhao, D. (1981). "A semi-linear model in infiltration theory." *Hydrological Res. Report*, 2, 246-255, P. R. China.

### APPENDIX III. NOTATION

*The following symbols are used in this paper:*

- $a$  = proportional factor of infiltration model;
- $F$  = cumulative infiltrated water depth (cm, L);
- $f$  = infiltration rate (cm/h, L/T);
- $f_c$  = steady-state infiltration rate (cm/h, L/T);
- $f_s$  = seepage rate (cm/h, L/T);
- $h$  = ponding water depth (cm, L);
- $K$  = hydraulic conductivity in transmission zone (cm/h, L/T);
- $L$  = soil depth (cm, L);
- $m$  = exponent (dimensionless);
- $n$  = exponent (dimensionless);
- $S$  = potential storage (cm or cm<sup>3</sup>, L or L<sup>3</sup>);
- $S_c$  = capillary suction head (cm, L);
- $S_0$  = initial soil space available (cm or cm<sup>3</sup>, L or L<sup>3</sup>);
- $t$  = time (min. T);
- $W$  = cumulative infiltrated water depth (cm, L); and
- $\theta_v$  = volumetric soil water content (cm<sup>3</sup>/cm<sup>3</sup>, L<sup>3</sup>/L<sup>3</sup>).